Characteristics and Modeling of Wireless LAN Channels for Multimedia Home Networks

von der Abteilung
Elektrotechnik und Informationstechnik
der Technischen Universität Dortmund
genehmigte
Dissertation
zur Erlangung des akademischen Grades
Doktor der Ingenieurwissenschaften

von
Beatriz Aznar Somolinos
Dortmund, 2009

Tag der mündlichen Prüfung: 27.02.2009

Hauptreferent: Prof. Dr.-Ing. R. Kays

Korreferent: Prof. Dr.-Ing. J. Götze

Vorwort

Die vorliegende Arbeit entstand während meiner Tätigkeit als wissenschaftliche Mitarbeterin am Lehrstuhl für Kommunikationstechnik der Technischen Universität Dortmund zwischen 2004 und 2008.

Dem Inhaber des Lehrstuhls, Herrn Prof. Dr.-Ing. R. Kays, möchte ich an dieser Stelle einen besonderen Dank dafür aussprechen, dass er diese Arbeit ermöglicht, betreut und begutachtet hat. Durch fruchtbare Diskussionen und viele Anregungen hat er zum Gelingen der Arbeit erheblich beigetragen.

Herrn Prof. Dr.-Ing. J. Götze vom Arbeitsgebiet Datentechnik, danke ich sehr für sein Interesse an der Arbeit und die Übernahme des Korreferats.

Darüber hinaus möchte ich mich bei allen Kollegen, studentischen Hilfskräften, Studien- und Diplomarbeiten am Lehrstuhl für Kommunikationstechnik bedanken, die durch ihre Einsatz, durch anregende Diskussionen und durch ein gutes Arbeitsklima zu der Entstehung dieser Arbeit beigetragen haben.

Mein besonderer Dank gilt meinem Freund Pablo für sein Verstädnis und seine Geduld während der Durchführung dieser Arbeit, sowie meinen Eltern dafür, dass sie mir das Studium ermöglicht haben und mit meinem Bruder mich immer unterstützt haben.

Beatriz Aznar

Prólogo

El presente trabajo se ha realizado durante mi actividad como trabajadora investigadora en departamento de Kommunikationstechnik de la Universidad Técnica de Dotmund entre 2004 y 2008.

Desde aquí me gustaría dar las gracias especialmente al titular del departamento, el Excelentísimo. Prof. Dr.-Ing. R. Kays, quien ha hecho posible, asesorado y dictaminado este trabajo. A través de fructuosos debates y muchas sugerencias ha aportado considerablemente al logro de este trabajo.

Al Excelentísimo Prof. Dr.-Ing. J. Götze del Área de Técnicas de Tratamiento Datos, le agradezco mucho su interés por el trabajo y la toma como segundo examinador.

Además me gustaría agradecer a todos mis compañeros, ayudantes estudiantiles y estudiantes de proyectos fin de carrera en el departamento de Kommunikationstechnik quienes con su esfuerzo, amenos debates y un buen clima de trabajo, han realizado su aportación a este trabajo.

Mi agradecimiento especial va para mi novio Pablo por su comprensión, ánimo y paciencia durante la realización de este trabajo, así como para mis padres, quienes hicieron posible que yo realizara estos estudios y junto a mi hermano siempre me han apoyado.

Beatriz Aznar

Index

Notation

Abbreviatures

ADSL	Asymmetric Digital Subscriber Lines
AGC	Automatic Gain Control
ARMA	Autoregressive Moving Average
AV	Audio-Visual
BER	Bit Error Rate
BFWA	Broadband Fixed Wireless Access
BPSK	Binary Phase-Shift Keying
BSC	Binary symmetric channel
BWA	Baum-Welch Algorithm
CDF	Cumulative Distribution Function
CRC	Cyclic Redundant Check
D/A	Digital to Analog
DAB	Digital Audio Broadcast
DANL	Displayed average noise level
DFS	Dynamic Frequency Selection
DFT	Discret Fourier Transformation
DLS	Direct Link Setup
DPCM	Differential (or Delta) Pulse Code Modulation
DSL	Digital Subscriber Line
DVB-T	Digital Video Broadcast Terrestrial
EM	Expectation-Maximization

ERP	Extended Rate PHY
FEC	Forward Error Correction
FDM	Frequency Division Multilex
FFT	Fast Fourier Transformation
GPIB	General Purpose Interface Bus
GSM	Global System for Mobile communications
HDSL	High-bit-rate Digital Subscriber Lines
HDTV	High-Definition Television
ICI	Inter Carrier Interference
IFS	Inter-frame spacing
IEEE	Institute of Electrical and Electronics Engineers
IIR	Infinite impulse response
ISDN	Integrated Services Digital Network or Isolated Subscriber Digital Network
ISI	Inter-Symbol-Interference
ISM	Industrial, Scientific and Medical
LLC	Logical Link Control
LOS	Line Of Sight
LTE	Long Term Evolution
LTI	Linear Time-Invariant
LTV	Linear Time-Variant
MAC	Medium Access Control
MIMO	Multiple Input, Multiple Output
MPC	Multipath Component
MSE	Minimum Square Error
MTU	Maximum Transmission Unit
NAS	Network Attached Storage
NLOS	Non Line of Sight

OBS	Obbstructed Sigth
OFDM	Orthogonal Frequency Division Multiplexing
PA	Power Amplifier
PAPR	Peak-to-Average Power Ratio
PC	Personal Computer
PHY	PHYsical layer
PLC	PowerLine Communications
PLCP	Physical Layer Convergence Procedure
PDF	Probability Density Function
PMD	Physical Medium Dependent
PPDU	PLCP Protocol Data Unit
PSDU	PLCP Service Data Unit
QAM	Quadrature Amplitude Modulation
QoS	Quality of Service
RAM	Random Access Memory
RF	Radio Frequency
RS 232	Recommended Standard 232
SIR	Signal to Interference Ratio
SINR	Signal to Interference plus Noise Ratio
SISO	Simple input simple output
SNR	Signal to Noise Ratio
TDL	Tapped Delay Line
UMTS	Universal Mobile Telecommunications System
VoIP	Voice over Internet Protocol
WAVE	Wireless Access for the Vehicular Environment
WLAN	Wireless Local Area Networks
WPP	Wireless Performance Prediction

WSSUS	Wide-Sense Stationary Uncorrelated Scattering
$\tau_n(t)$	Propagation delay
$\alpha_n(t)$	Attenuation factor
$\theta_n(t)$	Phase
T_m	Multipath delay
f_0	Carrier frequency
T_c	Coherence time
B_c	Coherence bandwidth
f_{Dmax}	Maximal frequency Doppler
$h(\tau,t)$	Time-varying impulse response
$H(f,t)$	Time-varying transfer function
$S(\tau,f_D)$	Doppler-varying impulse response
$T(f, f_D)$	Doppler-varying transfer function
$S_{hh}(\tau,\Delta t)$	Delay cross-power spectral density
$\varphi_{HH}(\Delta f,\Delta t)$	Time-frequency correlation function
$S(\tau,f_D)$	Scattering function
$S_{TT}(\Delta f,f_D)$	Doppler cross-power spectral density
$S_{\tau\tau}(\tau)$	Delay power spectrum
$\overline{\tau}$	Average excess delay
$\sigma_\tau = \tau_{rms}$	Delay spread or root mean square delay spread
$S_{\mu\mu}(f_D)$	Doppler power spectrum
$\overline{f_D}$	Average Doppler spread
σ_{f_D}	Doppler spread
$P_R(r)$	Channel amplitude probability density function
B_S	Transmission bandwidth

ChP	Received channel power
F	Frequency selective fading depth
λ	Wavelength
K	Rice factor
δ	Mapping symbols used by DPCM
$\gamma(n)$	Difference sequence between measured power samples
A	Transition matrix
B	Error matrix
π	Steady state vector
s_i	State

Abstract

With the introduction of new media distribution concepts such as “triple play”-offers, it is very important to provide reliable wireless networks for media transfer within the home. Wireless transmission of audio-visual data between multimedia devices in the home puts very high demands on the network and the underlying physical data transmission.

Furthermore, since a broad introduction of such systems to the consumer market can be expected, the available spectrum for wireless local networks will become a critical bottleneck. As radio propagation does not tend to stop at the boundaries of a single home, mutual interference between nodes of adjacent networks will arise. Such networks with high node density even increase the high demands on the performance of home media networks requiring network organization.

Channel modelling is one of the most critical aspects to be considered for the wireless networks design. The challenge is to obtain complete, descriptive and simple models, which allow developping simulations efficiently. Channel models predict among other effects the power loss suffered by a signal when propagates through an environment. Moreover, the in-house field is affected by dynamic attenuators.

This thesis contributes to the modeling of wireless in-house channels. In order to parameterize the models, numerous measurements were carried out. Both, static and dynamic scenarios with human influences were anlyzed. Several channel caracteristics are gained as consequence.The results are applied to improve the efficiency of wireless LAN for multimedia home networks.

1 Introduction

1.1 Thesis Objectives

The use of wireless technologies has been growing rapidly in the last years, evolving quickly from a novelty into a necessity. Currently, IEEE 802.11 (Institute of Electrical and Electronics Engineers) based wireless local area networks (WLANs) are frequently used to connect devices in the user's household. The wireless network technology is becoming very popular, making its way not only to the PC-related usage but also to other consumer electronic applications. These include Internet telephony, music streaming, gaming and in-home video transmission. Also, other AV storage appliances that contain multimedia material for enjoyment around the house are accelerating this tendency. Fig. 1.1 shows the forecast of the spectacular worldwide growth of the wireless devices until 2010.

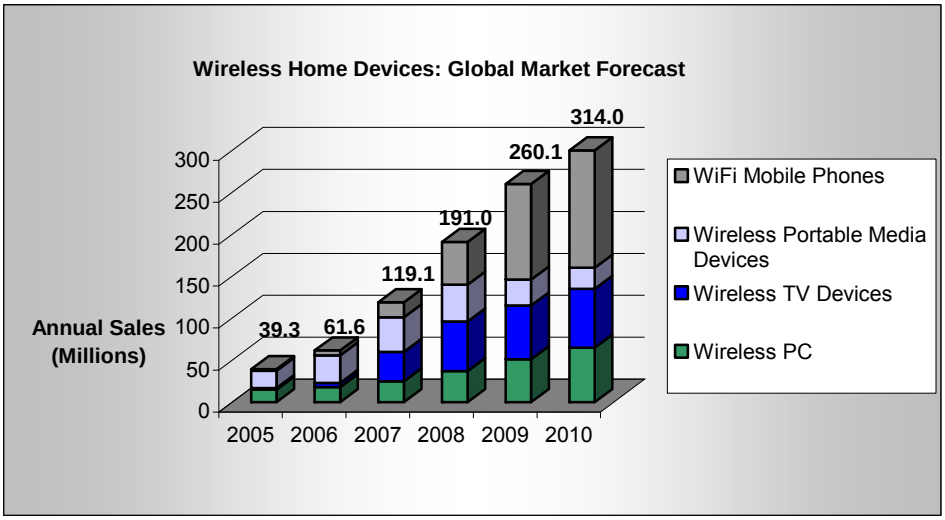

Fig. 1.1: Source: Strategy Analytics' Connected Home Devices service (Pyramid Research) [StratAnal]

There are predictions that an increasingly growing use of broadband wireless home networks will lead to the adoption of a multitude of new wireless home devices over the next years such as game consoles, wireless MP3 players and connected TVs. The digital household will be equipped with wireless home networking technologies, whereby the digital devices will interact with each other as well as with the available broadband and digital services.

Numerous alliances and consortia have been investigating how to develop the next generation of wireless broadband multimedia communication systems. The design of such systems needs to consider the demand on high data rates as well as a good quality of service (QoS). To fulfill these requirements, and to optimize them, it is essential to research the complex wireless channel time variability and its dependance on various effects during the transmission.

Characterising the dynamic behaviour of the channel is vital for the successful deployment of future wireless systems and/or optimization techniques for current wireless communication standards. That is the main objective of this dissertation, with particular emphasis on the analysis of the wireless channel characteristics in home environments. The work is divided into seven chapters. In this first chapter, a basic introduction of the wireless world is provided. Several multimedia applications and the scenario studied in this thesis are also outlined in this chapter.

The focus of Chapter 2 is on the wireless channel in the analyzed application scenario. The main characteristics such as time-varying fading or multipath propagation are also described together with some traditional statistical models and parameters.

The OFDM technique is introduced in Chapter 3. This includes a short overview of the evolution of the multicarrier systems followed by a description of some features of this technique. The insertion of OFDM in WLAN according to the standard IEEE 802.11 is also presented. Finally, several potential optimization procedures for this kind of transmission environment are listed at the end of this chapter.

To ilustrate the previous sections, numerous measurements of the in-house channel were carried out in the 2.4 GHz and 5 GHz frequency ISM (Industrial, Scientific and Medical) bands. Comprehensive evaluations are performed and the obtained results together with an in-house path loss model with attenuators are presented in Chapter 4. To gain a better insight into the wireless channel properties, additional sets of dynamic measurements are carried out and presented in detail in Chapter 5.

Based on the obtained time-varying channel characteristics, a model of the dynamic behaviour of the in-house WLAN channel is proposed. In Chapter 6, two different approaches are described: prediction for wireless network controllers and simulation of realistic time-varying situations. The first one can dynamically adapt the parameters of link adaptation techniques to the channel variations. The second approach reconstructs the measured received channel power traces, and models the distributions of bit errors through a Markov Model. This provides the possibility to simulate physical or link layer.

Finally, Chapter 7 points out the focuses of this work and summarizes the findings that have been presented.

1.2 Multimedia Applications

Some of the current and emerging home multimedia applications are Voice over IP (VoIP), video and music streaming, gaming and network attached storage (NAS). As confirmed by a user study [HOMEPLANE07], the wireless network is generally a preferred connection for multimedia devices. This is predominantly due to the increased flexibility of usage and the absence of cumbersome cable connections. Still, users expect the wireless network to be as reliable as the cable connections.

A good example of multimedia application whose usage has rapidly increased in the last years is VoIP. With the increased popularity of the Internet, (almost 50% of Europeans and 71% of North Americans have access to the Internet [IntWStat]), VoIP has become widely

accepted by users. Compared to the traditional phone services, VoIP phones are less expensive. The handsets are battery-powered and typically are connected to the Internet with built-in 802.11*b* or 802.11*g* adapter. Telephony does not demand high bandwidth, but it does require a reliable network connection with acceptable delays and jitters to be usable by the consumer.

Similarly, streaming demands a highly reliable connection, especially for video applications due to their very strict requirements. The consumers may prefer to have their digital audio and video collections in various rooms around the house.

Gaming is an application for which the home WLANs become increasingly more popular. There are different ways to use them. Users can be wirelessly connected to the Internet from their computers and portable gaming devices or they can use the network to compete with other players at home. They are also very demanding multimedia sessions.

NAS is an alternative for data backup for small offices as well as private households. An example of emerging applications for NAS are video storage centers that demand reliable and high-bandwidth connections to stream prerecorded TV programs, music videos or movies to TV sets or computers around the house.

Fig. 1.2 depicts examples of multimedia devices of the CE (consumer electronics) market that could take part in the wireless home network. Wireless connections provided with high data rate and QoS support will get rid of all the wires from the video and audio sources to the displays and loudspeakers. Some of these multimedia sources (live or stored) in our houses are set-top boxes, digital video cameras, media center PCs, IP phones or mp3 players, as shown in the picture. The display devices include DTV, HDTV and portable display appliances such as projectors.

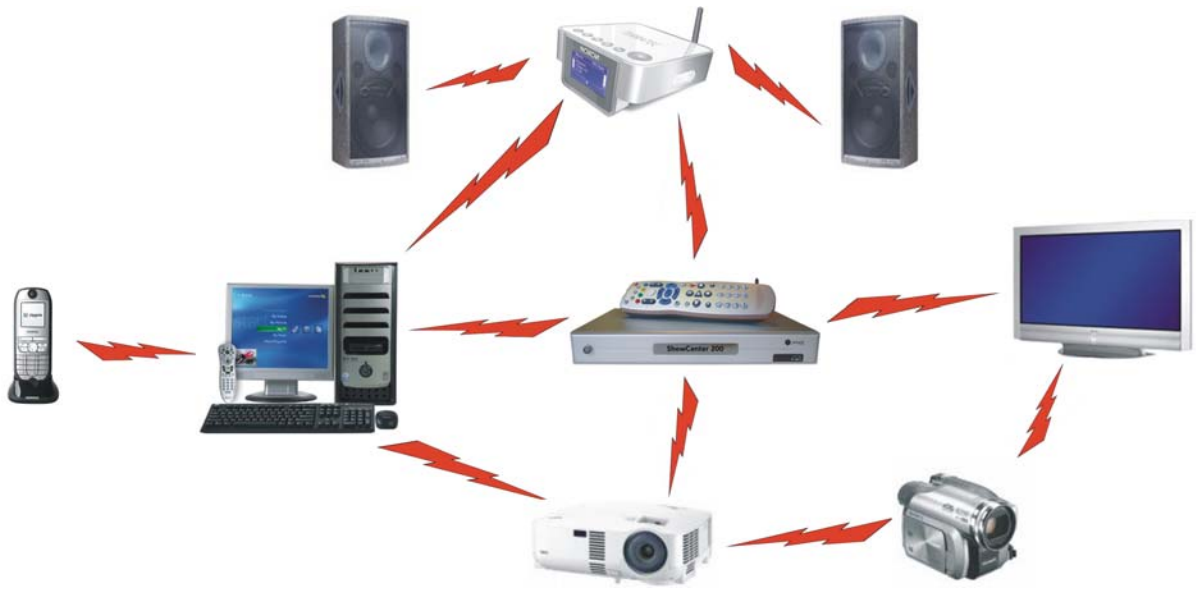

Fig. 1.2: Wireless multimedia home networking

The requirements for real time streaming in the wireless home network present a very demanding task, especially with regard to the QoS [KaJoEnN04]. QoS sets the requisites for specific applications to ensure satisfactory quality of their function. The parameters of interest include the data rate, the delay time and the delay jitter. For real time video, the required data rate should be provided to support various services in a stable and continuous

way. Depending on the application, data rates of up to 10 Mbit/s per link, e.g. for HDTV (High Definition Television), have to be supported. The transmission has to be quasi error free and latency should be kept very low, since a delay higher than 0.5 s will not be acceptable for fast zapping in online applications. Table 1.1 shows the different QoS requirements of possible applications regarding to the datarate, the delay time and the delay jitter [Brak99] completed with modern systems such as H264 HDTV.

Table 1.1: Requirements of several multimedia applications

Application	Data rate	Delay time	Delay jitter
MPEG-2 Video	3-6 Mbps	1 s	50 ms
H264 HDTV	6-10 Mbps	1-2 s	30 ms
MPEG-2 Audio	192 kbps	24 ms	100 ms
ISDN	64 kbps	50-100 ms	n.s. (not specified)
MPEG-2 DVD	2-10 Mbps	n. s.	n.s.
Videoconference	112 kbps	150-300 ms	130-400 ms
Gaming	n. s.	<40 ms	20-30 ms
Modem	≤ 64 kbps	-	-
Ethernet	10 Mbps	-	-
Control	< 100 bps	-	-
Remote control	< 100 bps	100-500 ms	n. s.

1.3 Application Scenario

Wireless transmission of audio-visual (AV) data between multimedia devices in the home environment puts very high demands on the network, on the underlying physical data transmission and on the quality of service (QoS) for which the IEEE 802.11 standard family is not optimized yet, even with the extension of IEEE 802.11e [IEEEe05].

A constant data rate and a reliable quality of each link are critical requirements for AV transmissions and have to be guaranteed over longer periods of time. In many situations off-the-shelf media products that are already available on the market do not achieve the required QoS. A typical video or audio transmission will run for a long time, often for several hours. During this period of time, the performance of the service could be degradated by changes of the transmission channel such as variable environments or new links interfering on the same frequency band. Such degradation can exist either for a short time or permanently. In any case the transmission's QoS requirements have to be guaranteed all the time. To determine the influence of these effects is the most challenging task of the modeling, since these changes are unpredictable.

In order to distribute electronic media in home environments, stable wireless links between media servers or gateways and presentation devices have to be supplied. Fig. 1.3 shows an

application scenario for a self-contained house, where the home network is made up of different links between the devices within. Further external networks such as satellite reception or DSL Internet are available through the corresponding access point and different devices may also link to terrestrial mobile communication such as GSM or UMTS or to digital broadcast networks such as DVB-T, DVB-H or DAB.

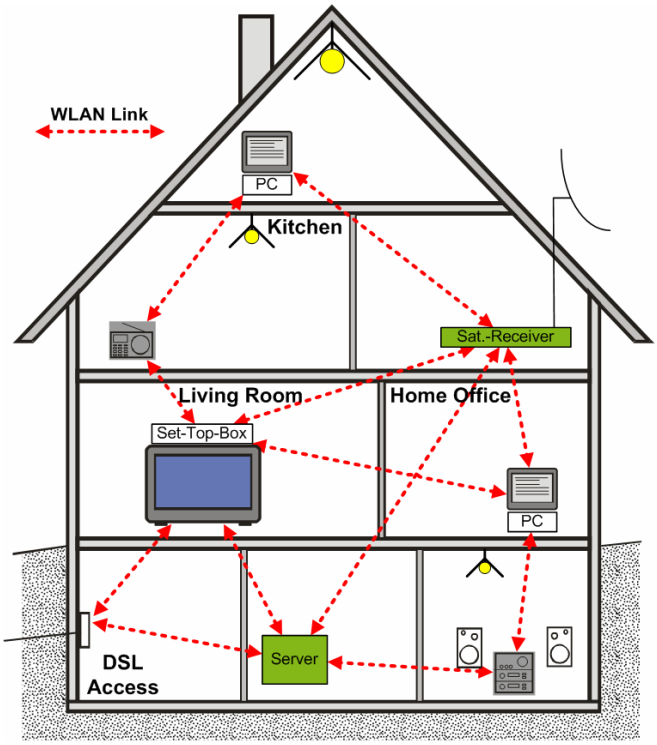

Fig. 1.3: Typical home media environment

Services are provided using individual links, and the devices offering such services are distributed in different rooms. The density of active network nodes is high, with the typical distance between two devices being in the order of 5 – 15 meters. Attenuation by walls, floors, and furniture heavily limits channel capacity. These links may be not only one stream for one device (unicast) but also one stream for several devices (multicast/broadcast) like a set of surround speakers.

A critical network situation is the simultaneous use of different video services by several members of the household. There will be a competition between the different wireless transmissions. Assuming a four-person household, typical in many industrial countries, the capacity of one single channel when using existing wireless LAN products is not sufficient. Due to the limited spectrum (e.g. only four non-overlapping channels in the 2.4 GHz ISM band), each link should be as efficient as possible to support the needs of all users in a neighborhood.

In comparison to the PC networks, the challenges for the multimedia local area network are quite different in many aspects. Three of them are particularly important and should be pointed out:

- Multimedia applications can require high data rates up to 10 Mbit/s in real time (e.g. DVD transmission, HDTV...).

- The network must be robust against short channel interferences, e.g. originated by movements or changes in a room.

- The user must be able to disconnect any device at any time without affecting the network function. Hence, the network should be preferably self-organised. For this reason, ad-hoc is the adequate topology to the analyzed application scenario.

1.3.1 Self-organised Ad-hoc Wireless Networks

In the development of an autarkicly configurable ad-hoc network for application scenarios such as the one shown in Fig. 1.3, seems plausible, since more than one node should be sufficient for managing different channel resources.

A wireless ad-hoc network is a collection of autonomous nodes or terminals that communicate with each other maintaining connectivity in a decentralized manner. The network topology is in general dynamic, because the connectivity among the nodes may vary with time due to node departures, new node arrivals and the possibility of having mobile nodes.

Application of link adaptation schemes should not cause users any difficulties. Therefore, self-organizing networks are necessary. Furthermore, for an optimum network management, an overall coordination of interfering logical networks of different users is required, especially in case of high node density. Intervention of a user is not desirable or even not possible in such an organization scheme. Moreover, changes of transmission parameters of a single link can not be treated as isolated processes. Every adaptation of a parameter has an impact on the whole network and can require parameter adaptation elsewhere.

Thus, self-organization does not just mean node discovery, synchronization and link establishment. Self-organization is a concept of cooperation. According to this concept, each node autonomously selects and adapts the transmission parameters that are necessary for an optimum networking. At the same time, the properties and behavior of its neighboring nodes are taken into account.

2 Wireless In-House Channel

2.1 Introduction

There are a number of differences between the terrestrial radio channel and the in-house radio channel. The cellular phone systems initiated a rapid growth of wireless communication. At the same time, with the growth of these systems, cell sizes became smaller to increase user capacity. The interest in indoor wireless systems for data services, e.g. wireless LANs, also began to be very significant.

The main difference between indoor and outdoor propagation lies in the accuracy of propagation prediction. In outdoor macro-cellular network propagation a topographical database can be used to determine the cell shape with a base station somewhere. Due to further causes of signal degradation the in-house channel can not be modeled only with path loss exponents. The primary causes for attenuation in indoor scenarios are distance, penetration losses through walls and floors and multipath propagation. Therefore, the characteristics of the outdoor radio channel cannot be directly adapted to the home enviroment, since the spatial proportions and the appeared velocities differ from one scenario to the other.

This chapter will present a mathematical description of the indoor wireless channels and demonstrate the importance of their crucial characteristic parameters. Furthermore, the principal causes of signal fading will be analyzed and the diverse examples in which it appears will be outlined. Finally, the most frequently published models will be presented.

2.2 Mathematical description of wireless channels

2.2.1 The channel impulse response approach

The random time-varying indoor radio propagation channel can be modeled in the three dimensional space as a linear time-varying (LTV) filter with the impulse response given by:

$$h(\tau,t) = \sum_{n=0}^{N(t)-1} \alpha_n(t) \cdot \delta(\tau - \tau_n(t)) \cdot e^{-j2\pi f_c \tau_n(t)} \tag{2.1}$$

where $h(\tau,t)$ represents the response of the channel at time t due to an impulse applied at time t-τ (see Fig. 2.5). $N(t)$ is the number of multipath components (typically considered N constant) and $\{\alpha_n(t)\}$, $\{\tau_n(t)\}$ and $\{\theta_n(t)\}$ are the random time-varying amplitude, arrival time and phase sequence, respectively (see also Fig. 2.5). The impulse response completely characterizes the channel and is a function of both t and τ. This mathematical model is illustrated in Fig. 2.1.

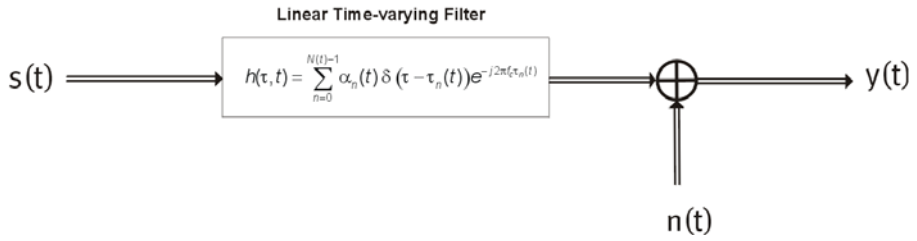

Fig. 2.1: Mathematical channel model

The channel output $y(t)$ to a transmitted signal $s(t)$ is given by:

$$y(t) = \int_{-\infty}^{\infty} s(\tau) \cdot h(t,\tau)\, d\tau + n(t) \tag{2.2}$$

where $n(t)$ is the low-pass complex-valued additive Gaussian noise.

If the equivalent low-pass signal of the input signal is represented with $s_l(t)$ and f_c is the carrier frequency, $s(t)$ can be formulated as follows:

$$s(t) = \mathrm{Re}\left[s_l(t) \cdot e^{j2\pi f_c t} \right] \tag{2.3}$$

Using the mathematically description of $h(\tau,t)$ in (2.1), the received band-pass signal may be expressed as:

$$y(t) = \sum_{n=0}^{N(t)-1} \alpha_n(t) \cdot s\left(\tau - \tau_n(t)\right) \cdot e^{-j2\pi f_c \tau_n(t)} \tag{2.4}$$

Substituting $s(t)$, defined in (2.3), in (2.4) :

$$y(t) = \mathrm{Re}\left[\left\{ \sum_{n=0}^{N(t)-1} \alpha_n(t) \cdot e^{-j2\pi f_c \tau_n(t)} \cdot s_l(t - \tau_n(t)) \right\} \cdot e^{j2\pi f_c t} \right] \tag{2.5}$$

From equation (2.5) it can be derived that the equivalent low-pass of the received signal is:

$$y_l(t) = \sum_{n=0}^{N(t)-1} \alpha_n(t) \cdot e^{j2\pi f_c \tau_n(t)} s_l(t - \tau_n(t)) \tag{2.6}$$

Considering the transmission of an unmodulated carrier frequency f_c, $s_l(t)=1$, the received signal is reduced to:

$$y_l(t) = \sum_{n=0}^{N-1} \alpha_n(t) \cdot e^{-j2\pi f_c \tau_n(t)} = \sum_{n=0}^{N-1} \alpha_n(t) \cdot e^{-j\theta_n(t)} \tag{2.7}$$

where $\theta_n(t) = 2\pi f_c \tau_n(t)$ varies by 2π rad whenever τ_n changes by $1/f_c$, which is a small number. Consequently, θ_n is a random variable that changes with relatively small variations of the medium, and therefore the received signal $y_l(t)$ can be modeled as a random process.

If the channel is assumed to be linear time invariant (LTI), then the impulse response in (2.1) may be simplified as:

$$h(\tau) = \sum_{n=0}^{N-1} \alpha_n \cdot \delta(\tau - \tau_n) \cdot e^{-j2\pi f_c \tau_n} = \sum_{n=0}^{N-1} \alpha_n \cdot \delta(\tau - \tau_n) \cdot e^{-j\theta_n} \tag{2.8}$$

2.3 Fading channel manifestations

In general, it is differentiated between large scale and small scale fading. Large scale fading describes the behavior of the signal strength relative to the long distance between the transmitter and the receiver causing the local average signal level to decrease gradually. On the contrary, small scale fading depicts the fast fluctuations of the received signal over very short distances. Fig. 2.2 shows the two kinds of attenuations. The factors causing these attenuations will be described in the next section.

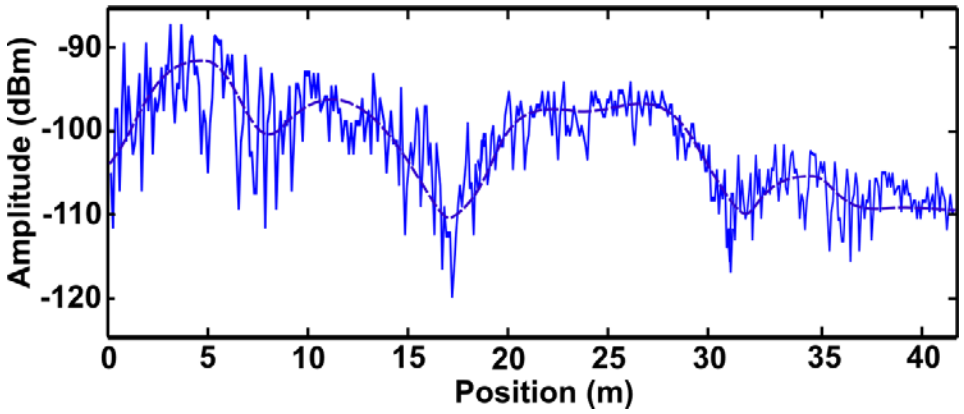

Fig. 2.2: Example of large and small scale fading

2.3.1 Large scale fading

Large scale fading represents an average signal power attenuation or a path loss due to the motion over large areas.The most important parameter predicted by large scale propagation models is typically the received power (or its reciprocal, path loss).

In the indoor scenarios, this phenomenon is mainly affected by walls and floors between the transmitter and the receiver. The statistics of large scale fading provide a way to estimate the path loss as a function of the distance.

2.3.2 Small scale fading

Small scale fading (often referred to as just fading) is used to describe the rapid fluctuations of the amplitudes $\{\alpha_n(t)\}$, phases $\{\theta_n(t)\}$ or multipath delays $\{\tau_n(t)\}$ of a radio signal over a short period of time or travel distance (as small as a half-wavelength).

Small scale fading manifests itself in two consequences, time-spreading of the signal (or signal dispersion) and time-variant behavior of the channel. The multipath creates time-spreading, whereas the time-variant channel is provoked by propagation path changes along the time between the transmitter and the receiver. The change rate of these propagation conditions accounts for the fading rapidity.

2.3.2.1 Multipath propagation

The signal transmitted through the radio channel reaches the receiver not only over the direct path (the shortest way from the transmitter to the receiver) but also by other ways mainly due to the three basic propagation mechanisms for radio waves: reflection, diffraction and scattering at immobile and mobile objects moving in different propagation paths.

Reflection occurs when electromagnetic waves bounce against objects whose dimensions are large compared with the wavelength of the propagating wave. Part of the energy is transmitted into the second medium and part is reflected back into the first one. When a radio wave is forced to deviate from a straight trajectory by one or more localized non-uniformities in the medium through which it passes, the reflected energy is spread out in all directions due to scattering.

All points on a wavefront can be considered as sources for the generation of secondary wavelets, which combined with each other produce a new wavefront. Diffraction is caused by the propagation of the secondary wavelets. Reflection, diffraction and scattering are collectively referred to as scattering.

The direct visibility between a transmitter and a receiver is designated as line of sight (LOS). Even when a LOS exists, multipath still occurs due to reflections caused by the floor or surrounding structures. Given that there are no moving objects in the channel, fading is purely a spatial phenomenon. Shadowing effects through walls or pieces of furniture constitute an additional attenuation. Such paths are referred to as obstructed sigth (OBS) or non line of sight (NLOS). The single propagation paths that arrive at the receiver have different lengths, which is referred to as multipath propagation. Fig. 2.3 depicts a possible multipath situation in a house. A LOS path exists between the laptop and the TV set, with other reflections (NLOS) being also involved.

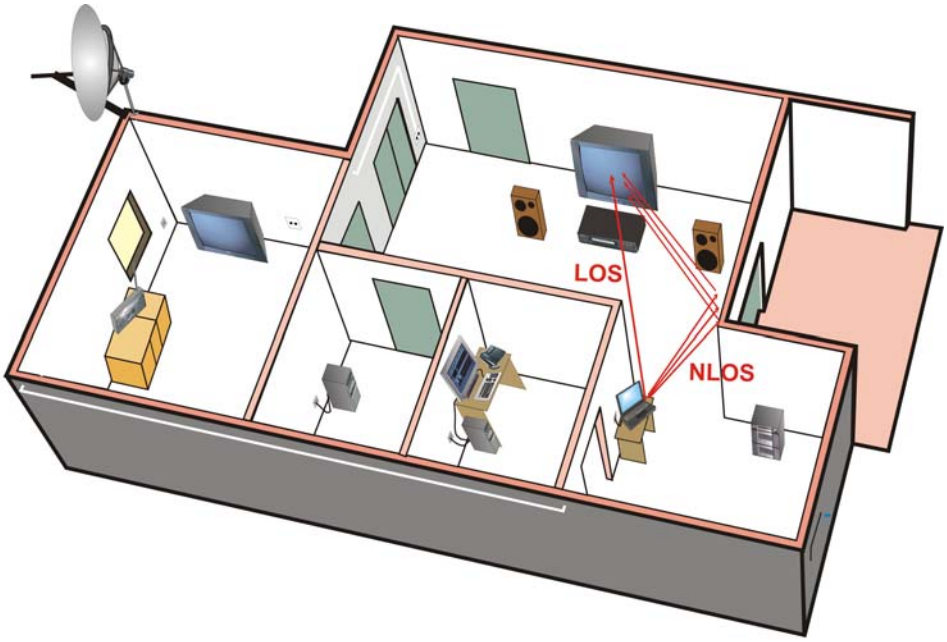

Fig. 2.3: Multipath situation with LOS and NLOS paths.

The received signal is composed by strongly attenuated, delayed and phase shifted copies of the transmitted signal, mathematically modeled in (2.4). Associated with each path there is a propagation delay $\{\tau_n(t)\}$, an attenuation factor $\{\alpha_n(t)\}$ and a phase $\{\theta_n(t)\}$. All of these parameters are time-varying as a result of changes in the propagation medium.

The multipath propagation model for the channel embodied in the signal $y_l(t)$ (2.6) results in signal fading. The fading phenomenon is primarily a result of the time variations in the phases. The path length determines the delay, $\tau_n(t)$, and depending on the phase, $\theta_n(t)$, can interfere with each other in a constructive or destructive mode.

Occasionally, the random phases $\theta_n(t)$ associated with the vectors $\alpha_n e^{-j\theta n}$ result in the vectors adding destructively and consequently, $y_l(t)$ becomes very small or practically zero (see Fig. 2.4 a)). At other times, they are adding constructively, so that the received signal is large (see Fig. 2.4 b)). Thus, the amplitude variations in the received signal, signal fading, are due to the time-varying multipath characteristics of the channel.

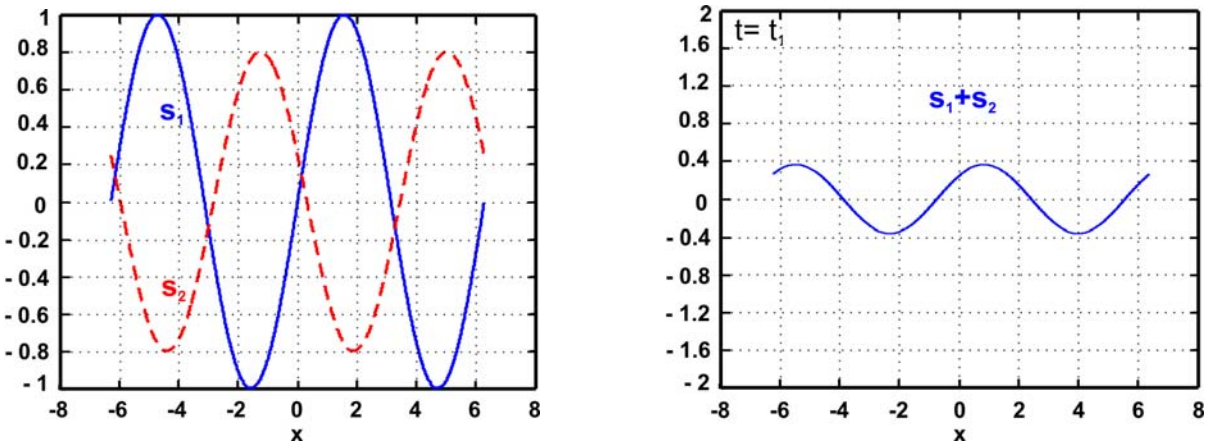

a)

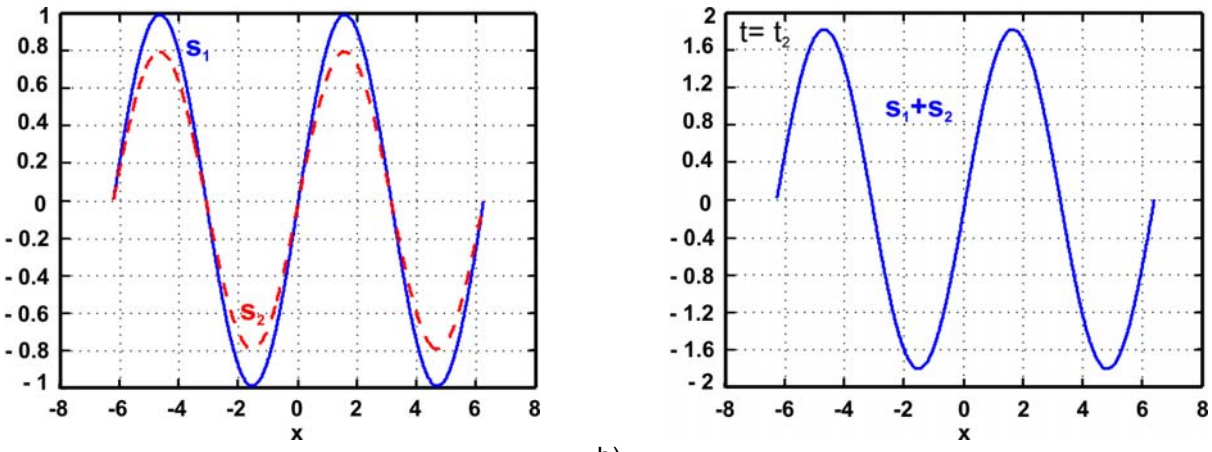

b)

Fig. 2.4: Representation of a) destructive and b) constructive interference between two signals. The key role is played by the phase difference between s_1 and s_2

As already mentioned, one feature of the fading channels is the time spread introduced in the transmitted signal. In Fig. 2.5 it is demostrated how a train of pulses is received as response to a short pulse transmitted over a time-varying multipath channel. The second feature that can be observed is a consequence of time variations. Changes in the number of pulses at the receiver, in relative delays between them as well as in their amplitudes are typical for such a channel. This phenomem is referred to as impulse dispersion and cannot be predicted.

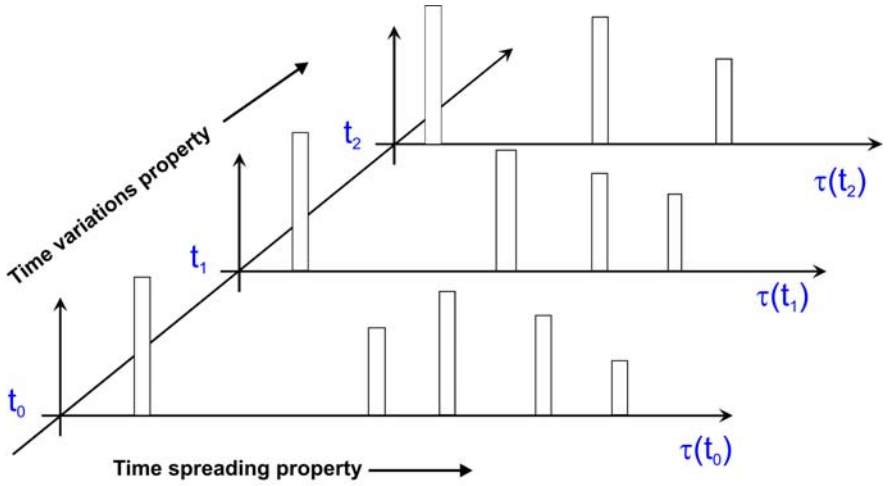

Fig. 2.5: Impulse response $h(\tau,t)$: time spreading because of multipath.

For a single transmitted impulse, the time between the first and the last received component, represents the maximum or multipath delay, T_m. The last component is defined as the fall of the multipath signal power to some threshold level below the strongest component. This indicator, T_m, is not necessarily the best to describe the channel performance. Different channels with the same multipath delay can exhibit very different profiles of signal intensity over the delay span. A more useful measurement of multipath is provided by the root mean squared (rms) delay spread that will be described in more detail in Section 2.4.1.1.

Large delay spread values cause inter-symbol-interference (ISI) in the single-carrier modulation system. For this reason, equalizers have to be used. In high data rate systems and/or high delay spread environments, the complexity and cost of equalizers can pose a

fundamental barrier. Another alternative is to use Orthogonal Frequency Division Multiplexing (OFDM) systems (see Chapter 3), which do not require equalizers. However, for a reliable deployment of OFDM systems, low delay spread values have to be assumed, e.g. in home environments, as it will be confirmed by the obtained measurements (see Chapter 4).

2.3.2.2 Doppler Effect

The Doppler Effect describes the frequency offset, which is given by a moving transmitter and a receiver relatively to each other. This sort of time-variation has been extensively studied in the context of cellular communications and has been modeled stochastically by Jakes [Jakes93]. However, the same effect can be produced in fixed wireless communication systems where both, transmitter and receiver, are stationary and time-variations are actually caused by changing environments. If the receiver and the transmitter are stationary but reflectors such as people move in the house, the interference pattern will change over the time.

The Doppler Effect can be observed for acoustic waves as well as for electromagnetic ones. The Doppler frequency shift of the *n*th echo path follows the next dependency:

$$f_{D_n} = f_{D_{\max}} \cdot \cos(\phi_n) \tag{2.9}$$

where Φ_n is the angle of incidence of the path at the receiver and f_{Dmax} is the maximal Doppler frequency, which is related to the moving speed v_{max}, the speed of light c_0 and the carrier frequency f_0:

$$f_{D_{\max}} = \frac{v_{\max}}{c_0} f_0 \tag{2.10}$$

Because of the Doppler Effect, the spectrum of the transmitted signal experiences a broadening through the channel. This effect is usually referred to as frequency spreading. In time domain such dispersion provokes a time variant impulse response (time selective). The larger the value of f_{Dmax}, the more rapidly the channel is changing with the time. This leads to define another channel parameter called channel coherence time T_c (will be described in detail in Section 2.4.1.1). As a simple empirical formula for the coherence time, it is often related to the maximal Doppler frequency [Rappaport02]:

$$T_c = \frac{1}{f_{D_{\max}}} \tag{2.11}$$

T_c is a statistical measure of the time over which the time correlation function of the channel is higher than 0.5, i.e. over which the received signal does not change considerably. In this case, the next approximation is valid [GrHa94]:

$$T_c = \frac{9}{16\pi \cdot f_{D_{\max}}} \tag{2.12}$$

In practice, the relation in (2.11) suggests a time duration in which a Rayleigh fading signal may fluctuate wildely, and (2.12) is mostly restrictive. Therefore, the coherence time can be estimated by a popular rule of thumb for modern digital communications through the geometric mean between both (2.11) and (2.12):

$$T_c = \sqrt{\frac{9}{16\pi \cdot f_{D_{\max}}^2}} = \frac{0.423}{f_{D_{\max}}} \tag{2.13}$$

Fig. 2.6 summarizes the fading manifestations described above. This diagram depicts a classification of different types of fading and factors causing them in time and frequency domain. At the bottom of the flow-diagram, the small scale fadings are reclassified as fast, slow, frequency-selective and flat fading. The parameters and criteria for the channel classification will be defined in Section 2.4.2.

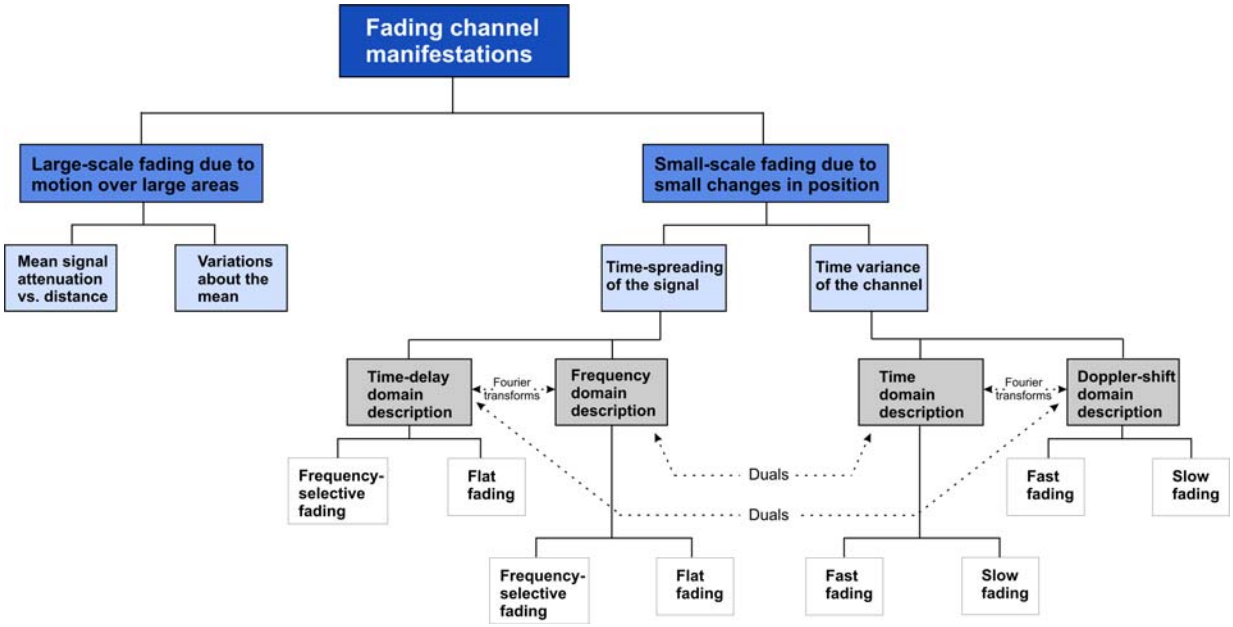

Fig. 2.6: Fading channel manifestations [BernSkl97]

2.4 Stochastic description of wireless channels

2.4.1 System functions

The theoretical description of radio channels can be essentially done by four system functions [Bello63], [Paetzold99]:

- Time-varying impulse response $h(\tau,t)$: describes the channel reaction at time t to a dirac impuls transmitted at time t-τ.

- Time-varying transfer function $H(f,t)$: characterizes the transmission behavior of signal with frequency f at time t.

- Doppler-varying impulse response $S(\tau,f_D)$: gives the dispersive behavior of the channel in dependency on the delay τ and the Doppler frequency f_D.

- Doppler-varying transfer function $T(f, f_D)$: with this function it is possible to stablish a relation between input and output spectra.

These functions are related to each other through the Fourier transformation. Since the radio channels are generally not deterministic, the four system functions are treated as stochastic magnitudes and described by autocorrelation functions, which are equally related through the Fourier transformation functions [Bello63], [Paetzold99].

Significant simplifications can be made by assuming that the time-variant impulse response h(τ, t) is stationary in the wide sense with respect to *t* and that the scattering components with different propagation delays are statistically uncorrelated. Based on these assumptions, Philip Bello introduced the WSSUS (wide-sense stationary uncorrelated scattering) model. The description of the WSSUS model is the topic of the following subsection.

2.4.1.1 WSSUS-Channel model

Important and simple classes of stochastic, time-varying and linear channel models are the WSSUS-Models introduced by P. Bello [Bello63]. They allow for an easy description of the input and output behavior of channels for the transmission of bandpass signals in the equivalent base band. For that, the stationarity of the channel must be guaranteed.

The time-frequency correlation function by WSSUS channel models is given by:

$$\varphi_{HH}(f,f',t,t') = E\left\{H^*(f,t)\cdot H(f',t')\right\} \tag{2.14}$$

It only depends on the time difference $\Delta t = t-t'$ and frequency difference $\Delta f = f-f'$. WSSUS-channel models can benefit from the Fourier transformation relations and thus, some simplification for the generic autocorrelation functions take place:

$$\begin{aligned}
&\varphi_{hh}(\tau,\tau';t,t') = S_{hh}(\tau,\Delta t)\cdot\delta(\tau-\tau')\\
&\varphi_{HH}(f,f';t,t') = \varphi_{HH}(\Delta f,\Delta t)\\
&\varphi_{SS}(\tau,\tau';f_D,f_D^{'}) = S(\tau,f_D)\cdot\delta(f_D-f_D')\\
&\varphi_{TT}(f,f';f_D,f_D^{'}) = S_{TT}(\Delta f,f_D)\cdot\delta(f_D-f_D')
\end{aligned} \tag{2.15}$$

where:

$S_{hh}(\tau,\Delta t)$:delay cross-power spectral density
$\varphi_{HH}(\Delta f,\Delta t)$: time-frequency correlation function
$S(\tau,f_D)$: scattering function
$S_{TT}(\Delta f,f_D)$: Doppler cross-power spectral density

For Δt=0 it is possible to derive the delay power spectrum $S_{\tau\tau}$ of the channel from the delay cross-power spectral density $S_{hh}(\tau,\Delta t)$:

$$S_{\tau\tau}(\tau) = S_{hh}(\tau,0) = \int_{-\infty}^{\infty} S(\tau,f_D)\, df_D \tag{2.16}$$

The delay power spectrum $S_{\tau\tau}(\tau)$ indicates the average power of the scattered components with a delay τ. It leads directly to two important parameters of the WSSUS-models:

- Average excess delay:

$$\bar{\tau} = \frac{\int_{-\infty}^{\infty} \tau \cdot S_{\tau\tau}(\tau)\, d\tau}{\int_{-\infty}^{\infty} S_{\tau\tau}(\tau)\, d\tau} \tag{2.17}$$

is the first moment of $S_{\tau\tau}$.

- Delay spread or root mean square (rms) delay spread:

$$\sigma_\tau = \tau_{rms} = \left[\frac{\int_{-\infty}^{\infty} \left(\tau - \bar{\tau}\right)^2 S_{\tau\tau}(\tau)\, d\tau}{\int_{-\infty}^{\infty} S_{\tau\tau}(\tau)\, d\tau} \right]^{1/2} \tag{2.18}$$

is the square root of the second central moment of the delay power.

For Δf=0 and from the doppler cross-power spectral density $S_{TT}(\Delta f, f_D)$ follows the Doppler power spectrum $S_{\mu\mu}(f_D)$:

$$S_{\mu\mu}(f_D) = S_{TT}(0,f_D) = \int_{-\infty}^{\infty} S(\tau,f_D)\, d\tau \tag{2.19}$$

It indicates the average power of the scattered components with a Doppler frequency f_D and is proportional to the probability density of f_D. Its mean and standard deviation also have a special significance:

- Average Doppler spread:

$$\overline{f_D} = \frac{\int_{-\infty}^{\infty} f_D \cdot S_{\mu\mu}(f_D)\, df_D}{\int_{-\infty}^{\infty} S_{\mu\mu}(f_D)\, df_D} \tag{2.20}$$

describes the average frequency shift that a carrier signal suffers during the transmission over the channel and represents the first moment of $S_{\mu\mu}(f_D)$.

- Doppler spread:

$$\sigma_{f_D} = \left[\frac{\int_{-\infty}^{\infty} \left(f_D - \overline{f_D} \right)^2 S_{\mu\mu}(f_D)\, df_D}{\int_{-\infty}^{\infty} S_{\mu\mu}(f_D)\, df_D} \right]^{1/2} \tag{2.21}$$

is the standard deviation of $S_{\mu\mu}(f_D)$.

Moreover, from the time-frequency correlation function, $\varphi_{HH}(\Delta f, \Delta t)$, two additional parameters can be obtained.

For Δt=0 is deduced the frequency correlation function $\varphi_{HH}(\Delta f, 0)$ that characterizes the amplitude correlation depending on the frequency difference Δf. The bandwidth that fulfills:

$$|\varphi_{HH}(B_c, 0)| = 0.5 \cdot |\varphi_{HH}(0,0)| \tag{2.22}$$

is referred to as coherence bandwidth B_c.

The delay power spectrum, $S_{\tau\tau}(\tau)$, and the frequency correlation function, $\varphi_{HH}(\Delta f, 0)$, build a Fourier transformation pair, so that the coherence bandwidth according to the time-bandwidth product [OhmLueke04] is approximately inversely proportional to the delay spread σ_τ.

For Δf=0 is deduced the time correlation function $\varphi_{HH}(0, \Delta t)$ that characterizes the amplitude correlation depending on the time difference Δt. Now, the parameter coherence time T_c is derived as the difference that fulfills:

$$\left|\varphi_{HH}(0, T_c)\right| = 0.5 \cdot \left|\varphi_{HH}(0,0)\right| \tag{2.23}$$

The coherence time, T_c, behaves approximately inversely proportional to the Doppler spreading, σ_{f_D}, since the time correlation function, $\varphi_{HH}(0, \Delta t)$, and the Doppler power spectrum, $S_{\mu\mu}(f_D)$, are associated to each other by the Fourier transformation.

The dependence of the system functions in WSSUS-models as well as other derived parameters are displayed in Fig. 2.7.

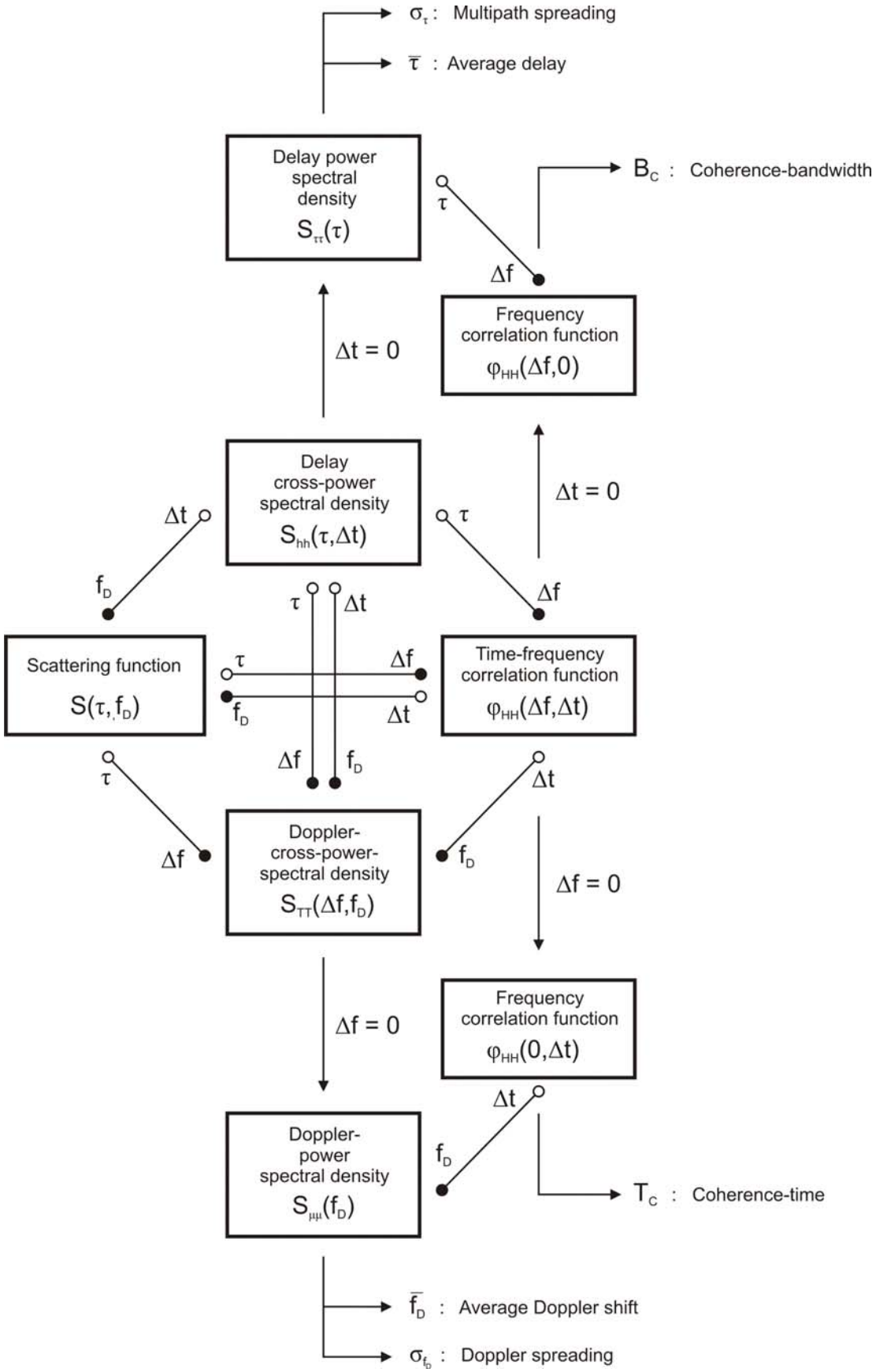

Fig. 2.7: Dependency between the correlation functions, spectral densities and the characteristical parameters according to WSSU channel models [Paetzold99].

2.4.2 Channel classification

Multipath propagation results in delay spreading whereas time variations in the channel impulse response or frequency response result in Doppler spreading. Consequently, a varying fading multipath channel may be generally characterized as a doubly spread channel, in time and in frequency. Both parameters deliver important information about the characteristic channel properties and are often used in the literature to describe and classify the radio channels.

According to these two spreading parameters there are two types of small-scale fading:

- Doppler spread-time selective fading due to σ_{f_D} .
- Delay spread-frequency selective fading due to σ_τ .

Fig. 2.8 summarizes the two small-scale fading manifestations, the two domains (time or time-delay and frequency or Doppler shift), whereby the fading degradation categories, and their consequences can be characterized.

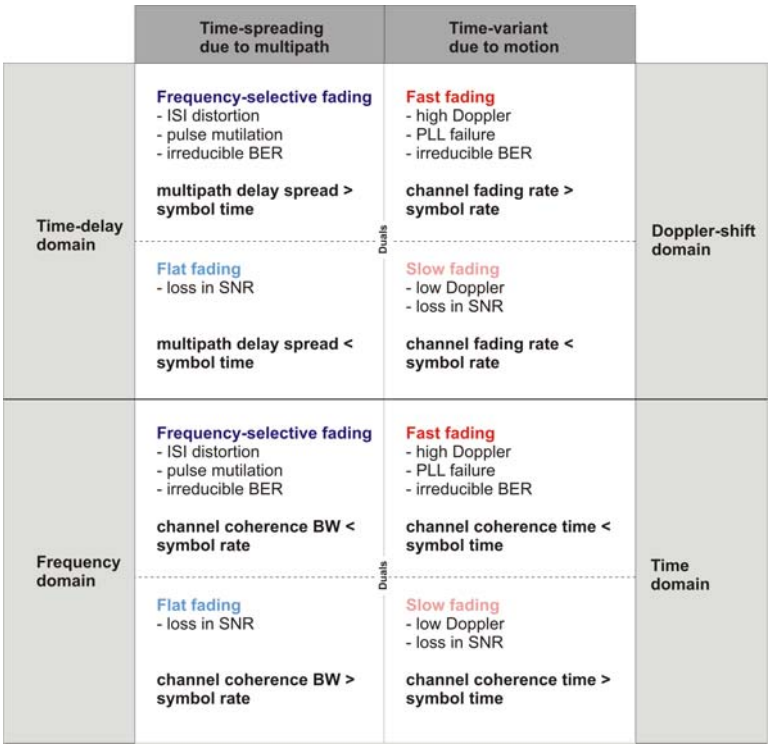

Fig. 2.8: Small scale fading: manifestations, degradations categories and effects [BernSkl97]

The manifestations identified in the time domain can be characterized equally in the frequency domain. Hence, the time spreading will be noted in the time-delay domain as a multipath delay spread and in the frequency domain as a channel coherence bandwidth. Similarly, the time-variant manifestation will be characterized in the time domain as a channel coherence time and in the Doppler-shift (frequency) domain as a channel fading rate or Doppler spread.

A signal suffers from frequency selective fading when the signal bandwidth B_s is

considerably higher than the coherence bandwidth B_c. Therefore, the symbol duration T_s is shorter than T_m and in the received spectrum can be generated strong incursions. When all the received multipath components of a symbol arrive within the symbol time duration, it is a flat fading.

On the other hand, a signal experiences fast fading if the symbol duration T_s is higher than the channel coherence time T_c and therefore, can cause the baseband pulse to be distorted, resulting in a loss of SNR that often yields an irreducible error rate.

2.5 Characterization of the impulse response

The channel impulse response can be anlyzed according to the distribution of path amplitudes, to the distribution of the arrival time sequence or to the distribution of path phases. In the next sections traditional and frequently used path loss models for the indoor channel will be presented concerning the amplitudes and arrival times.

Since the fading variations can not been forecasted, it is reasonable to characterise the time-varying multipath channel statistically. Statistical models of fading multipath channels which are often applied in the analysis and design of communication systems are: Rayleigh, Nakagami, Rician, Weibull, Lognormal, Suzuki or Saleh-Valenzuela.

2.5.1 Distribution of path amplitudes

In a multipath environment if the difference in time delay of a number of paths is much smaller than the reciprocal of the transmission bandwidth, the channel is considered to be underspread, otherwise it is overspread. Fig. 2.9 shows two examples of such situations. In the first example the received subpaths are resolved, however this is not the case in Fig. 2.9 b), where the signals are overlapping.

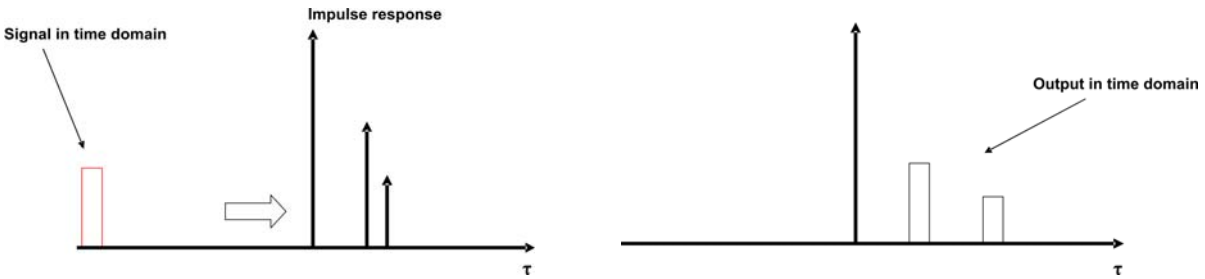

a) Overspread channel

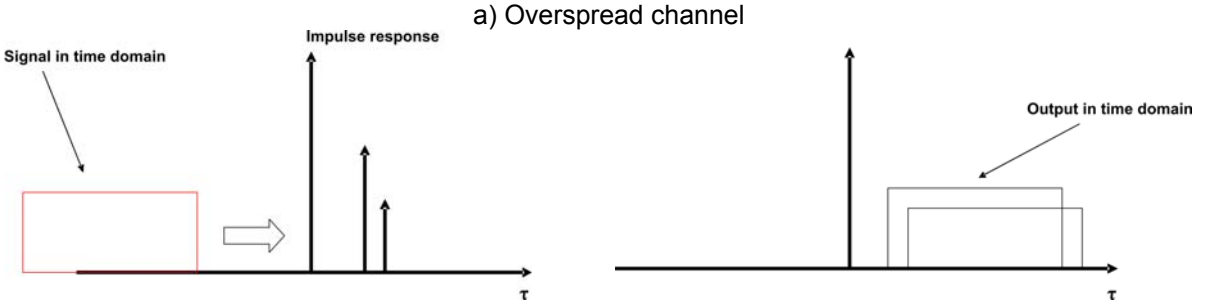

b) Underspread channel

Fig. 2.9

The unresolvable subpaths add vectorially (according to their relative strengths and phases) and the envelope of their sum is observed. The envelope value is therefore a random variable.

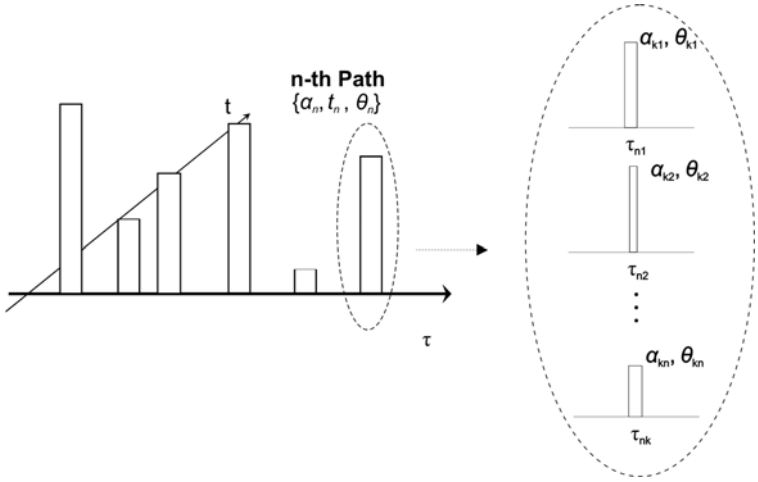

Fig. 2.10: An unresolved multipath component and its associated subpaths.

Mathematically, if $\tau_{ni} - \tau_{nj} < 1/B_S$, with $i, j = 1, 2, \ldots, k$, and B_S is the transmission bandwidth, then:

$$\alpha_n e^{j\theta_n} = \sum_{i=1}^{k} \alpha_{n_i} e^{j\theta_{n_i}} \tag{2.24}$$

is the resolved multipath component.

In the following $R = \alpha_n$ for any n to simplify the notation. Amplitude fading in a multipath environment may follow different distributions depending on the presence or absence of a dominating strong component and several other conditions. Major candidate distributions are described below.

2.5.1.1 Rayleigh distribution

When there is a large number of scatters in the channel that contribute to the signal at the receiver, an application of the central limit theorem leads to a Gaussian process model for the channel impulse response. This is the case in ionospheric or tropospheric signal propagation. If the process is zero-mean, then the envelope of the channel impulse response at any time instant has a Rayleigh probability distribution and the phase is uniformly distributed in the interval (0, 2π). The R envelope has the probability density function (pdf):

$$p_R(r) = \frac{2r}{\rho} e^{\frac{-r^2}{\rho}}, \quad r \geq 0 \tag{2.25}$$

where ρ is the Rayleigh parameter and is calculated as:

$$\rho = E\left[R^2\right] \tag{2.26}$$

The Rayleigh distribution is widely used to describe multipath. There are many reported empirical justifications for application of the Rayleigh distribution to the indoor propagation data [HorTanMor86], [SalehValenz87], [Alexander82], [AlexPugl83], [LoBeBo92], [KaEITaMa92]. Several measurements at 900 MHz, 1800 MHz, and 2.4 GHz showed that the small scale variations were Rayleigh distributed [ToTur92].

2.5.1.2 Nakagami distribution

This distribution, also referred to as the *m*-distribution, contains many other distributions as special cases. The pdf for this distribution is as follows:

$$p_R(r) = \frac{2}{\Gamma(m)}\left(\frac{m}{\rho}\right)^m r^{2m-1} e^{-mr^2/\rho}, \quad r \geq 0 \tag{2.27}$$

where ρ is defined as in (2.26), $\Gamma(m)$ is the Gamma function and the parameter *m*, called fading figure, is defined as the ratio of moments:

$$m = \frac{\rho^2}{E\left[\left(R^2 - \rho^2\right)\right]}, \quad m \geq \frac{1}{2} \tag{2.28}$$

The Nakagami-*m* is a two parameter distribution, *m* and *ρ*. Consequently, this distribution provides more flexibility and accuracy in matching the observed statistics. This includes the Rayleigh distribution as a special case (*m*=1).

Turin [Turin72] and Suzuki [Suzuki77] showed that the Nakagami distribution provides the best fit for the data signal received in urban radio channels. The application of this distribution to the indoor radio propagation data has been generally neglected.

2.5.1.3 Rician distribution

The Rician distribution is also a two parameter distribution that may be used to characterize the signal in a fading multipath channel. This distribution is appropiate for modeling a Gaussian fading channel in which the impulse response has a non-zero component, usually called as specular component, *s*. The pdf for the Rice distribution is as follows:

$$p_R(r) = \frac{r}{\sigma^2} e^{\frac{-(r^2+s^2)}{2\sigma^2}} I_0\left(\frac{r \cdot s}{\sigma^2}\right), \quad r \geq 0 \tag{2.29}$$

where s represents the amplitude of the LOS path or dominant signal, $I_0(\cdot)$ is the zeroth order modified Bessel function of the first kind and σ^2 is proportional to the power of the all multipath components. When s^2=0, (2.29) reduces to the Rayleigh pdf with $\sigma^2=\rho/2$. When s is large, the distribution approaches a Gaussian distribution centered at *s*:

$$p(x \mid \mu,\sigma) = \frac{1}{\sigma\sqrt{2\pi}} \exp\left(-\frac{(x-\mu)^2}{2\sigma^2} \right) \tag{2.30}$$

The Rice distribution is a particularly appropiate model for LOS communication links, where there is a direct propagating signal component (the specular component) and multipath components arising from secondary reflections that arrive with different delays, as was shown in Fig. 2.2.

In conclusion, the Rayleigh and Rice distributions are the most widely used statistical models for signals transmitted through fading multipath in-house channels [ThMcGee88], [KaBo92].

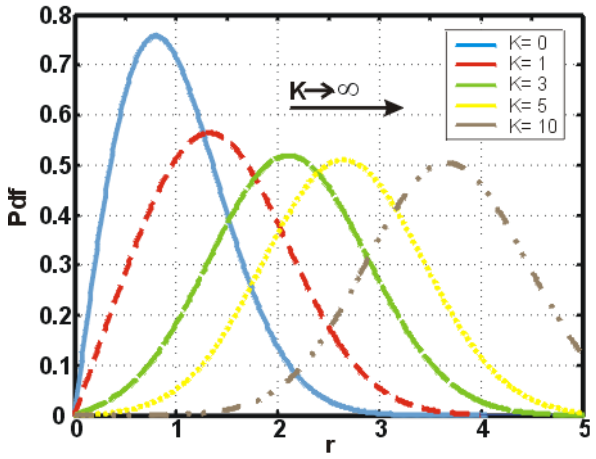

Fig. 2.11: Rayleigh and Rice distribution functions

2.5.1.4 Weibull, Lognormal and Suzuki distributions

Weibull distribution represents yet another generalization of the Rayleigh function. The Lognormal distribution has often been used to explain large scale variations of the signal amplitudes in a multipath fading environment. And the Suzuki distribution is a mixture of both. It phenomenologically explains the transition between the local Rayleigh distribution to the global lognormal one.

A review of indoor propagation literature indicates that these three distributions have been generally neglected.

2.5.2 Distribution of the arrival time sequence

The impulse response approach to characterize the indoor radio propagation channel based on the distribution of the arrival time sequence has been described in several models: Standard Poisson Model, Modijied Poisson-The A-K Model [Suzuki77], Modijied Poisson-Nonexponential Interarrivals and the Neyman-Scott Clustering Model. However, none of these models have taken hold in indoor scenarios. Far from the Saleh-Valenzuela model which has been the standard model for Indoor NLOS wireless propagation.

2.5.2.1 Saleh-Valenzuela model

Saleh-Valenzuela model is a statistical model whose basic assumption is that multipath components (MPCs) arrive in clusters formed by the multiple reflections from the objects in the vicinity of receiver and transmitter. The model proposes that both of these decaying patterns are exponential with time and are controlled by two time constants: the cluster arrival decay constant and the ray arrival decay constant.

The clusters, as well as the MPCs within a cluster, arrive according to Poisson processes with different rates and have interarrival times that are exponentially distributed. The MPCs amplitudes are independent Rayleigh random variables and the corresponding phase angles are independent uniform random variables over [0,2π). The power decays exponentially with the cluster decay constant as well as with the excess delay within a cluster.

The complex, low-pass impulse response of the channel is given by:

$$h(\tau,t)=\sum_{l=0}^{\infty}\sum_{k=0}^{\infty}\beta_{kl}e^{j\theta_{kl}}\delta(t-T_l-\tau_{kl}) \tag{2.31}$$

where T_l is the arrival time of the lth cluster, τ_{kl} is the arrival time of the kth ray measured from the beginning of the lth cluster, and β_{kl} and θ_{kl} are the gain and phase of the kth ray of the lth cluster. The mean square values of the amplitudes are given by:

$$\overline{\beta_{kl}^2}\equiv\overline{\beta^2(T_l,\tau_{kl})}=\overline{\beta^2(0,0)}e^{-\frac{T_l}{\Gamma}}e^{-\frac{\tau_{kl}}{\gamma}} \tag{2.32}$$

where $\overline{\beta^2(0,0)}$ is the average power of the first arrival of the first cluster, and Γ and γ are the power decay constants for the clusters and rays, respectively. T_l and τ_{kl} are described by the independent interarrival exponential probability density functions:

$$\begin{aligned}p(T_l\mid T_{l-1})&=\Lambda e^{(-\Lambda(T_l-T_{l-1}))}\\ p(\tau_{kl}\mid\tau_{(k-1)l})&=\lambda e^{(-\lambda(\tau_{kl}-\tau_{(k-1)l}))}\end{aligned} \tag{2.33}$$

where Λ and λ is the cluster and ray arrival rate, respectively.

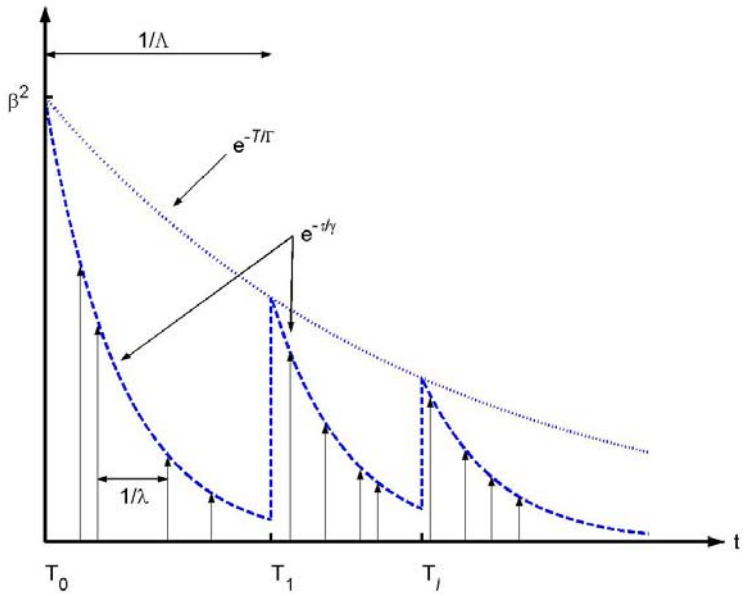

Fig. 2.12: An exponential decay of the mean cluster power and the ray power within the cluster.

A generalized version of the Saleh-Valenzuela model can be found for ultra-wideband channels (see 802.15.4a) [Molish05].

2.6 Modeling of frequency selective channels

2.6.1 Tapped-Delay-Line model

Frequency selective channels classified according to the criteria listed in Fig. 2.8, can be implemented by means of FIR (finite impulse response) filters [Paetzold99]. In the literature the TDL (tapped-delay-line) channel models are frequently used.

When the channel is overspread, Fig. 2.9 a), the sampling theorem may be used to represent the resolvable received signal components through the time-varying channel impulse response as:

$$h(\tau,t)=\sum_{n=0}^{N-1}h_n(t)\cdot\delta(\tau-\frac{n}{B_s}) \tag{2.34}$$

and the corresponding time-varying transfer function as

$$H(f,t)=\sum_{n=0}^{N-1}h_n(t)\cdot e^{j2\pi f_c\frac{n}{B_s}} \tag{2.35}$$

where N is the number of resolvable multipath components. If the multipath spread is T_m and the time resolution of the multipath $1/B_s$, it follows that

$$N = \lfloor T_m B_s \rfloor + 1 \tag{2.36}$$

A channel having the impulse response given by (2.34) may be represented by a tapped-delay line with N taps and complex time-varying tap coefficients $\{h_n(t)\}$.

The tap gains $\{h_n(t)\}$ are usually modeled as stationary (wide-sense) mutually uncorrelated random processes (WSSUS, see section 2.4.1.1). Thus, each resolvable multipath component may be modeled with its own appropiate Doppler power spectrum and corresponding Doppler spread. Fig. 2.13 illustrates the tapped-delay-line channel model.

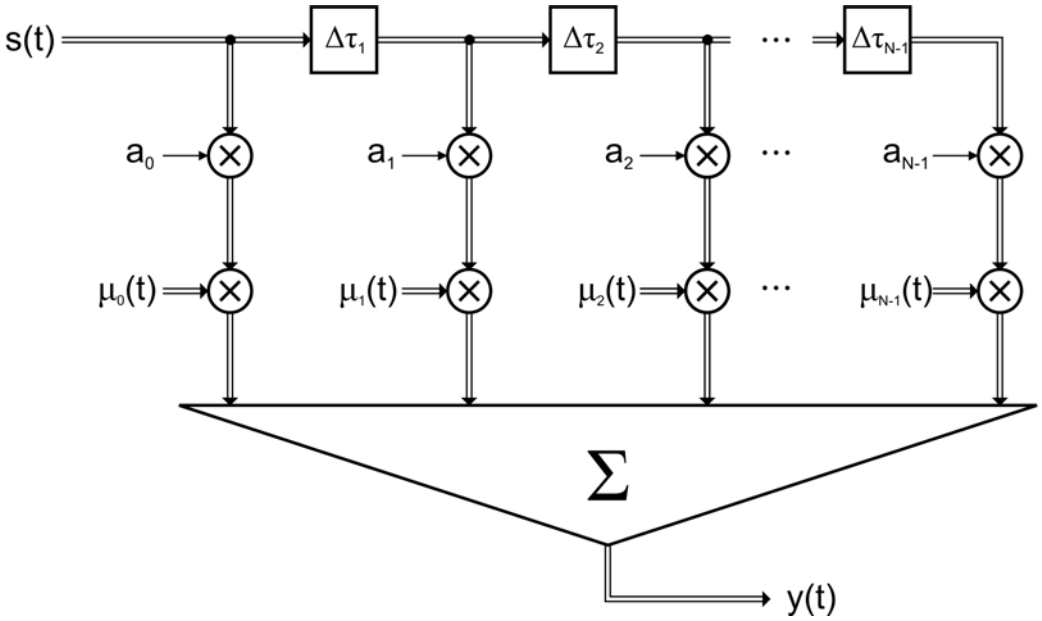

Fig. 2.13: Tapped-delay-line channel model

Each of the delayed versions of the input signal $s(t)$ is weighted by a constant delay coefficient a_n. Both the delay coefficients a_n and the discrete propagation delays $\Delta\tau_n$ determine the delay power spectral density, $S_{\tau\tau}(\tau)$, of frequency-selective channel models. In general, the delay coefficients and the discrete propagation delays determine the frequency-selective behavior of the channel, which can be attributed to the effect of multipath propagation. The disturbances of the channel caused by the Doppler effect are modelled according to the principle of deterministic channel modelling, by a time-variant complex deterministic Gaussian process $\mu_n(t)$. Therefore, $h(\tau,t)$ can be also formulated as:

$$h(\tau,t) = \sum_{n=0}^{N-1} a_n \mu_n(t) \cdot \delta(\tau - \frac{n}{B_s}) \tag{2.37}$$

A discrete-time model required for the computer simulations can be obtained from the continuous-time structure, e.g., by sampling $\tau_n \rightarrow n \cdot T_s$, $s(t) \rightarrow s(k \cdot T_s)$, $y(t) \rightarrow y(k \cdot T_s)$ and $\mu_n \rightarrow \mu_n(k \cdot T_s)$ with $T_s \leq T_{symbol}$.

2.6.2 Finite State Markov Model

TDL is a continuous-time-based channel model. When the number of multiple delayed fading paths is large and/or the differential delay between paths is small, which is usually true for wideband systems in practice, then a significant amount of computational effort is required in simulations with continuous-time channel models [JeBaSha00].

In digital mobile communication systems, baseband signal processing is typically carried out in the discrete-time domain. Correspondingly, an end-to-end discrete-time channel model that comprises the continuous-time physical channel model, the (analog) transmit and receive filters, as well as the sampling process at the receiver is of great interest. The simulation of a system is carried out in a pure discrete manner at the symbol rate, which is 1/8 to 1/16 the sample rate, leading to a higher computational efficiency.

The discrete-time channel model was firstly presented by Forney in the early 1970's [Forney72], and simulation models in the discrete-time domain were discussed in [Hoeher92], [YipNg95] and [YipNg96] for single-input single-output (SISO) wireless channels. These papers qualitatively showed the computational efficiency in favor of the discrete-time models.

Discrete channel models describe the errors over the channel by means of probabilities. There are two categories: with and without memory. A feature of the frequency selective channels is that they have memory due to the emergence of error bursts and therefore, this section will focus on this kind of channel models.

Markov processes are popular in modeling fading because they can model processes with memory and their theory is well developed. The study of the finite-state Markov channel started from early work of Gilbert [Gillbert60] and Elliot [Elliot63]. They studied a two-state Markov channel known as the Gilbert-Elliot channel. In their channel model, each state corresponds to a specific channel quality, which is either good or bad. In general, a binary symmetric channel (BSC) with a given crossover probability can be associated with each state so that the channel quality for each state can be identified.

Fig. 2.14 represents the received channel power over time-varying channel. Typical behavior of multipath channels provokes a deep fade reducing strongly the received signal strength at certain times. It can be defined a threshold to limit the power range with an acceptable bit error rate from the range with a not admissible one. This threshold value indicates the criterium a channel to stay in a good or a bad state.

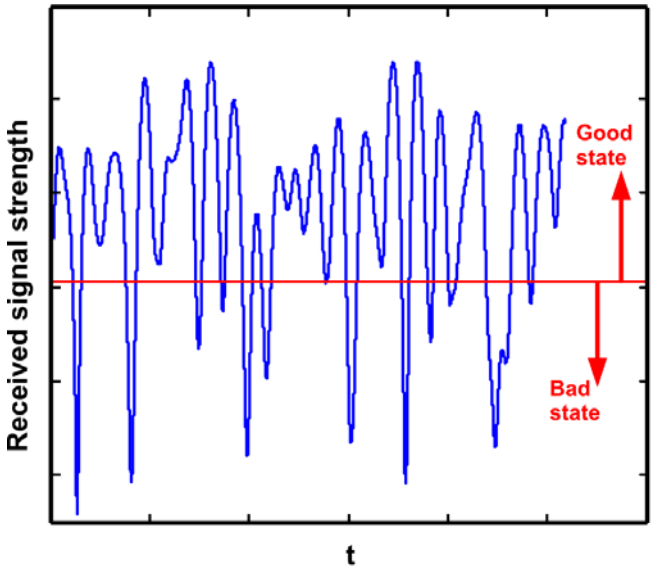

Fig. 2.14: Received channel power and threshold value for a model with two states

The channel can be defined by the probabilities corresponding to two states: S= { g, b }. In the first state, “good state”, g, the error probability is quite low, whereas if the channel is in the “bad state” the error probability is relative high.

Along the time the channel transits from “good state“ into the “bad state“ and vice versa. The time correlation of the physical channel determines how often a transition takes place and how long the channel remains in one state.

To describe these state transitions, the transition probabilities a have been defined:

$$\begin{aligned} a_{gg} &= P(S_{t+1} = g \mid S_t = g) \\ a_{gb} &= P(S_{t+1} = b \mid S_t = g) \\ a_{gb} &= P(S_{t+1} = b \mid S_t = g) \\ a_{bb} &= P(S_{t+1} = b \mid S_t = b) \end{aligned} \tag{2.38}$$

where S_t and S_{t+1} are the channel states at time t und t+1 respectively. These probabilities can be resumed by the transition matrix:

$$A = \begin{pmatrix} a_{gg} & a_{gb} \\ a_{bg} & a_{bb} \end{pmatrix} \tag{2.39}$$

The addition of each row in the matrix A will result one. A graphic representation of the Gilbert-Elliot model is shown in Fig. 2.15.

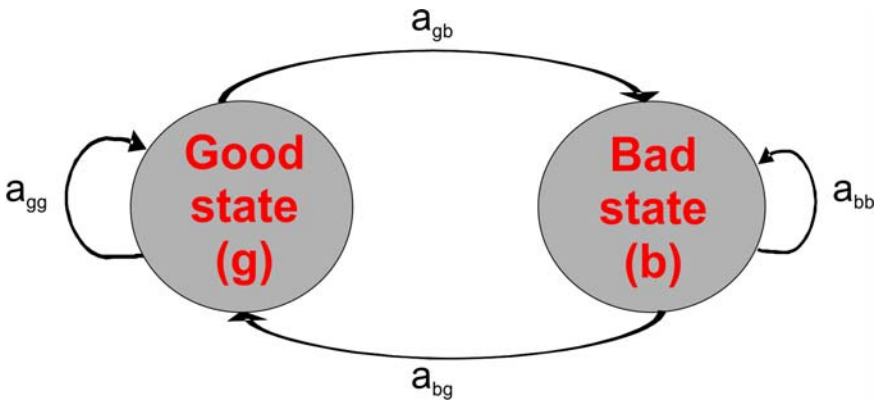

Fig. 2.15: Two-states Markov model

Other stastistics such as the probability that the channel stays in a given state are interesting. The steady state probabilities are defined by Π_{ss}.

In some cases, modeling a radio communication channel as a two-state Gilbert-Elliot channel is not enough when the channel quality varies dramatically, e.g. in in-house channels. A straighforward solution is to form a channel model with more than two states. There are different model structures commonly used in describing Markov model channels:

Multiple Markov chains

The Markov Model of order *m* (in the literature also named as "memory *m*") defines the state probability at *t*+1 as follows:

$$P(S_{t+1} \mid S_t, S_{t-1}...) = P(S_{t+1} \mid S_t, S_{t-1},...S_{t-m-1}) \tag{2.40}$$

It implies that the state at time *t* depends on the last *m* states. By a first order markov model this dependency only affects to the previous state:

$$P(S_{t+1} \mid S_t, S_{t-1}...) = P(S_{t+1} \mid S_t) \tag{2.41}$$

The presented Gilbert-Elliot channel model is a special case of first order Markov models with *N*=2 states.

There have been some attempts to use higher order Markov models to represent fading channels [BaLom00], [BaKeLom99]. Babich [BaKeLom99] used the context tree approach to model fading channels, where the derived Markov model has a variable order. New methods are being studied, capable of fitting Markov models with arbitrary order to the actual process.

However, it was shown in [BaLom00] and [BaKeLom00] that a model of first order approximates quite accurately the reproduction of the multipath channel characteristics. It would be only meaningful to apply a higher order model in special cases due to the computing costs of such models.

Quantized autoregressive and moving average (ARMA)

The fading power spectral density is approximated with a rational function using standard methods of the infinite impulse response (IIR) filter design [RaGo75]. As in the case of the multiple Markov chains, the size of this model transition probability matrix grows exponentially with the process memory.

Birth and death processes

Birth and death processes are a special case of a first order Markov model (m=1) with N states. These models assume that the quantized fading amplitude from the current ith level can jump only to the adjacent levels. Thus, a_{ij}=0 if $|j - i| > 1$. This structure allows to model slowly varying processes, and its accuracy depends on the selection of quantization levels.

The mapping from a physical fading channel to the first-order discrete Markov model (birth-death process) was proposed by Wang and Moayeri [WaMo95]. There, it was established a connection between Rayleigh fading channels and their markov models, by partitioning the received signal to noise ratio (SNR) into a finite number of intervals leading to a finite state Markov model. Thus, the quality of the Rayleigh fading channel is characterized in terms of the average error probability given a specific digital modulation scheme.

Assumed that the SNR remains at a certain level for the time duration of channel symbol and that the channel states associated with consecutive symbols are neighboring states, the fading channel is represented in Fig. 2.16. This structure allows to model slowly varying processes, flat fading.

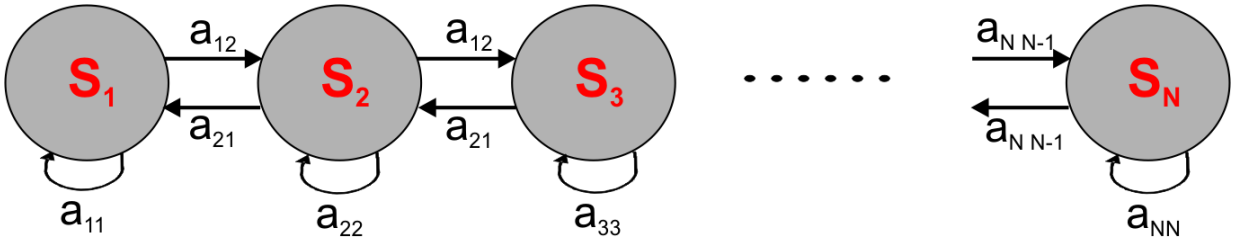

Fig. 2.16: Birth and death process assumed slow fading

Similarly, Zhang [ZhKa99] examined the first-order Markov model to represent the Rayleigh fading channel.

Due to the non-linearity between SNR and the average error probability, the SNR intervals may have to be non-uniform to be useful. Optimization of thresholds for a particular environment under mean square error criterion has been addressed in [WaMo93].

Monte Carlo method

The model parameters for the Markov process approximation are estimated by computer simulations. Several methods to fit Markov chains are described in [Billingsley61].

Hidden Markov Models

For the flat-fading channel, the Gilbert–Elliot model [Elliot63] or birth and death processes are used since its model parameter can be analytically expressed in terms of the Rayleigh

fading parameters. For frequency selective channels, however, the model parameters cannot be analytically determined.

A more generalized scheme for the frequency selective fading is used based on hidden-markov model (HMM). The HMM parameters must be extracted from error-sequences derived through either field measurements or more thorough simulations of the physical layer. In general, the model parameters are extracted for a *N*-state Markov model with *N*>2 for more accuracy [GaCr97].

3 OFDM-Transmission Technique

3.1 History

The principle of the OFDM-transmission (Orthogonal Frequency Division Multiplexing) was published in mid-1960s. The first ideas regarding multicarrier systems were discussed even in the 1950s.

Basically, OFDM is a special case of multicarrier transmission, where a single data stream is transmitted over a number of lower rate subcarriers. The uniqueness of OFDM in comparison to other multicarrier systems is that it is an orthogonal method, in which the data are modulated and separated into individual subcarriers without obvious inter carrier interference (ICI). Furthermore, OFDM offers the possibility of reducing inter symbol interference (ISI) by introducing an additional guard interval to efficiently handle the multipath delay spread (factors causing a multipath delay spread are described in Chapter 2).

It was already shown in 1971 [WeEb71] that it is possible to use the discret Fourier transformation (DFT) for the OFDM-baseband signal processing. Through the fast Fourier transformation (FFT) and the advances in the microelectronic and digital signal processing, a low-cost demonstration of the OFDM method was achieved and became a key technology for the modern transmission techniques.

In the 1980s, OFDM was studied for high-speed modems, digital mobile communications and high-density recording. Moreover, various-speed modems were developed for telephone networks [KeBi80].

In the 1990s, OFDM was introduced for wideband data communications, high-bit-rate digital subscriber lines (HDSL) supporting data rates up to 1.6 Mbps, asymmetric digital subscriber lines (ADSL) up to 6 Mbps and very-high-speed digital subscriber lines (VDSL) up to 100 Mbps.

The Digital Audio Broadcast (DAB) standard [DAB95] was the first OFDM-based standard, 1995, followed by the digital video broadcast terrestrial standard DVB-T [DVB97] in 1997.

The OFDM-based IEEE wireless standards were the first ones to use the OFDM in packet-based wireless communication. Since the beginning of the 1990s the 900 MHz, 2.4 GHz and 5 GHz ISM (Industrial, Scientific & Medical) bands have been available for license-exempt use in Europe, the United States and Japan. In June 1997, an international interoperability standard was approved by the IEEE. In July 1998, the IEEE 802.11 standardization group selected OFDM as the basis for its new 5 GHz standard, IEEE 802.11 a, yielding data rates from 6 up to 54 Mbps. In June 2003, the other standard that uses OFDM as physical layer, IEEE 802.11 *g* was released.

Another transmission system where OFDM is used is PLC (Power Line Communications) also referred to as power line carrier or power line networking (PLN), which describes several

different systems using elecric power lines to carry information. Moreover, the OFDM technique is also considered for further development of current mobile radio systems like 3GPP LTE (Long Term Evolution), or as more commonly called Super3G, to improve UMTS.

This chapter introduces the multicarrier system and provides an overview of an OFDM system according to the IEEE 802.11 *a*/*g* standard.

3.2 Multicarrier sytems

To fulfill the requirements of current applications for high data rates, either higher modulations should be applied or a larger system bandwidth should be used. Disadvantages of higher modulations include a greater noise sensitivity and the limitation of the maximal transmission power. The use of a higher system bandwidth results in shorter symbol durations through the time-bandwidth product [OhmLueke04] and thus, more complex equalisers would be required to counteract the ISI.

In the case of a maximal delay spread, $\tau_{\max}$, every symbol with duration T_s, will be influenced by the previously transmitted N_{ISI} symbols:

$$\mathrm{N_{ISI}} \approx \frac{\tau_{\max}}{T_S} \tag{3.1}$$

Thus, the basic idea of multicarrier transmissions consists of partitioning one data stream into N parallel data streams that are simultaneously transmitted in parallel frequency bands, without altering the overall used bandwidth. Due to the parallelisation, the symbol duration can be multiplied by N in each channel, maintainig the same bandwidth efficiency. With the new symbol duration, $T_s = N \cdot T_s$, the number of symbols influenced by ISI is N times smaller.

Fig. 3.1 shows the transmitter block diagram of a multicarrier system. The source data stream is first separated into N parallel data streams. Thereafter, according to the modulation step, ld(M) bits are mapped to one of the M-corresponding datasymbols. Before the superposition takes place, each signal is multiplied by the complex carrier $e^{j2\pi f_n t}$, where f_n is the midfrequency of the used frequency band.

The final signal at the transmitter is as follows:

$$s(t) = T_S \sum_{n=0}^{N-1} d_n(i) \cdot h_S(t - iT_S) \cdot e^{j2\pi f_n t} \quad \text{for} \quad iT_S \le t < (i+1)T_S \tag{3.2}$$

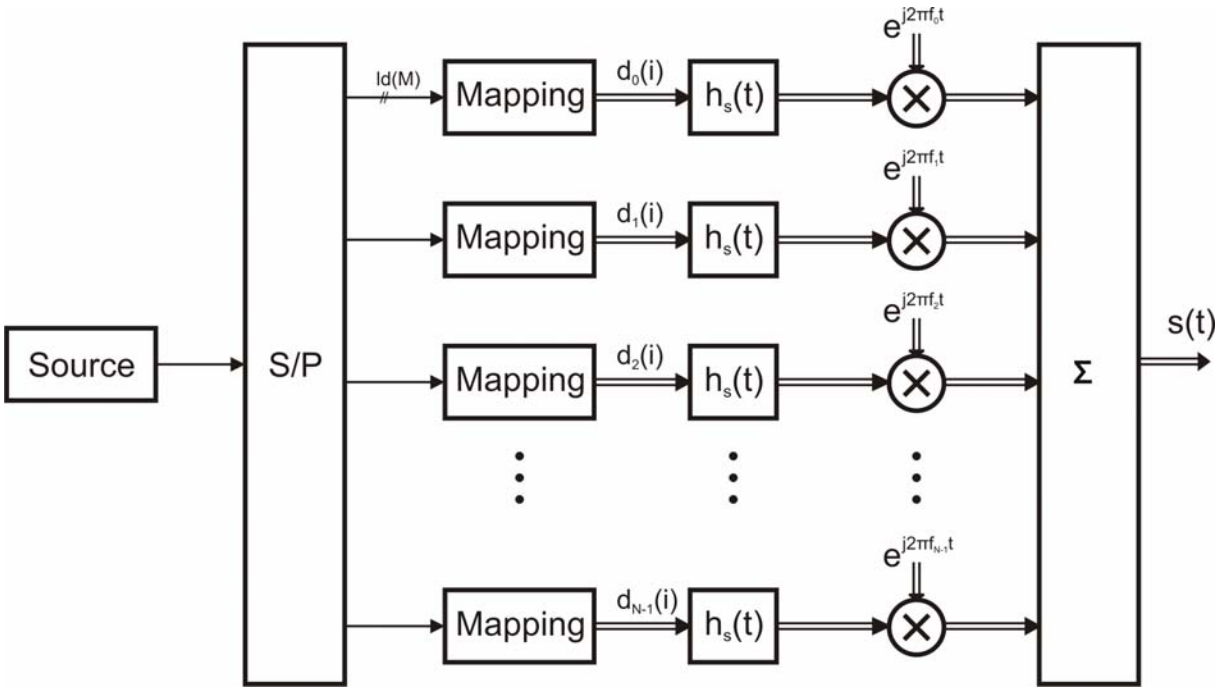

Fig. 3.1: Transmit block diagram of a multicarrier system

For a good function of the overlapping multicarrier modulation technique, a crosstalk between subcarriers must be reduced. If the filter $h_s(t)$ is not adequatly selected, ICI can appear between the single carriers and then the subcarrier spectra could not be detected correctly. This situation is represented in Fig. 3.2 b).

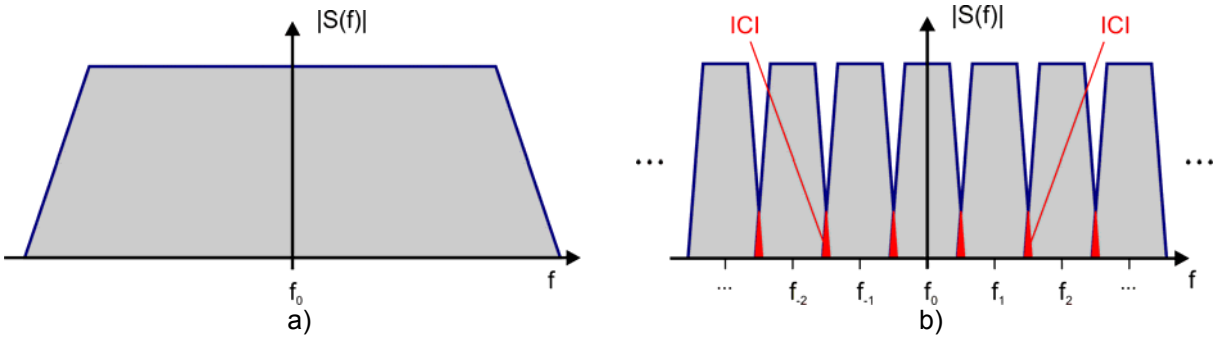

Fig. 3.2: Spectra: a) of a single carrier system b) of a multicarrier system

Hence, the orthogonal multicarrier techniques like OFDM are very interesting for transmission sytems. The reason is that with a correct filter dimensioning between a transmitter and a receiver the ICI will completely disappear.

3.3 OFDM Principle

The property of orthogonality indicates a precise mathematical relationship between the system subcarriers. In conventional frequency division multiplex (FDM) systems, a separating filter for each sub-channel is required to introduce guard bands in the frequency domain that reduce the spectra efficiency.

To conform to the orthogonal condition, the symbol duration must accomplish:

$$T_S = \frac{1}{f_S} \tag{3.3}$$

where f_S denotes the subcarriers spacing and T_s the symbol duration.

The impulse response of the transmitter filter in Fig. 3.1 is a rectangular function of duration T_S:

$$h_s(t) = \begin{cases} \frac{1}{T_S} & \text{for} \quad 0 \le t < T_S \\ 0 & \text{for} \quad \text{sonst} \end{cases} \tag{3.4}$$

If the definition of the transmitter filter in (3.4) is inserted in (3.2):

$$s(t) = \sum_{n=0}^{N-1} d_n(i) \cdot e^{j2\pi f_n t} \tag{3.5}$$

The rectangular functions of the single transmitter filters correspond to a si-shaped spectrum in frequency domain. The OFDM signal multiplexes the individual spectra with frequency spacing equal to the transmission speed of each subcarrier, f_S, as shown in Fig. 3.3. It also depicts that at the center frequency of each subcarrier the other channels present a zero because of (3.3). Therefore, the transmitted data are recovered at the receiver with no crosstalk. Moreover, using the FFT-based multicarrier technique, frequency-division multiplex is achieved not by bandpass filtering but by baseband processing.

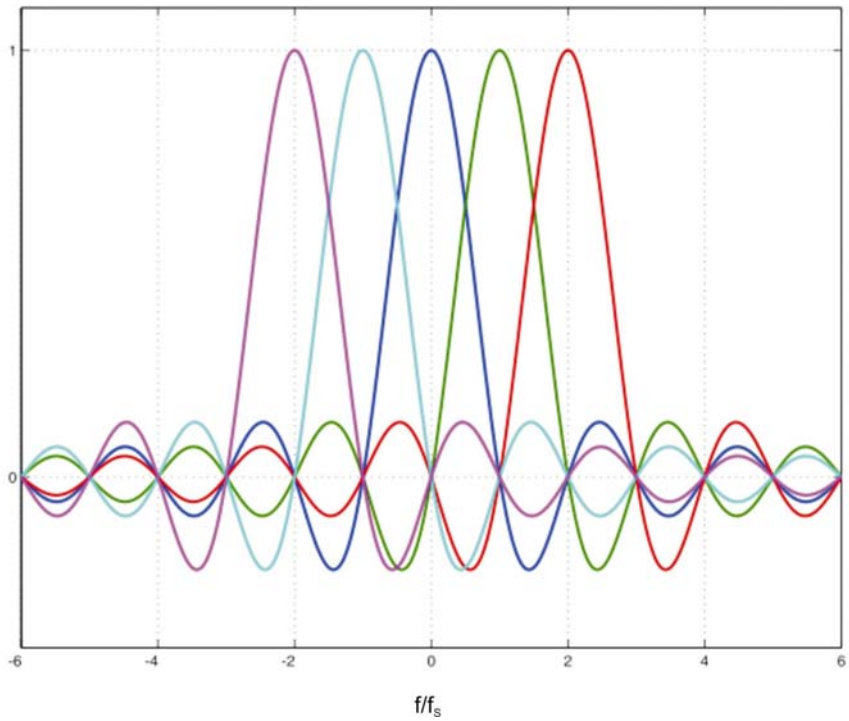

Fig. 3.3: Spectra of several subcarriers in an OFDM- system

In order to obtain a maximal signal to noise ratio (SNR) for the transmission, the transmitter and the receiver filters are designed as matched-filters:

$$h_R(t) = h_S(t) \tag{3.6}$$

where $h_R(t)$ is the filter at the receiver.

3.3.1 Guard interval

The delay spread, which also generates intersymbol interference (see Chapter 2) appears for the transmission through radio channels. Fig. 3.4 shows the ISI and ICI effects over three OFDM symbols.

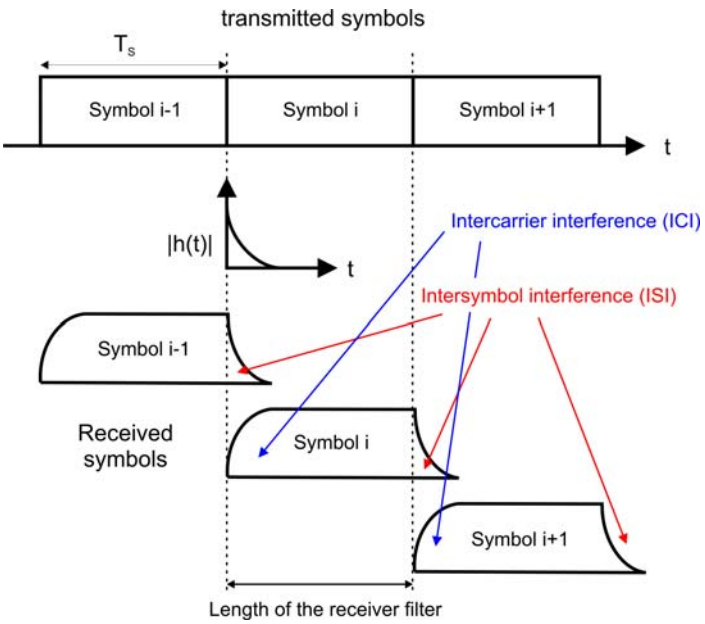

Fig. 3.4: Influence of the multipath propagation on the OFDM-transmission

It is possible to suppress both ISI and ICI using a guard interval. The cyclic prefix, which is transmitted during the guard interval, is the end of the OFDM symbol. This copy into the guard interval is transmitted followed by the OFDM symbol. Fig. 3.5 represents how the guard interval can help against the echos.

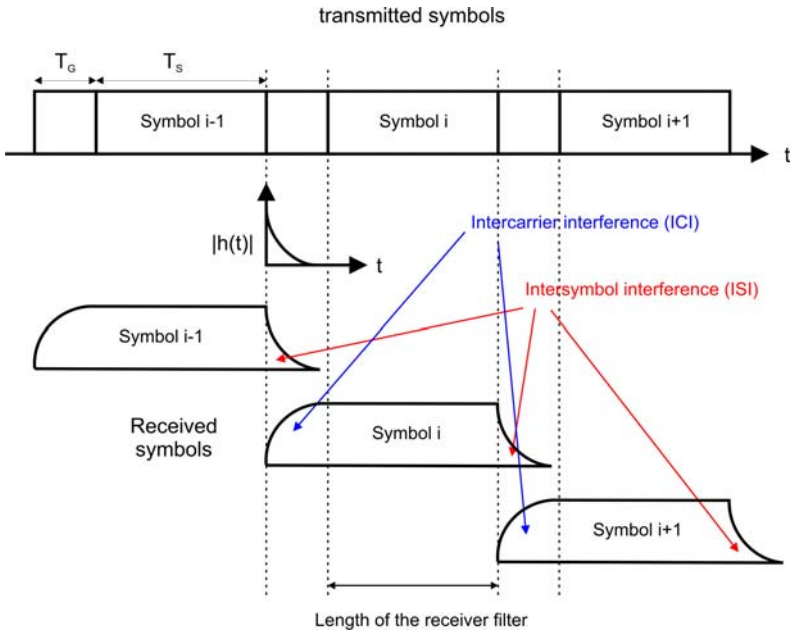

Fig. 3.5: OFDM transmission with guard interval by multipath propagation

By demodulating with the FFT at the receiver, it will be integrated over an integer number of sinusoid cycles for each of the multipaths. The guard interval will contain crosstalk of the previous transmitted OFDM symbols. The received data in this time will be discarded, so that the FFT-window will be applied to the rest of the data. If the guard interval is larger than the delay spread, the transmission will be ISI free. Hence, follows that:

$$T_G \geq \tau_{max} \tag{3.7}$$

Since after τ_{max} all the past values dissapear from the channel memory, ISI can be avoided by using the cyclic extension during the guard interval. At the receiver, an accurate continued and periodic signal is always available even in the case of the delayed version of the OFDM symbols.

That implies that for OFDM transmission, correctly dimensioning the guard interval allows for interference free transmissions for ISI and ICI through multipath channels.

The application of a guard interval requires an extension of the transmitter filter by a time span of T_G, leading to a loss of SNR. If N_{FFT} and N_g are the samples corresponding to the OFDM symbol and guard interval respectively, the SNR loss at the receiver input can be determined by:

$$\gamma_G^2(\text{dB}) = 10 \cdot \log\left(\frac{T_S}{T_S + T_G}\right) = 10 \cdot \log\left(\frac{N_{FFT} \cdot T_{sample}}{(N_{FFT} + N_G) \cdot T_{sample}}\right) = 10 \cdot \log\left(\frac{N_{FFT}}{(N_{FFT} + N_G)}\right) \tag{3.8}$$

For an OFDM-system with a guard interval duration of T_G=1/4·T_S, an SNR loss of 0.97 dB is generated.

3.3.2 Benefits and drawbacks of the OFDM Technique

The OFDM transmission scheme has the following key advantages:

- OFDM is an efficient way to deal with the multipath through the guard interval, as seen in Section 3.3.1. For a given delay spread, the implementation complexity is significantly lower than that of a single carrier system with an equalizer. The delay spread due to a multipath propagation is generally less than 50 ns in households, 100 ns in offices and 300 ns in industrial environments [VanPr00].

- OFDM is robust against narrowband interference, because such interference affects only a small percentage of the subcarriers. Error control systems can be utilized to correct them.

- With link adaptation techniques, the transmission can be adapted to the channel conditions individually for each sub-carrier. Therefore, it is possible to significantly enhance the capacity in relatively slow time-varying channels

However, OFDM also has some drawbacks compared to single carrier modulation:

- OFDM is more sensitive to frequency offset and phase noise by demodulating. In such cases an ICI-free decoding can not be guaranteed.

- OFDM has a relatively large peak-to-average power ratio (PAPR), which tends to reduce the power efficiency of the RF (radio frequency) amplifier.

In OFDM system design, a number of parameters are up for considerations, such as the number of subcarriers, guard time, symbol duration, subcarrier spacing, modulation type per subcarrier and the type of forward error correction (FEC) coding. The choice of parameters is influenced by system requirements such as available bandwidth, required bit rate, tolerable delay spread and Doppler values. Some requirements are conflicting and must be appropriate to each application and transmission system. In the next section, the selected parameters for the wireless systems based on the IEEE 802.11 standards will be presented.

3.4 WLAN according to the standard IEEE 802.11

Wireless Local Area Network is a wireless network with a maximal distance of approximately 100 meters between the nodes. A number of standards for the wireless transmission were specified. In Table 3.1 the released IEEE standards are listed.

In June 1997, the IEEE approved an international interoperability standard [IEEE97]. The standard specifies both medium access control (MAC) procedures and three different physical layers (PHY). In Europe there are a total of 19 licence free frequency channels in the 5 GHz-band, which can be used by an IEEE 802.11 *a* system. For the *g* alternative there are 13 channels in the 2.4 GHz band, which can be employed without license. Only four of them are not overlapped.

For both, 11*a* and 11*g* standards were defined as a physical layer with OFDM. Moreover, the *g* alternative is compatible with the *a* standard and both work at the 2.4 GHz band. A preamble assures that *b* and *g* stations could interchange data.

Table 3.1: Overview of several important WLAN-Standards

Standard	Description	Release year
IEEE 802.11	Basic standard Layer 2: LLC, MAC Layer 1: DSSS, FHSS, IR	1997
IEEE 802.11 *a*	Layer 1: OFDM at 5GHZ band	1999
IEEE 802.11 *b*	Layer 1: DSSS	1999
IEEE 802.11 *g*	Layer 1: OFDM, CCK, PBCC	2003
IEEE 802.11 *e*	Better QoS in MAC layer	2005

In March 2007, the current standard IEEE 802.11-2007 was approved. It contains cumulative changes from multiple sub-letter task groups as a single document that merged 8 amendments (802.11 *a*, *b*, *d*, *e*, *g*, *h*, *i*, *j*) with the base standard IEEE 802.11.

The following list contains the IEEE 802.11 standards, which have not been released yet. Their scheduled dates of publication are also indicated according to the official timelines [IEEE802.11WG]:

- IEEE 802.11k - Radio resource measurement enhancements (final process approval Sept. 2008, ANSI approval N.A.)
- IEEE 802.11n - Higher throughput improvements using MIMO (multiple input, multiple output antennas) (Nov. 2009)
- IEEE 802.11p - WAVE - Wireless Access for the Vehicular Environment (such as ambulances and passenger cars) (Dec. 2009)
- IEEE 802.11r - Fast roaming. (final process approval Sept. 2008, ANSI approval N.A).
- IEEE 802.11s - ESS Extended Service Set Mesh Networking (Dec. 2009)
- IEEE 802.11.2 - Wireless Performance Prediction (WPP) - test methods and metrics Recommendation (Dec. 2009)
- IEEE 802.11u - Interworking with external networks, for example, cellular (March 2010)
- IEEE 802.11v - Wireless network management (Dec. 2009)
- IEEE 802.11w - Protected Management Frames (Sept. 2009)
- IEEE 802.11y - 3650-3700 MHz Operation in the U.S. (final process approval Sept. 2008, ANSI approval N.A)
- IEEE 802.11z - Extensions to Direct Link Setup (DLS) (Sept. 2009)

3.4.1 IEEE 802.11 WLAN Parameters

Table 3.2 lists the main parameters of the OFDM standard used for WLAN. A key parameter that determines the choice of other paramenters is the guard interval of 800 ns. To limit the SNR loss at the receiver to approximately 1 dB (3.8), the chosen symbol duration is 4 μs (T_s=3.2 μs). This also determines the subcarriers spacing f_s = 1/ T_s = 312.5 kHz. By using 48 subcarriers with variable modulation and coding rates to correct subcarriers in deep fades, data rates from 6 up to 54 Mbps can be achieved. In addition to the 48 subcarriers, four pilot subcarriers track the residual carrier frequency offset that remains after initial frequency correction during the training phase of the packet. The outer 12 subcarriers in the 20 MHz WLAN channel (N = 64) are zeroed in order to reduce adjacent channel interference.

Table 3.2: Main OFDM parameters for WLAN

Data rate	6, 9 ,12, 18, 24, 36, 48, 54 Mbps
Modulation	BPSK, QPSK, 16-QAM, 64-QAM
Coding rate	1/2, 2/3, 3/4
Number of subcarriers	52 (48 for data)
Number of pilots	4
OFDM symbol duration	4 μs
Guard interval	800 ns
Subcarrier spacing	312.5 kHz
-3 dB Bandwidth	16.56 MHz
Channel spacing	20 MHz

3.4.2 IEEE 802.11 WLAN channelization

The frequency ranges allowed in Europe are listed in Table 3.3 as well as the power restrictions to devices, which use this band for communications.

Table 3.3: OFDM PHY frequency ranges for Europe in 2.4 GHz and 5 GHz bands

Regulatory range	**Maximum output power**	
2.400-2.4835 GHz	100 mW (EIRP*)	
5.15-5.25 GHz	50 mW	4 dBm +10 $\log_{10}$ B **
5.25-5.35 GHz	250 mW	11 dBm +10 $\log_{10}$ B
5.47-5.725 GHz	1000 mW	17 dBm +10 $\log_{10}$ B

*EIRP =effective isotropic radiated power
** B is the -26 dB emission bandwidth in MHz

Fig. 3.6 and Fig. 3.7 show the channelization for the 2.4 GHz and the lower and middle 5 GHz bands. One can see how the 13 channels in the ISM 2.4 GHz overlap with a space of 5

MHz. The overall 5 GHz band has 19 channels available in Europe. A total of 455 MHz is divided in three bands. In the 5.15-5.35 GHz bands the center frequencies are separated by 20 MHz. Eight channels are available in these two bands with guard spacings of 30 MHz at the band edges. The third band from 5.470 to 5.725 GHz has a guard spacing from the band edges of just 20 MHz.

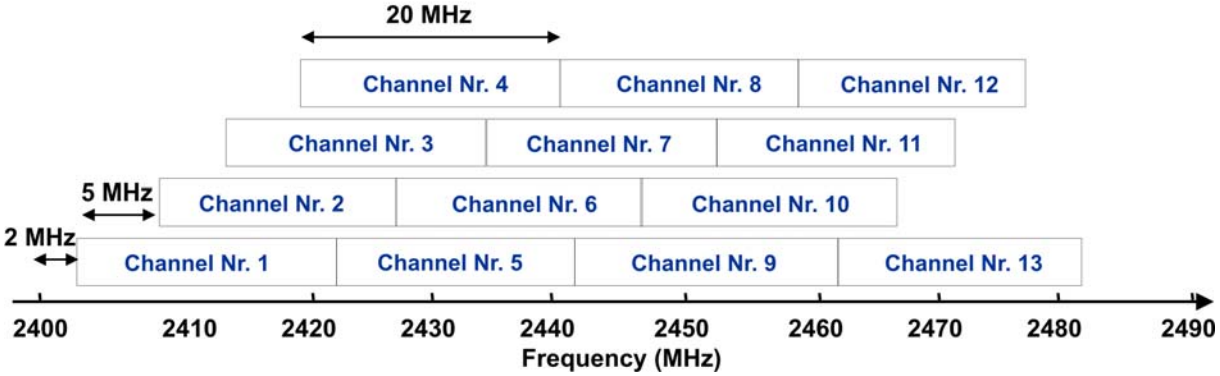

Fig. 3.6: OFDM PHY frequency channel plan for Europe in 2.4-2.4835 GHz band.

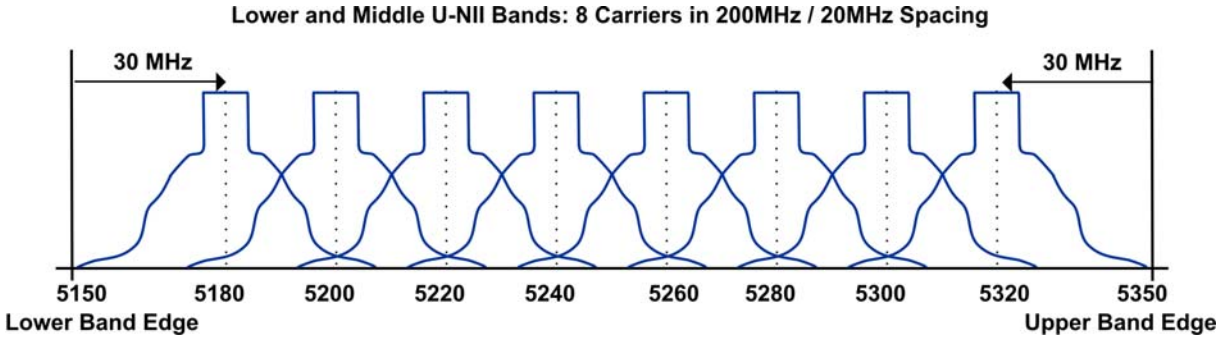

Fig. 3.7: OFDM PHY frequency channel plan for Europe in 5.15-5.35 GHz band

3.4.3 IEEE 802.11 *g* OFDM frame

An OFDM frame is composed of several OFDM symbols, which are preceded with a short and a long preamble as well as the signal field. The long preamble is used among other things for the channel estimation that is applied to the equalization of all OFDM symbols in a frame. In Fig. 3.8 the OFDM frame formats in the physical sublayers PLCP (physical layer convergence procedure) and PMD (physical medium dependent) can be seen for the IEEE802.11 *g* standard, as an example.

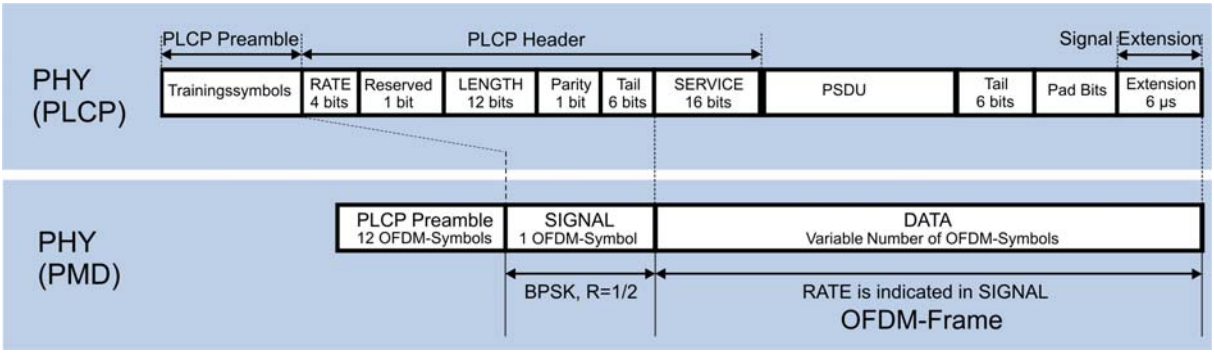

Fig. 3.8: PPDU frame format according to IEEE 802.11*g* standard

PLCP provides a convergence procedure in which PSDUs (PLCP service data unit) are converted to and from PPDUs (PLCP protocol data unit) by means of a PLCP preamble and header. The PPDU includes the OFDM PLCP preamble, OFDM PLCP header, PSDU, tail bits, and pad bits. The PLCP header contains RATE, LENGTH, a reserved bit, an even parity bit, and the SERVICE fields. In terms of modulation, the LENGTH, RATE, reserved bit, and parity bit (with 6 “zero” tail bits appended) constitute a separate single OFDM symbol, denoted SIGNAL, which is transmitted with the most robust combination of BPSK modulation and a coding rate of R = 1/2. The SERVICE field of the PLCP header and the PSDU (with 6 “zero” tail bits and pad bits appended), denoted as DATA. For ERP-OFDM (extended rate PHY) modes, an ERP packet is followed by a period of no transmission with a length of 6 µs referred to as OFDM signal extension. This extra length extension is used to ensure that the transmitter computes the duration field incorporating this “idle time” in order to ensure the inter-frame spacing (IFS) time.

These data are scrambled, coded with a convolutional encoder, optionally punctured and mapped into complex symbols of the corresponding modulation (BPSK or QAM). Afterwards, the pilots are inserted and the transformation from frequency to time and the addition of a circular prefix is carried out. Finally, the OFDM symbols are concatenated into a single time-domain signal. This transmission procedure is represented as block diagram in Fig. 3.9.

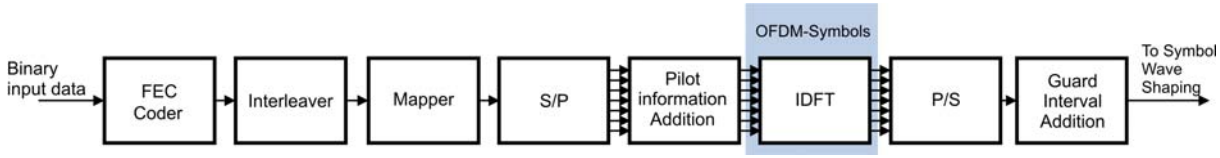

Fig. 3.9: Transmit block diagram according to IEEE 802.11 *g* standard

3.5 Optimizations for WLAN In-house transmissions

The strong market penetration of IEEE 802.11 and also low prices of the transceiver chipsets make it a good candidate for further applications in the user’s household. In an environment with high node density, the AV home network requirements can be only met by exploiting the limited physical channel very efficiently. This kind of intelligence can be introduced by compatible extensions of WLAN standards, designing all nodes as friendly and cooperative members in a global transmission environment.

Since these networks pose many complex issues, there are many questions for research and opportunities for making significant contributions. At the moment the transmission of multimedia data over IEEE 802.11 links is not as reliable as required for a broad consumer market. Of course both, the standards as well as the equipment, are continuously refined. However, from the technical point of view, limitations still exist with respect to the medium access (MAC) protocol and data transmission capabilities because of limitations of the physical layer (PHY). The methods for link efficiency enhancement in the PHY layer can be divided into link adaptation and static modifications of OFDM parameters.

Link adaptation is the dynamic optimization of the transmission parameters according to the current transmission conditions of the link. Different concepts of link adaptation have been analyzed (see overview in [KeHan00], for example).

Simulations have shown significant room for improvement when applying IEEE 802.11 *a*/*g* to home media networks. The results clearly show that the performance of such WLAN systems can be significantly enhanced. To further improve the transmission, the following factors can be optimized:

- MAC parameters
- Transmitter power
- Selection of the transmission mode
- Transmitted packet length
- Transmission frequency

Overall performance in typical scenarios can be increased significantly when all improvement options mentioned above are combined. For efficiency and feasibility reasons, these methods should be combined in a cross-layer concept designed for self-organizing networks.

Furthermore, in contrast to other scenarios, the delay spread in typical home environments is very short. The guard interval defined in current OFDM WLAN standards (800 ns) is oversized for such a scenario. By reducing the guard interval to an appropriate value of 200 ns, the capacity can be improved by 18% (0.7 dB).

In many cases data rate fluctuations of an individual link as well as link breakdowns might occur. These effects are very often originated from the transmission channel properties. Thus, knowledge about the channel characteristics in the house is necessary for the development of data transmission enhancements. For an acquisition of these characteristics a large amount of transmission channel measurements have been performed. The results of these investigations are presented in detail in the next sections.

4 WLAN In-House Channel Measurements and Evaluations

The wireless channel has numerous limitations with regard to the performance of wireless systems in comparison to the cable. At home, the transmission path can vary from one that is not blocked by people and objects to another that is severely obstructed. In contrast to the wired channels, wireless in-house channels are extremely random. Specific measurements and statistical methods are required to analyse the wireless effects and to model the channel parameters in a specific communication system.

This chapter presents the results of measurements and investigations attempting to enhance home AV-networks based on IEEE 802.11*a*/*g*. To improve data transmission, a detailed and reliable knowledge about the characteristics of the transmission channel is necessary. Therefore, several meaurements have been conducted at the frequency bands of 2.4 and 5 GHz in both LOS and NLOS situations at typical residential environments.

The main goal of these first measurement sets is to estimate fading effects, channel power and spatial correlation, without taking into account other effects such as dynamic changes of the environment or people moving in a room. The design of these static measurements is described in the following section.

4.1 Measurement set-up

The used set-up is depicted in Fig. 4.1. The radio transmitter consists of an OFDM signal generator (AMIQ + SMIQ) emitting a continuous 100 MHz bandwidth signal, which modulates a carrier. Because all physical layers of wireless LAN have to be covered, carrier frequencies of 2.45 GHz and 5.6 GHz are used to allow assessments of such ISM bands. To ensure a good coverage range the test signal is amplified.

At the receiver side the signal is detected using a spectrum analyzer (FSIQ) that is controlled by a PC. Thus, an automatic data acquisition can be carried out. To overcome the problem of strong spatial dependencies of the radio field, the antenna is automatically positioned using a specially designed antenna positioner. With this device the antenna can be placed automatically within an area of 80 cm x 80 cm with a maximum accuracy of 0.025 mm. The superstructural parts of this device are mainly built of non-conductive material to minimize influence on the radio field. With the help of this arrangement parts of a room can be surveyed without any user interaction. An optional control connection also exists between the PC and the transmitter, so that parameters like output power, frequency range, etc. can also be controlled automatically.

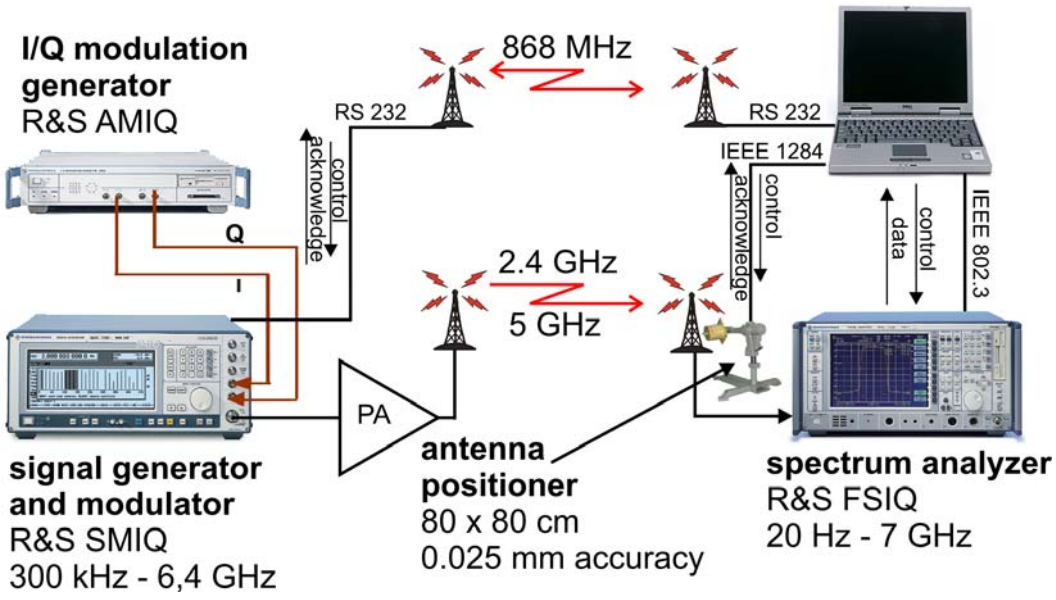

Fig. 4.1: An Measurement set-up for registering the channel characteristics.

The individual components of the measurement set-up are presented in Annex A.

4.2 Measurement campaigns

The environments selected for the static measurements represent two different scenarios in order to compare the results and to determine their statistical significance. The residential buildings are referred to as house A and house B in the following sections.

Several thousand measurements were carried out for each test house, creating an important database. In Table 4.1, the number of registered WLAN channel spectra per house and frequency band is specified. The results of the two houses will be usually presented as splitted in the way of transmission (LOS or NLOS) and frequency ranges, except in some cases, in which it will be explicitly indicated which scenario is dealt with.

Table 4.1: Number of registered channel spectra

	House A	*House B*
2.4 GHz	225000	65000
5 GHz	25000	10000

Both, house A and house B are multifamily residential buildings, with their structures, distributions and construction materials differing from each other.

House A has three stories. The two lower levels are the living space; the highest story is an attic. The separation between the lowest level and the medium level is a concrete ceiling with an open stairway. The walls are made of fibrous plaster. The separation between the living space and the attic is a lightweight construction. Fig. 4.2 gives an overview of the first test

environment.

House B has four levels with a cellar level as an additional story. The ceilings of this building are made of concrete, whereas the walls are made of bricks.

The analysis comprises two typical types of transmission situations. The first one is a LOS transmission. In this case, both stations are in the same room with no obstacles in the direct line between the two antennas. The second scenario is a NLOS transmission. This is the typical situation if two devices are placed in different rooms, so that the radio waves have to travel through doors, walls, ceilings, etc. Fig. 4.2 depicts such a situation with the transmitter on the attic and the receiver somewhere on the floors below. This is the typical allocation for in house distribution of a satellite signal.

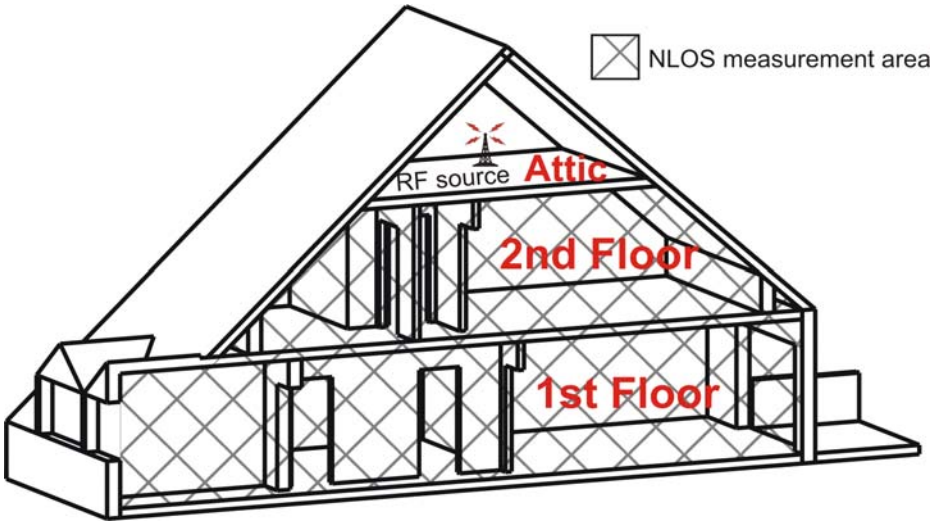

Fig. 4.2: An example of a NLOS-measurement in a three-storey apartment in a multifamily residence.

The floor plans in Fig. 4.3 illustrate individual measuring locations in different rooms. The transmitter, represented as a circle, is situated in the living room with both types of transmissions, LOS and NLOS. The measured area at the receiver is graphed by a square. Fig. 4.3 a) shows an example of a LOS measurement in the living room, whereas the NLOS measurements conducted over the same floor are depicted in Fig. 4.3 b).

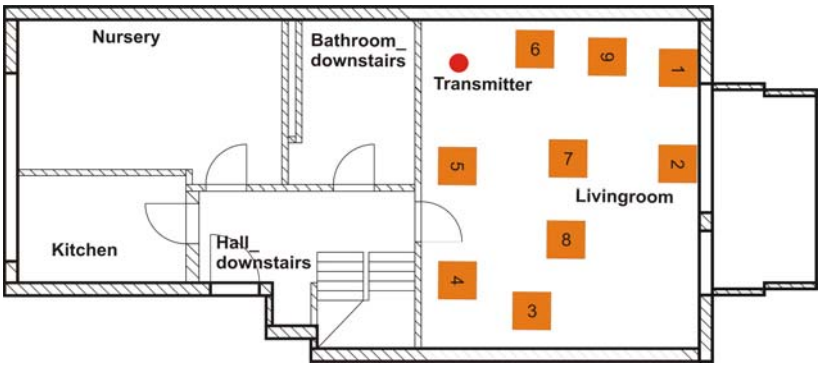

a) An example of a LOS-measurement

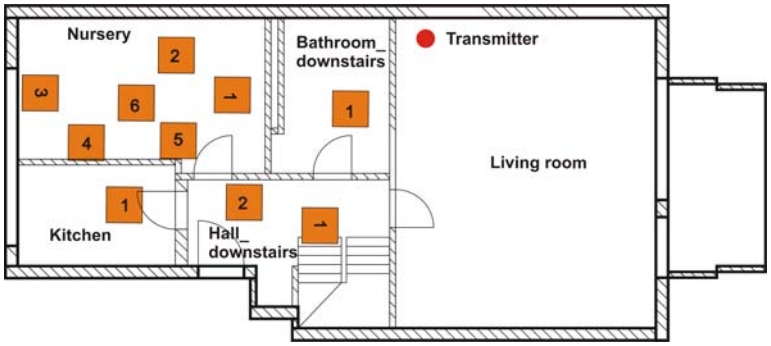

b) An example of a NLOS-measurement

Fig. 4.3

In Fig. 4.4 a) the receiving area is zoomed in. It can be seen in this picture that the measured points are separated by 5 cm. The reason why this distance has been chosen will be discussed in section 4.8.2. The received signal in the whole bandwidth of 100 MHz has been stored at every point of the grid, as plotted in Fig. 4.4 b) as an example for 2.4 GHz band.

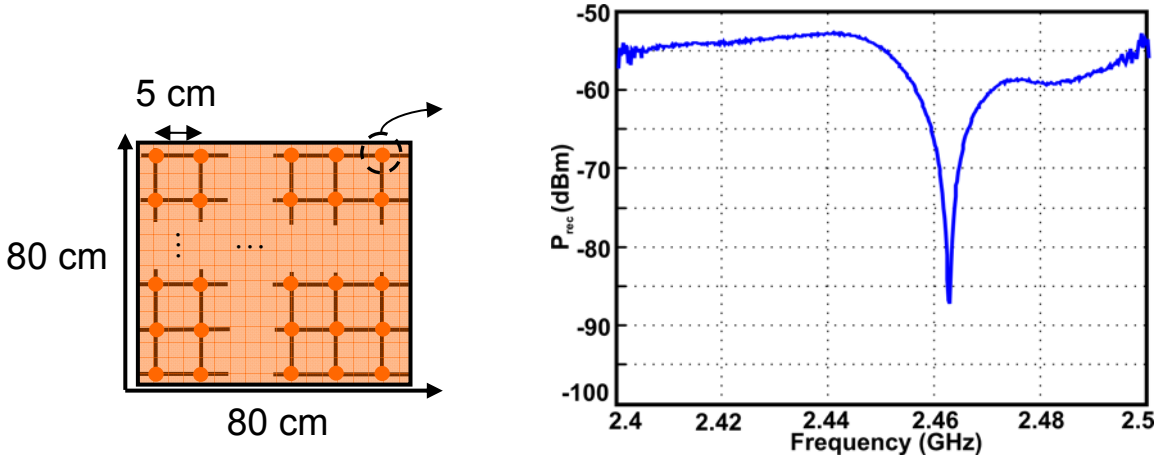

a) b)

Fig. 4.4: a) Measurement grid. b) An example of the measured spectrum in the 2.4 GHz ISM band.

4.3 Channel transfer function

To obtain the channel transfer function without distortion, $H_{channel}$, all of the measurements have been calibrated in order to cancel the effects of the measuring system frequency response, since they could distort the actual behavior of the radio channel.

The layout of the used set-up for the measurements shown in Fig. 4.1 is simplified in the following block diagram, Fig. 4.5:

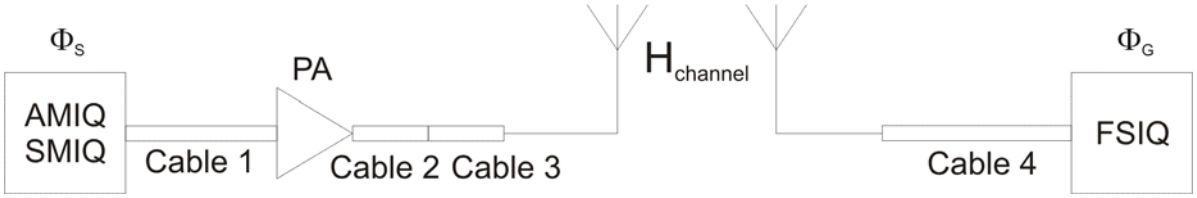

Fig. 4.5: Measurement set-up block diagram.

Each single element of the scheme presents a frequency response that could adulterate the validity of the measured data. An example is the frequency response of the power amplifier (PA) in the two bands 2.4 and 5 GHz, characterized as follows:

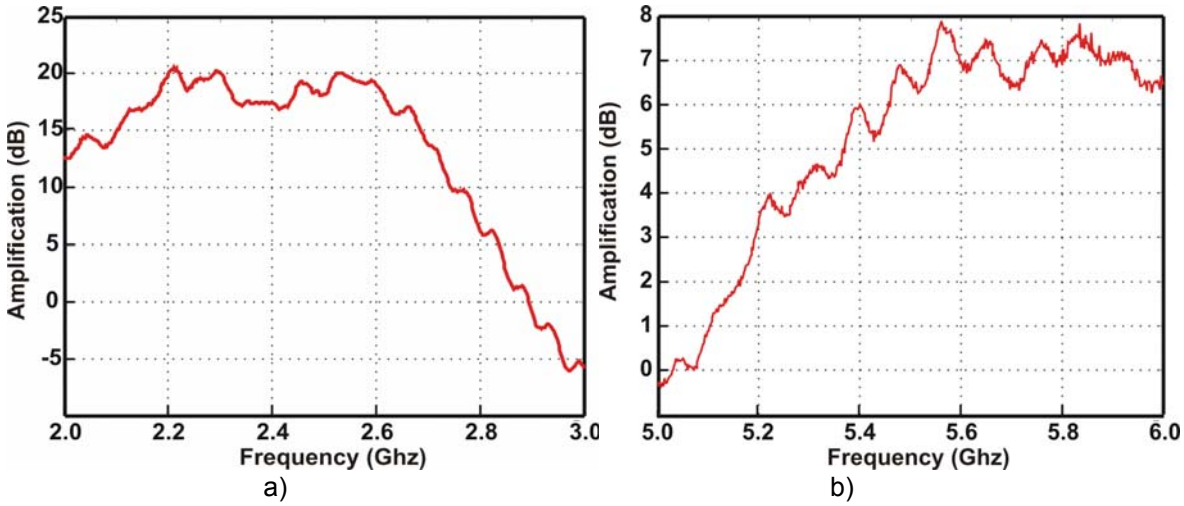

Fig. 4.6: Amplifier frequency response in a) 2-3 GHz band and b) 5-6 GHz band

Fig. 4.6 a) and b) show the amplifier response within 1 GHz range for both bands. These are not flat in any case. In the first one, the upper frequencies from 2.6 to 3 GHz are strongly attenuated. The same happens for the first 400 MHz in the 5 GHz band. The frequency range of interest for the WLAN channel analysis is limited to 100 MHz in each band, from 2.4 to 2.5 GHz and from 5.6 to 5.7 GHz.

The length of different cables is chosen according to the measuring equipment specifications such as saturation parameters or input power restrictions. The following can be derived from the outline in Fig. 4.5:

$$\Phi_G / \Phi_S = |H_{Cable1}|^2 \cdot |H_{PA}|^2 \cdot |H_{Cable2}|^2 \cdot |H_{Cable3}|^2 \cdot |H_{Channel}|^2 \cdot |H_{Cable4}|^2 \qquad (4.1)$$

where Φ is the power spectral density, and H represents the different frequency responses correspondig to the diverse components of the system.

In order to determine the transfer function of the channel, $H_{channel}$, the spectral densities Φ_G, Φ_{G1}, Φ_{G2} and Φ_{G3} are measured as shown in Fig. 4.7, and it is assumed that: $H_{Cable3} \approx 1$. Three arrangements are necessary for the calibration, one for the measurement of each power spectral density.

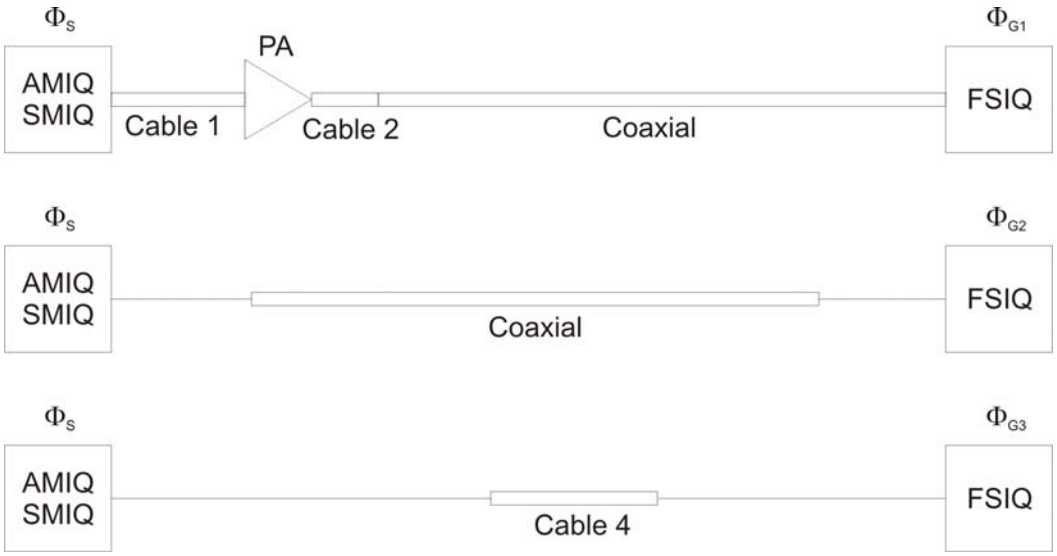

Fig. 4.7: Layouts for the determination of a) Φ_{G1} b) Φ_{G2} and c) Φ_{G3}

Thus:

$$\Phi_{G1} / \Phi_S = H^2_{Cable1} \cdot H^2_{PA} \cdot H^2_{Cable2} \cdot H^2_{Coaxial} \tag{4.2}$$

$$\Phi_{G2} / \Phi_S = H^2_{Coaxial} \tag{4.3}$$

$$\Phi_{G3} / \Phi_S = H^2_{Cable4} \tag{4.4}$$

from (4.1) and (4.2):

$$H^2_{Channel} = \frac{\Phi_G}{\Phi_S} \cdot \frac{H^2_{Coaxial} \cdot \Phi_S}{\Phi_{G1} \cdot H^2_{Cable3} \cdot H^2_{Cable4}} \tag{4.5}$$

from (4.5) and (4.3) follows:

$$H^2_{Channel} = \frac{\Phi_G}{\Phi_S} \cdot \frac{\Phi_{G2}}{\Phi_{G1} \cdot H^2_{Cable3} \cdot H^2_{Cable4}} \tag{4.6}$$

and therefore, from (4.6), (4.4) and $H_{Cable3} \approx 1$ follows:

$$H^2_{Channel} = \frac{\Phi_G \cdot \Phi_{G2}}{\Phi_{G1} \cdot \Phi_{G3}} \tag{4.7}$$

Based on this method, and from the measured data, the actual channel transfer function can be obtained without any additional implication of the measuring set-up.

In a typical transfer function in the 2.4 GHz band, there are several deep fades in the 100 MHz wide band. This performance is known as frequency selective behavior, and this characteristic becomes apparent in the example shown in the Fig. 4.8. However, the wireless channel within typical home environments is characterized by a very short delay spread, due to the size of rooms, and high attenuation due to walls, floors, and furniture. This is why the detour lengths are typically so short that there is at most one deep fade within one 20 MHz channel, the typical bandwidth of OFDM-based WLAN. In general, a fade deteriorates more than one subcarrier depending on the width of the fade.

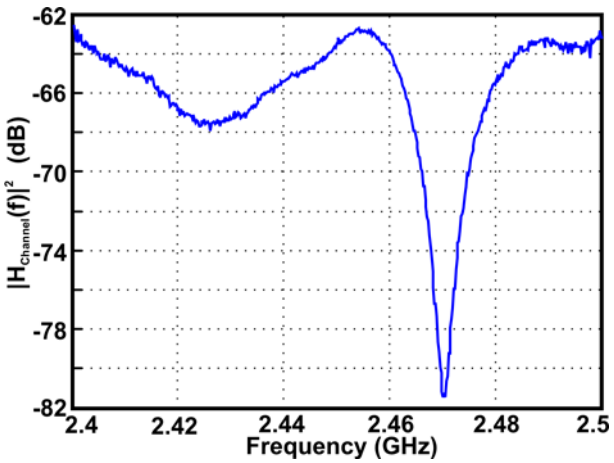

Fig. 4.8: Sample of a transfer function in the 2.4 GHz ISM band in a typical home environment

To continue a thorough analysis of the WLAN channel, the 100 MHz measured and calibrated transfer functions are subdivided into the 20 MHz frequency ranges corresponding to the different channels (see Section 3.4.2 for channelization).

4.4 Channel amplitude distribution

In radio propagation environments the multipath fading is the fluctuation of the signal amplitude caused by the interference of multipath signals from scatters and reflections, as described in Chapter 2. The attenuation of the received signal consists of a fixed component (large scale fading) plus a zero-mean fluctuating component, small scale fading, as has been shown in Fig. 2.2.

Since small scale fading has an irregular appearance, its statistical properties have been used to anticipate system performance. The most common statistical models for in-house fading channels were presented in Section 2.5.1. To verify these models, the amplitude distribution of the transfer functions obtained from the empirical measurements has been analyzed.

First, to distinguish between small scale fading and large scale fading, the linear amplitude of the received and calibrated channel spectra, $10 \log_{10}|H(f)|^2$, is averaged in frequency in each measuring position:

$$A_{mesasuring\ position}(f) = \text{mean}\ (|H(f)|) \tag{4.8}$$

The normalized transfer function $\overline{|H(f)|} = \frac{|H(f)|}{A_{measuring\ position}(f)}$ supplies small scale fading alone.

Fig. 4.9 represents the preprocessing steps that were followed to obtain the small scale fading *r*.

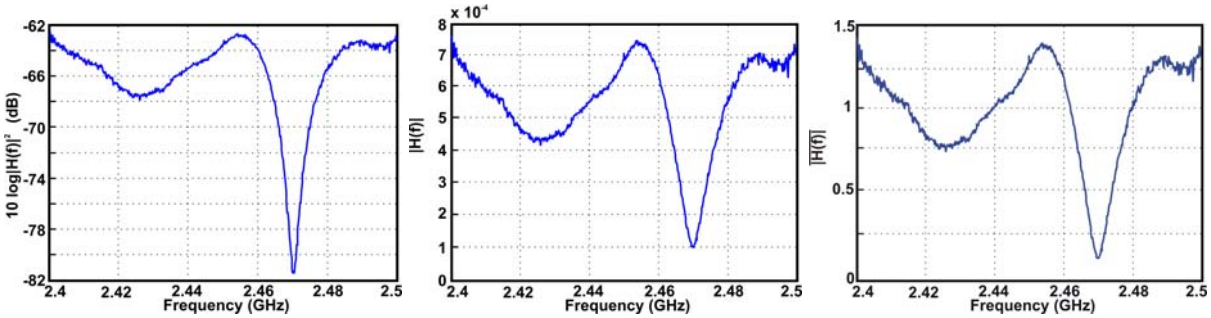

a) b) c)

Fig. 4.9: Prepocessing steps to obtain the small scale fading: a) Calibrated spectrum b) Linear amplitude and c) Small scale fading

The random variable *r* is the set of channel amplitude variations due to small scale fading independent from the frequency:

$$[r] = \overline{|H(f)|}\Big|_f \text{ evaluated for } f = 2.4\text{: } 0.0002\text{: } 2.5 \text{ GHz} \tag{4.9}$$

In the following, the spectral data of LOS and NLOS scenarios are treated separately for the multipath analysis.

4.4.1 LOS Spectra

Using many values of the random variable *r*, a probability distribution function can be obtained. In Fig. 4.10 the more than 200000 measured channel amplitude variations in house A are depicted as a distribution function.

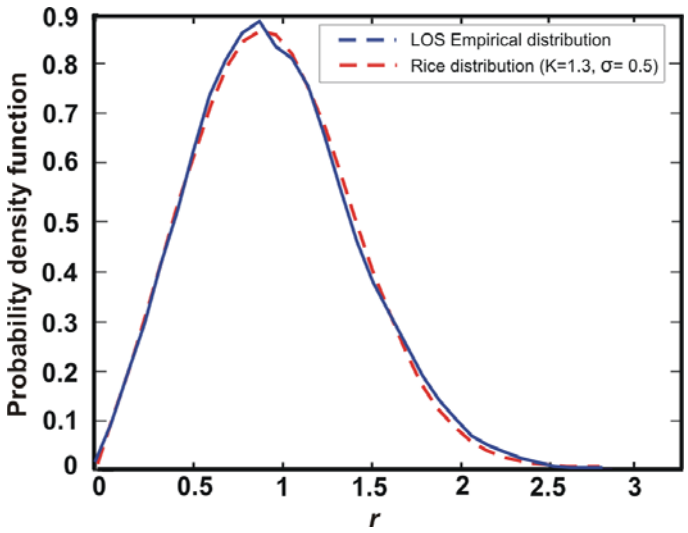

Fig. 4.10: LOS, House A: empirical and theoretical distribution of *r*.

From Section 2.5.1.3 the Rician distribution is given by:

$$p_R(r) = \frac{r}{\sigma^2} e^{\frac{-(r^2+s^2)}{2\sigma^2}} I_0\left(\frac{r \cdot s}{\sigma^2}\right), \quad r \geq 0 \tag{4.10}$$

The relative amplitude of the dominant signal is often measured by means of the Rice parameter *K*:

$$K = \frac{s^2}{2\sigma^2} \tag{4.11}$$

There are a number of possibilities to estimate the *K*-factor from the measured data. One approach is to compute the empirical distribution and then compare the result to a set of hypothetical distributions using a suitable goodness of fit, as described in [Parsons92] [GrHa94]. Another one is to compute a maximum-likelihood estimation using an EM (expectation-maximization) algorithm, as suggested in [MaNiWa95]. Finally, a traditional used method calculates the first and second moments of the received signal and from them the *K*-factor resolving the equation (4.12), as described in [TaLa91]. A similar method using the statistical moments is used in [GrMiEr99] to characterize a narrowband wireless channel. Two of these methods have been applied to obtain the *K*- factor of the presented measurements.

The first method attempts to fit the empirical distribution. To determine which distribution is the best approximation to describe the amplitude fading variation, the MSE (minimum square error) test was employed between experimental and theoretical distribution, Ricean for LOS. The parameters involved in the theoretical distribution functions, *K*-Rice factor and σ, have been varied. The smallest MSE indicates the best distribution function, yielding *K*=1.3 the best parameter to fit the curve to the experimental data (MSE=0.016). The theoretical Rice distribution for this type of transmission is also plotted in Fig. 4.10.

K values from 0.33 (= -4.815 dB) (approximately Rayleigh distribution) to 3.5515 (= 5.5 dB) have been obtained depending on the receiver position in the LOS situations, e.g. Fig. 4.3a).

In the second test, the *K* factor is extracted from the received power by using the well-known method of moments [TaLa91] and is given by the following expression:

$$\frac{E[r]}{\sqrt{E[r^2]}} = \frac{\Gamma(3/2)}{\sqrt{1+K}} \exp\left(\frac{K}{2}\right) \cdot \left[(1+K) \cdot I_0\left(\frac{K}{2}\right) + K \cdot I_1\left(\frac{K}{2}\right)\right] \tag{4.12}$$

where $E[r^2] = \frac{s^2 + 2\sigma^2}{2}$ is the local mean received power. Fig. 4.11 shows equation (4.12) graphically.

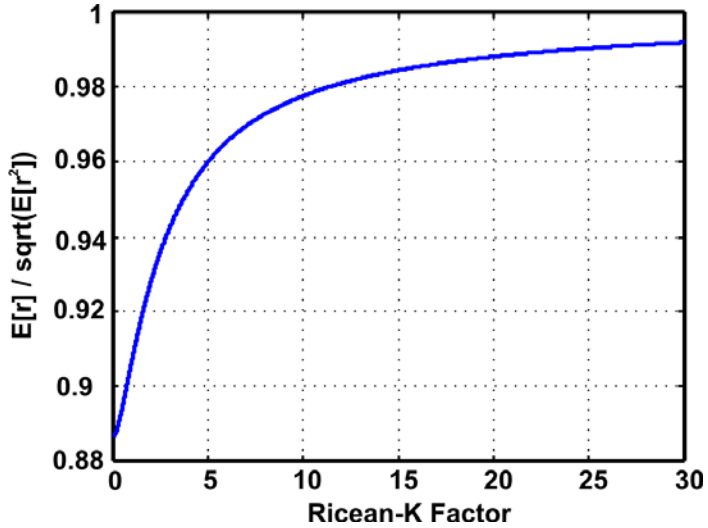

Fig. 4.11 *K*-factor calculation method using statistical moments [GaCr97]

Based on all of the measurements in house A, it has been obtained in average:

$$\frac{E[r]}{\sqrt{E[r^2]}} = \frac{1}{1.2885} = 0.9127 \tag{4.13}$$

and consequently, from Fig. 4.11 can be read: K=1.2625.

Both methods yield almost the same value. This result agrees with the ones found in the literature for indoor measurements [WyZe00]. For example, the *K*-values measured in a laboratory environment [JaStPr95] evaluated in [JanSen96] are presented in Fig. 4.12. Based on the 2.4 GHz LOS (a) curves, it can be seen that in 50% of the cases $K \leq 3$ dB that is in the same range of the in-house measuremets.

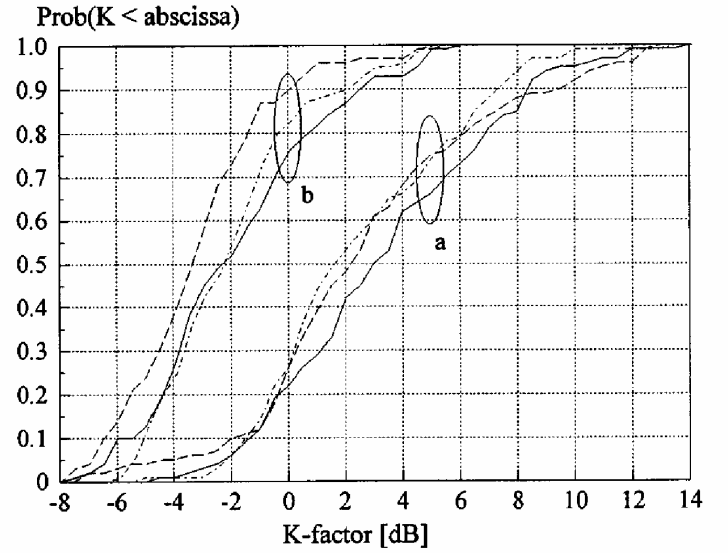

Fig. 4.12: CDF of the Rice-factor K for (a) LOS, (b) NLOS indoor channels and for: 2.4 GHz (-), 4.75 GHz (----) and 11.5 GHz (-·-·-·-) [JanSen96]

Therefore, it has been verified that the Rician fading is an adequate model for LOS communication links.

4.4.2 NLOS Spectra

The measurements corresponding to a NLOS situation are now evaluated. The results of the amplitude distribution are plotted in Fig. 4.13 for house A and B. The empirical values are in the continuous curves and the dotted ones represent the theoretical distribution, in this case Rayleigh one:

$$p_R(r) = \frac{2r}{\rho} e^{\frac{-r^2}{\rho}}, \quad r \geq 0 \tag{4.14}$$

The peak of the distribution occurs at $r = \rho$, and the mean value of r is:

$$\text{mean}(r) = < r > = \rho\sqrt{\frac{\pi}{2}} \tag{4.15}$$

Because of the normalization to obtain the small scale fading, $< r > = 1$, and so that, $\rho = 0.8$. Substituting this value of ρ into (4.14), it is seen that the Rayleigh distribution for the normalized received signal in a channel is completely determined. It can be observed that in both environments, house A and B, the theoretical curve adjusts perfectly and the channel spread is almost the same because of the similarity of reflection coefficients of the construction materials [Bertoni00]. As described in Section 4.2, house B contains brick walls whereas walls of house A are made of plaster.

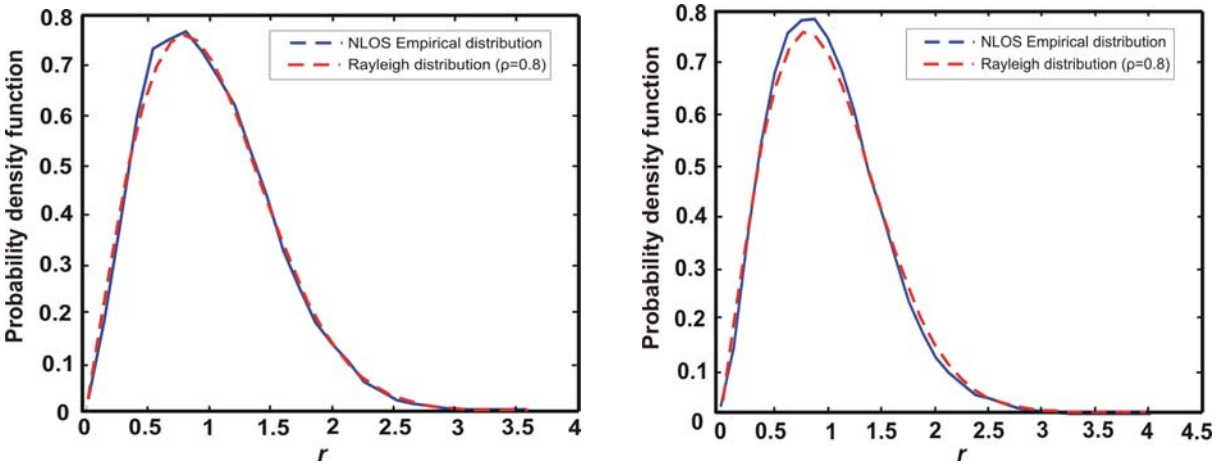

a) b)

Fig. 4.13: a) NLOS, House A: empirical and theoretical distribution of channel amplitudes. b) NLOS, House B: empirical and theoretical distribution of *r*.

4.5 Coherence Bandwidth

In Fig. 2.8 it was pointed out that the multipath delay spread can lead to frequency selective fading. Since the measurements in frequency domain provide such channel information, the coherence bandwidth can be used to characterize the frequency dependency.

The coherence of the 20 MHz WLAN channel is obtained by calculating the autocorrelation function of each channel transfer function measured in frequency domain (2.4 and 5 GHz). The coherence bandwith is defined as in (2.22), where φ_{HH} decreases by 3 dB:

$$\varphi_{HH}(\Delta f) = \sum_{n=1}^{500} H(f) \cdot H(f + \Delta f)\, df \qquad \Delta f = -80....80\,\text{MHz} \tag{4.16}$$

For LOS paths, where the direct ray gives the dominant contribution to the signal, the frequency response shows a coherence bandwith of 14 MHz in average in 2.4 GHz. Practically the same range is observed in the 5 GHz band, as shown in Fig. 4.14.

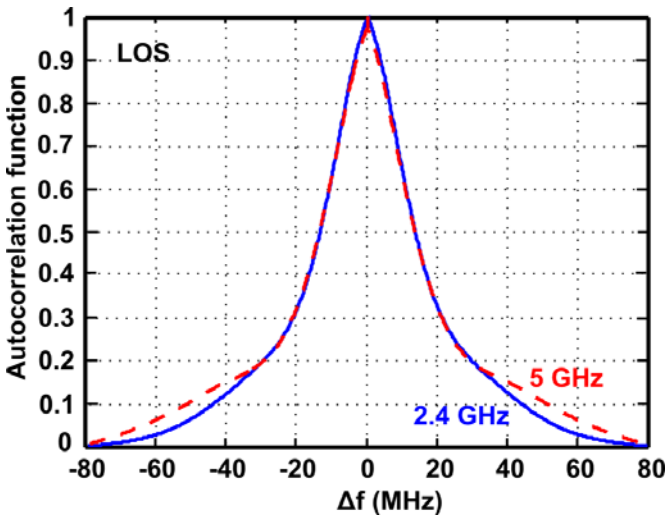

Fig. 4.14: LOS, House A: coherence bandwidth in 2.4 GHz and 5 GHz.

As for NLOS paths, the received signal is expanded in time due to many multipath arrivals with approximately equal amplitudes. The channel transfer function in this case will show rapid variation with frequency and hence, a smaller coherence bandwdith in comparison to the LOS scenario. The channel coherence bandwidth is defined as the reciprocal of the multipath spread, as confirmed in [JaStPr96] and [DoSu97]. Thus, it is expected to obtain a slightly higher coherence bandwidth in the measurements belonging to house A than in the ones from house B. The calculations of B_c by the autocorrelation function confirm it. In 2.4 GHz, house A presents a coherence bandwidth of approximately 13 MHz while house B shows barely 12 MHz.

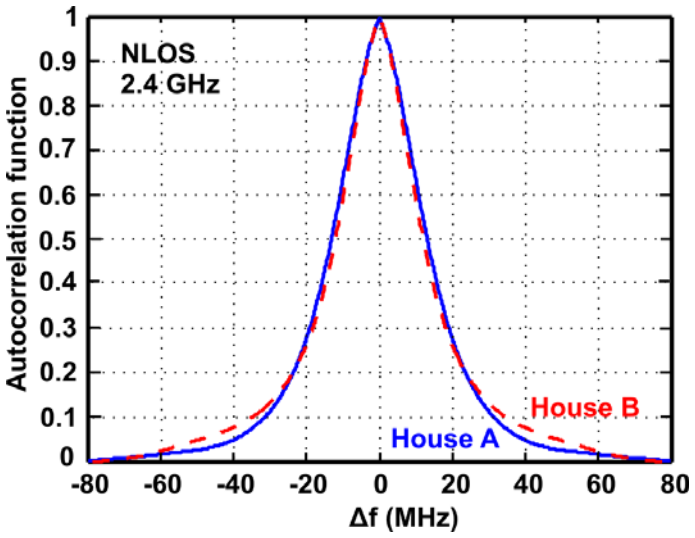

Fig. 4.15: NLOS, House A and B: coherence bandwidth in 2.4 GHz.

Thereby, the WLAN bandwidth and the channel coherence bandwidth have the same order of magnitude for a typical home environment.

An exact relationship between coherence bandwidth and delay spread does not exist, and must be derived from signal analysis (usually using Fourier techniques) of actual signal dispersion measurements in particular channels. Several approximate relationships have been described. A popular approximation of B_c generally accepted, corresponding to a

bandwidth interval having an interval over which the channel frequency transfer function has a correlation of at least 0.5 has been defined in [Rappaport02] [Durgin02]. The relation can be estimated using:

$$B_c \approx \frac{1}{5\sigma_\tau} \tag{4.17}$$

where σ_τ is the delay spread of the channels impulse response. From this identity, the delay spreads can be estimated for the test scenarios [PoonHo03].

Table 4.2: RMS delay spreads in 2.4 GHz.

		σ_τ (ns)
LOS	House A	14.81
NLOS	House A	15.26
	House B	16.26

The delay spread estimation was also computed and analyzed in [PooonHo03], [Papadakis97], [YaSmHe05] where the results of the measurements from 2 to 8 GHz in both LOS and NLOS scenarios, at both office and residential environments present a delay spread range from 10 to 30 ns.

4.6 Received channel power

The WLAN channel power at the receiver is calculated by integrating the received spectrum into the corresponding 20 MHz band:

$$ChP_j = \int_{f_0-10\,\mathrm{MHz}}^{f_0+10\,\mathrm{MHz}} S_j(f)\,df \tag{4.18}$$

where f_0 is the center frequency of any channel and $S_j(f)$ the received signal in this frequency band.

For the measured discrete data:

$$ChP_j = 10 \cdot \log_{10}\left(\sum_{i=1}^{100} \frac{S_j(f_i)*f_A}{\Delta f_{rbw}}\right) \tag{4.19}$$

where $S(f_i)$ are the 100 frequency samples corresponding to a 20 MHz channel, the sampling rate is f_A= 200 KHz, and the resolution bandwidth in the spectrum analyzer is set to Δf_{rbw}= 200 KHz.

The received channel power has been studied in each house, and the results are presented separately to account for the different construction materials and architecture of the houses.

4.6.1 House A

In Fig. 4.16 the cumulative distribution functions (cdf) are plotted for the channel power measured in house A in the 2.4 GHz band. The dashed curve in Fig. 4.16 resumes the LOS scenarios where transmitter and receiver stand in the livingroom. The power range is situated between -65 and -20 dBm and in 50% of the cases it is lower than -30 dBm. Also the NLOS scenarios are depicted. The transmitter was placed at the attic and the receiver anywhere in the 2 stories below, as depicted in Fig. 4.2. The dash-dotted line contains the receiving positions on the 2nd floor (the signal crosses one ceiling) in bedroom, bathroom upstairs, hall upstairs and workroom. The continuous curve belongs to the measurements carried out with the receiver in the 1st floor (two ceilings): livingroom, bathroom downstairs, hall downstairs, nursery and kitchen.

The variation margin of the received channel power values for the 1st floor is from -80 to -40 dBm, whereas on the 2nd floor the magnitude varies from approximately -70 to -25 dBm.

It is interesting to see the attenuation that a signal undergoes when crossing one or multiple floors. The attenuation added for crossing the 1st ceiling (lightweight construction) is 11 dB comparing to case of LOS. Additional 20 dB are lost for crossing a 2nd ceiling (concrete ceiling with an open stairway).

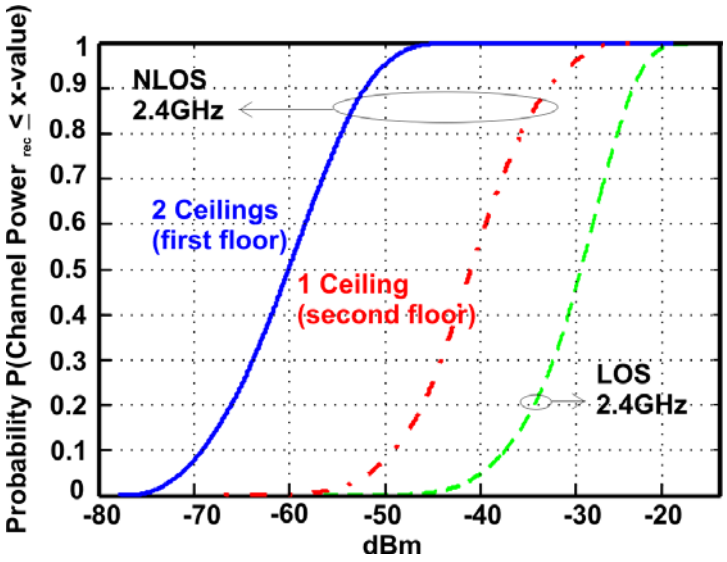

Fig. 4.16: LOS and NLOS, House A: Received channel power cdf 2.4 GHz

Fig. 4.17 shows the received power cdf for the 2nd floor in the two examined frequency bands, 2.4 and 5 GHz. The attenuation caused by obstacles in the path of the link, such as the building's structures and furniture, tends to increase with higher frequencies. Moreover, the active area of the receiver's antenna, and therefore the received power, is proportional to λ^2 and $1/f^2$ respectively. In this measurement, the reduction in the received channel power reaches 10 dB in average comparing to measurements in 2.4 GHz band.

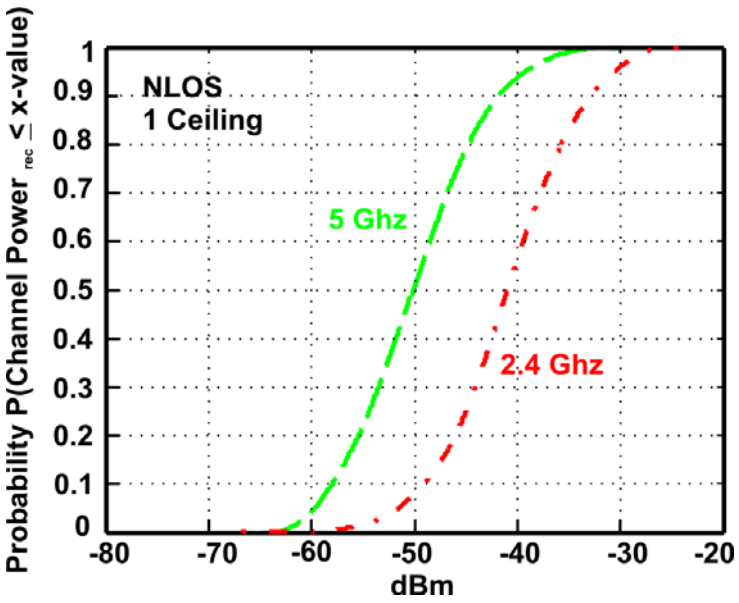

Fig. 4.17: NLOS (Transmitter Attic), House A: Received channel power cdf 2.4 GHz–5 GHz in the 2nd floor

Further analyses have demonstrated that the power distribution in a room is non-uniform. In the NLOS case there is an averaged reception power in the middle of the room up to 14 dB higher compared to near-wall positions. As an example, Fig. 4.19 depicts the cdfs for the measured channel powers in different positions in the livingroom marked in Fig. 4.18. The transmitter was in the attic.

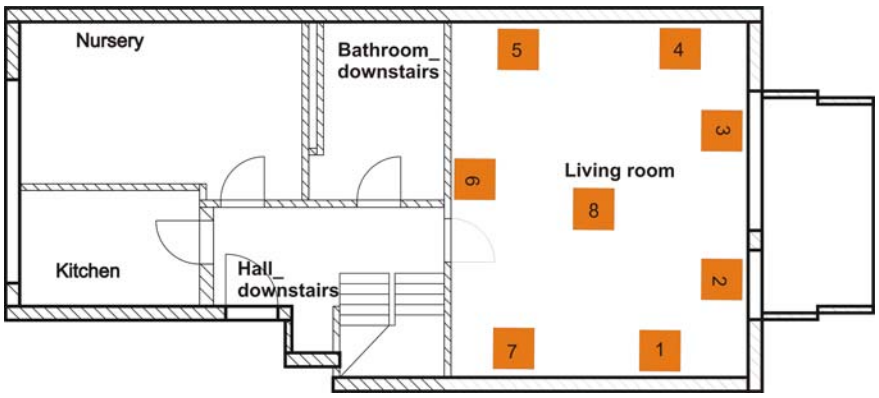

Fig. 4.18: Measured positions in the 1st floor

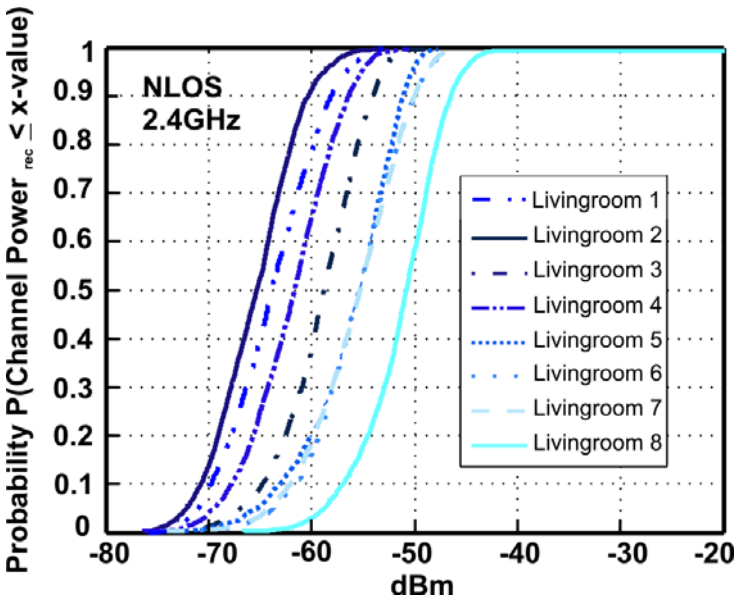

Fig. 4.19: NLOS (Transmitter Attic), House A: Received channel power cdf 2.4 GHz in the 1st floor

These curves pinpoint that the most convenient receiving area is exactly in the center of the room identified with the number 8. The acquisitions in positions 5, 6 and 7 have a very similar performance and not far from the best one, maybe due to the proximity to the open stairs. On the contrary, the less favourable positions are situated near to the wall and to a window. The worst case is the measurement number 2.

Therefore, it is to emphasize the important role of the antenna position in a wireless transmission. Even under same conditions and number of ceilings to cross the difference between the best and the worst standpoint can reach 15 dB.

4.6.2 House B

In contrast to house A, the transmitter is placed in different locations in house B. In particular, the transmitter is situated in three different floors: in the attic, in the 1st floor and in the basement.

Fig. 4.20 depicts three curves of received power when the transmitter is placed in the 1st floor. In the cdf labelled as “1 Ceiling (2nd floor)”, the receiver stands in the bedroom on the 2nd floor. The second cdf “1 Wall” also reproduces a NLOS scenario but on the same floor. The reception antenna is placed in the workroom, a neighbor room in the 1st floor. Finally, the LOS scenario is mapped on the dotted curve. All these bring out the attenuation that a wireless signal suffers by crossing walls and floors comparing to the LOS transmission. A loss of almost 15 dB experiences the received power to expand one room (“1 Wall”). If the wireless signal continues one floor upper, the loss amounts 23 dB. That is in the range of crossing a concrete ceiling in house A.

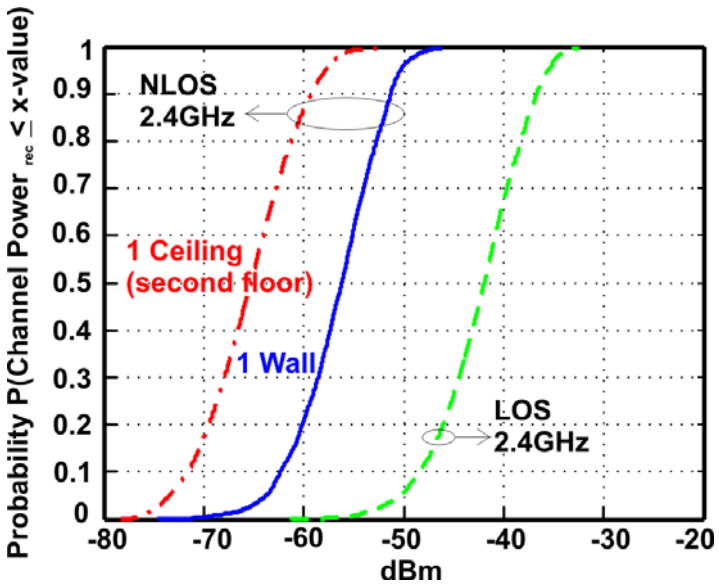

Fig. 4.20: LOS and NLOS (Transmitter Livingroom), House B: Received channel power cdf 2.4 GHz through 1 ceiling, 1 wall and LOS

Another analysis has been conducted fixing the receiving area in the bedroom on the 2nd floor. Two measurements have been carried out sending from the attic and from the 1st floor respectively. In both cases the signal must cross just one floor. The results in Fig. 4.21 show a slightly higher attenuation, lower than 4 dB, by the upper ceiling between the attic and the 2nd floor than by the ceiling between 1st and 2nd floor.

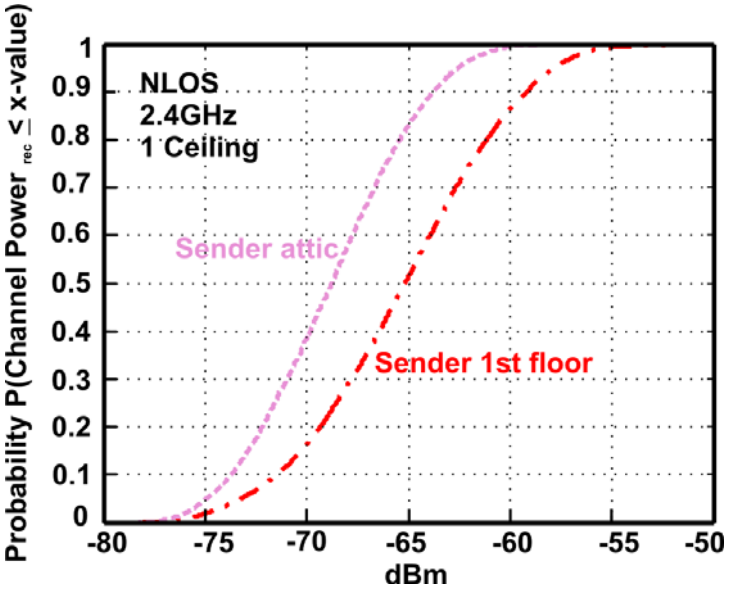

Fig. 4.21: NLOS (transmitter attic and 1st floor), House B: Received channel power cdf in the 2nd floor:

4.7 Frequency selective fading

Not only the channel power is important for the reception of a signal but also the attenuation suffered from several single subcarriers. It is known as selective frequency fading and its causes have been described in Chapter 2.

Even in the case of a line-of-sight between two devices deep fades can occur. In Fig. 4.22 the cdf for the maximum relative fading within a 20 MHz frequency band is depicted. The term relative fading attenuation specifies the difference between the highest and the lowest value within 20 MHz of the corresponding channel spectrum. The figure shows that 50% of the locations have fading depths of more than 3 dB in the LOS case. For NLOS transmissions fading is worse. Here the 50% value is at 4.5 dB. Another interesting result of these measurements is the remarkably high probability for fading attenuations of more than 20 dB in both scenarios, reaching degradations of up to 30 dB in the worst cases.

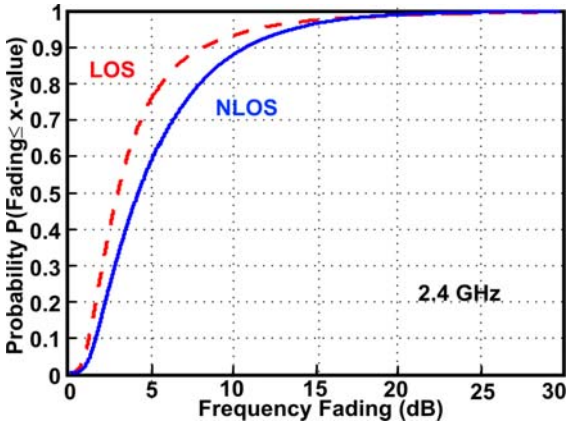

Fig. 4.22: Maximum channel frequency fading in 2.4 GHz band

A similar analysis can be performed, if the fading depth is analyzed for the channel with the highest and lowest received power. This is relevant for systems that dynamically change their working frequency. The resulting CDFs for 2.4 GHz and 5 GHz are depicted in Fig. 4.23 a) and b) respectively.

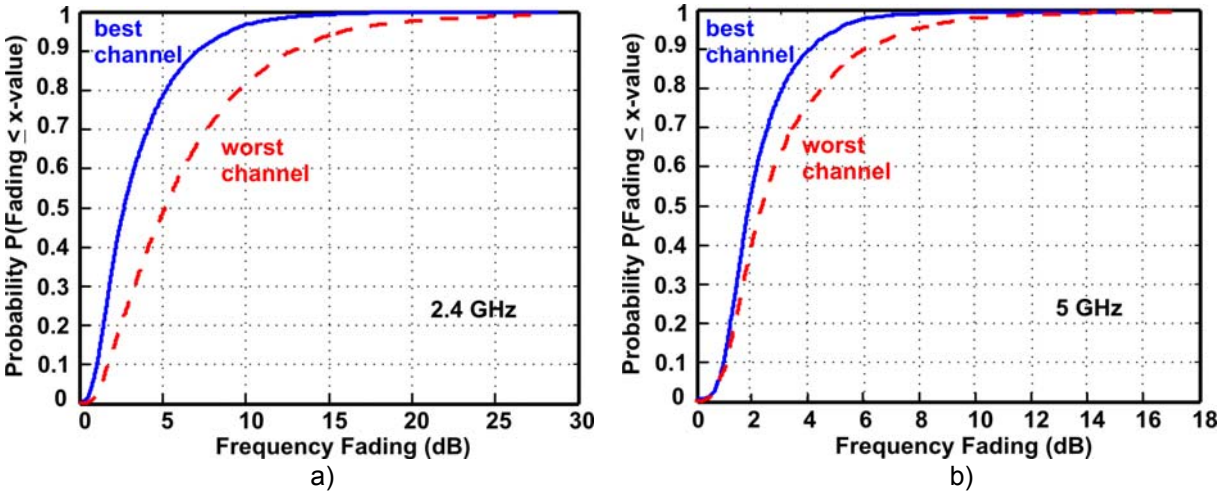

Fig. 4.23: Maximum channel frequency fading for the best and the worst channel in a) 2.4 GHz and b) 5 GHz bands

These figures emphasize that the choice of the channel with the highest average reception power usually delivers lower fading effects than the choice of the worst channel, as expected. The 50% value for the best channel is 2.65 dB and 1.82 dB for 2.4 GHz and 5 GHz respectively, and for the worst one, 5 dB and 2.35 dB.

It can also be seen that the maximal depth for the 2.4 GHz is much larger than for the 5 GHz band, almost double. Therefore, although the 5 GHz band is more sensitive to a reduction of the power it is not the case for the fading impact.

4.8 Physical Layer enhancements

The overall purpose is to conduct a reliable wireless multimedia transmission in home environment. To achieve this goal, several optimization techniques have been proposed in section 3.5. Two of these approaches are investigated and evaluated on the basis of the presented measurements. These are the dynamic frequency selection (DFS) and the diversity technique.

4.8.1 Dynamic frequency selection

If some carriers of the OFDM multiplex are affected by fading or if the overall received power is comparably low, the whole transmission can be shifted to another physical channel.

In Fig. 4.24 it can be seen that the total transmitted power differs very much between adjacent WLAN channels. This fact pinpoints the potential of the dynamic selection of the best channel at any time that can yield a significant gain with regard to the received power.

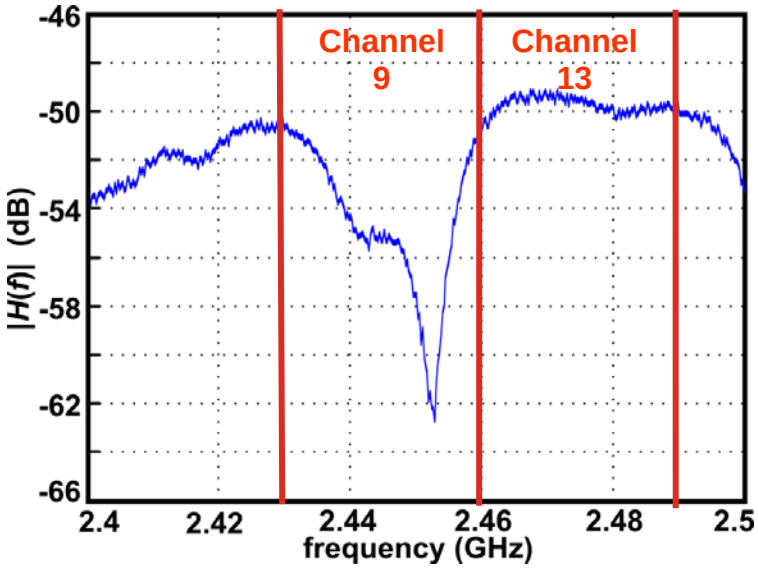

Fig. 4.24: Example of 100 MHz measured Spectrum

Taking into account the transmission channel power, the effect of changing the transmission channel to a less disturbed frequency is investigated with the static measurements. The effect of this method is evaluated and the gain using the worst WLAN channel compared to the best one is quantified Fig 4.25 a) and b) present the difference between the power of the channel with the highest and lowest channel power in 2.4 GHz and 5 GHz bands. The results show that in 50% of all cases this gain is at least 5.4 dB for a LOS transmission and 7.23 dB for a NLOS transmission in the 2.4 GHz band. The fact that the gain is typically higher at NLOS situations is very interesting, because this is usually the

more critical case for a link. These promising first results led us to a more comprehensive analysis of this method (see Chapter 5).

At 5 GHz, the situation is slightly different. Here there is usually a higher gain for LOS situations. But in either case the probability for a certain gain is usually higher compared to 2.4 GHz. So, the 50% values are at 10.38 dB for a LOS situation and 9.45 dB for NLOS transmissions.

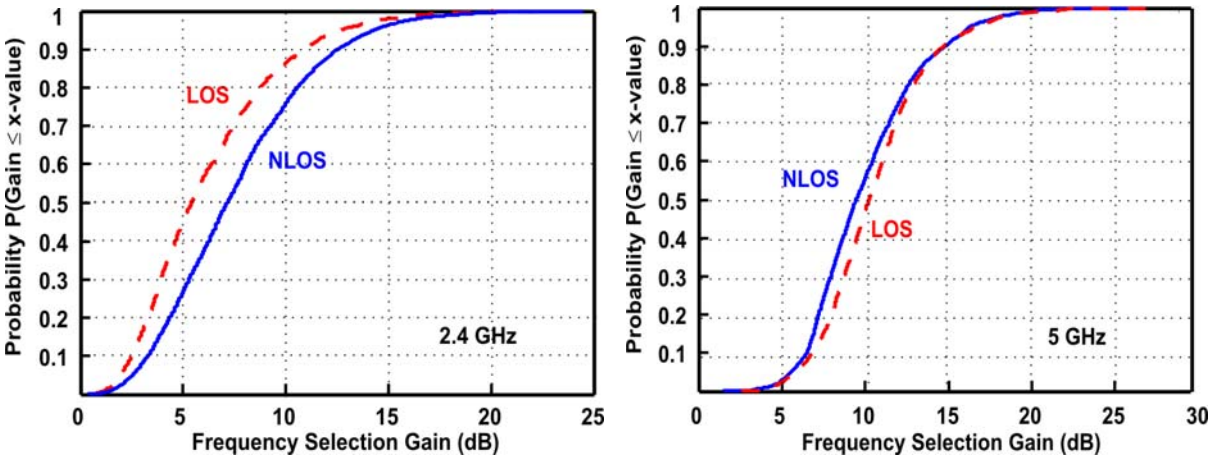

a) b)

Fig. 4.25: CDF for improvements realized by dynamic frequency selection in a) 2.4 GHz and b) 5 GHz bands

The organization of this frequency selection is not covered by the standard and can be organised as an application operating on higher network layers. As a framework for realizing dynamic frequency selection the amendment of IEEE 802.11h [IEEEh03] could be used.

4.8.2 Antenna Diversity

A lot of media devices in the household allow for deployment of two or more antennas with sufficient distance. Taking into account the spatial coherence of the in-house channel, antenna diversity is therefore another very powerful method for link adaptation.

Even very simple antenna diversity with antenna switching can offer high gains. The reason for this effect is the spatial coherence of the channel. In [Bertoni00] it is pointed out that for a channel situation with equally distributed angles of incidence and equal path amplitudes a spatial decorrelation can be assumed for distances *s*:

$$s > 0.4\lambda \tag{4.20}$$

with λ the wavelength of the radio signal.

Taking this into account, two antenna diversity with an antenna distance of 40% of the signal's wavelength would be sufficient. So even for 2.4 GHz it results in a minimum required antenna distance of 5 cm, for 5 GHz even less.

Similarly to frequency selection the possible gain for antenna diversity with respect to

channel power can be analyzed. The cdf for the achievable gain, if two antennas with a distance of 5 cm are used, is depicted in Fig. 4.26 a) for 2.4 GHz and in Fig. 4.26 b) for 5 GHz. The reason that both figures start at a value of 0.5 is due to the fact, that a second antenna is advantageous only in every second case. In both frequency areas there is a probability of about 10% that the gain is 5 dB or more. In some cases gains of nearly 20 dB with an antenna distance of 5 cm have been found.

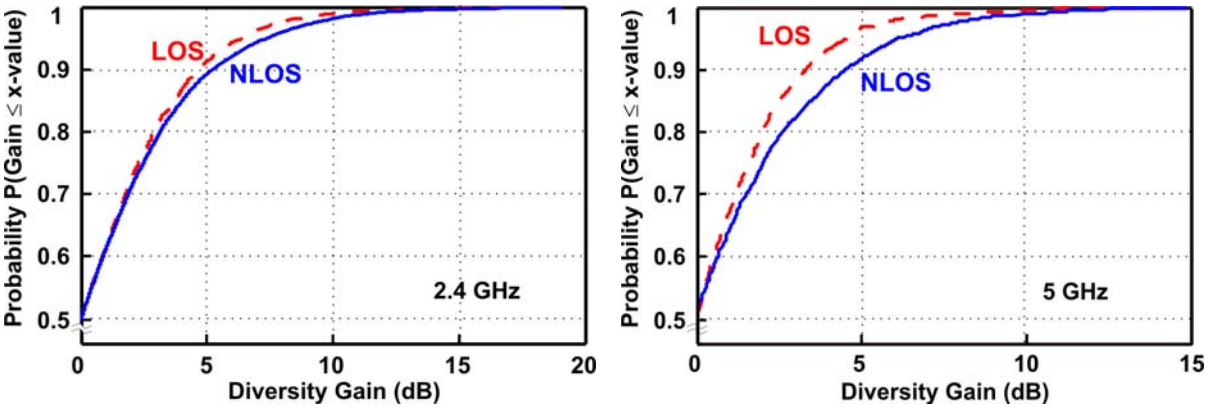

Fig. 4.26: CDF for the achievable diversity gain using two antennas with a distance of 5 cm in a) 2.4 GHz and b) 5 GHz bands

Of course in reality the wave incidence is not as in the idealized case. The distributions of angles of incidence and path amplitudes will be different. For this reason, the result is that the correlation distance can be still of the same order of magnitude of the wavelength. Other distances between both receiver antennas have also been studied. In Table 4.3, the corresponding gains are listed for the 90 % of the cases with the corresponding distances.

Table 4.3: P(Diversity Gain ≤ x-value) = 0.9 using two antennas with different distances

Diversity Gain (dB)	**2.4 GHz:**		**5 GHz:**	
	LOS	NLOS	LOS	NLOS
5 cm.	4.88	5.08	3.72	4.9
10 cm.	5.44	6.12	4.7	5.75
15 cm.	6.21	6.76	6.62	6.22
20 cm.	6.27	7.22	7.092	6.34
25 cm.	6.40	7.44	6.924	6.74
30 cm.	6.5	7.51	6.982	6.66
35 cm.	6.75	7.63	6.928	6.81
40 cm.	6.99	7.57	6.964	6.71

4.9 Summary of the measurement results

In this chapter, a setup for carrying out in-house measurements in the 2.45 GHz and 5GHz

ISM bands has been described. With this configuration the studied transmission channel characteristics have been detected. The numerous measurements performed in two different home scenarios, A and B, have been thoroughly analyzed. Several results regarding the channel amplitude distributions, coherence bandwidth, received channel power and frequency selective fading have been presented.

Furthermore, two powerful methods for link adaptation have been evaluated: dynamic frequency selection and antenna diversity. The analysis of the comprehensive channel measurements substantiates that these methods can give a significant improvement in average received power.

4.10 In-house path loss model with attenuators

Using the previous measurement results, a real WLAN scenario with different concurrent links could be simulated for a typical home environment.

Ideal path loss with additional attenuation caused by building structures plotted in a logarithmic scale of attenuation vs. linear distance will result in a straight line with discontinuities at the spatial positions of the respective attenuators. The step height directly corresponds to the attenuation, whereas the slope is equivalent to the path loss exponent.

As both parameters had to be estimated, the spatial position of the attenuators (walls, floors) with respect to the antennas is needed. In case of non trivial situations, basic architecture models of the buildings have to be set up. An example of such an architecture model is given in Fig. 4.27 for house A. The transmitter position is marked with a red spot. The “links” are represented from the transmitter to the respective receiver positions (black spot) and the intersections of the structures of the building with the respective link are purple.

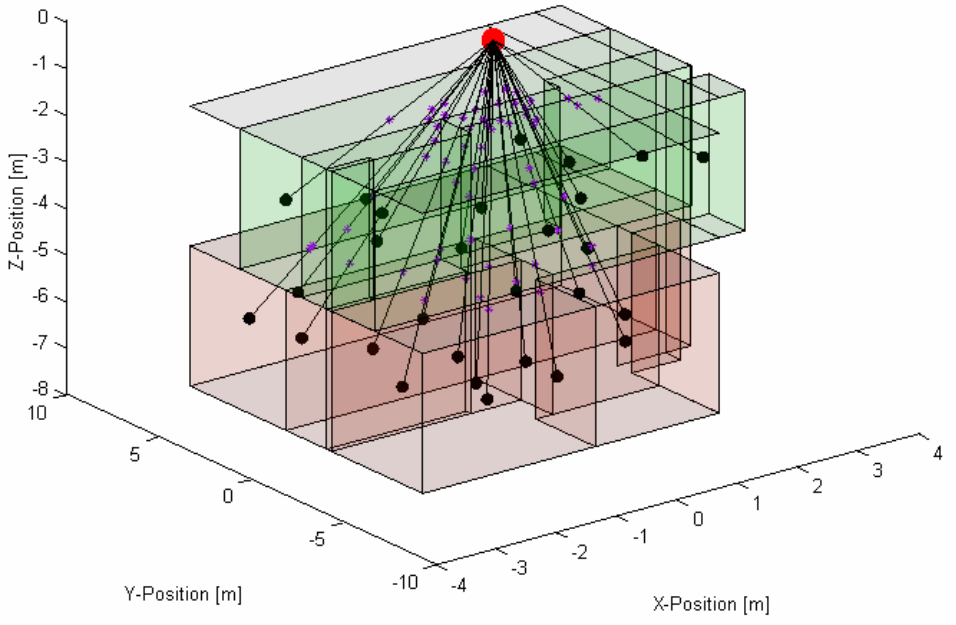

Fig. 4.27: Measurements in House A.

The following model was used to find the optimum set of parameters to fit the measurements for a certain link (for the sake of clarity in a non logarithmic version)

$$a = a_0 \cdot a_d \cdot d^n \cdot \prod_i^{m_{walls}} \left(a_{wall,i}^{\left(\frac{1}{\sin \beta_i}\right)} \right) \cdot \prod_j^{m_{floors}} \left(a_{floor,j}^{\left(\frac{1}{\sin \beta_j}\right)} \right) \tag{4.21}$$

with the parameters listed in the following table:

Table 4.4 Parameters of the path loss model with attenuators

Parameter	
a	Total link attenuation
d	Link distance
m_{walls}	Number of intersected walls
β_i	Angle between the i-th wall intersecting the actual link
β_j	Angle of the j-th floor intersecting the actual link
a_d	Attenuation caused by the directional diagram of the antennas
a_0	Modelling the transmitter's power, the antenna's gain as well as physical constants
n	Path loss exponent
a_{wall}	Attenuation of a wall (same for all walls)
$a_{floor,j}$	Attenuation of an individual floor

In order to reduce the number of parameters, all walls are assumed to have the same attenuation. The parameter a_0 is taken from the calibration of the respective antenna. In [Miniwatt06] it was found out, that the consideration of the intersection angles showed few or no positive effects. Therefore, $\beta_i = \beta_j = 90°$.

Moreover, it was evaluated whether the consideration of the penetration angle and the antenna's directional diagram results in a better fit and therefore in a more reliable parameter estimation. Several sets of measurements were evaluated. Comparing the results of the parameter estimation ("antenna directional diagram ignored / penetration angle ignored" to "select the combination with the best match") yielded results in only fractional differences in the estimated parameters. This may result from the rich scatter present in residential homes. In order to simplify the propagation model, the influence of penetration angle and directional diagram is abandoned as well, $a_d = 1$.

$$a = a_0 \cdot d^n \cdot a_{wall}^{m_{walls}} \cdot \prod_{floors\ j} \left(a_{floor,j} \right) \tag{4.22}$$

Several objectives for the optimization process were evaluated. In the end, reasonable results were achieved with a coring function to minimize the deviations between the

measurements and the path loss model.

The parameters are estimated by means of a full search algorithm with a heuristic objective. The following parameters have to be estimated:

- Path Loss Exponent**: *n***
- Attenuation of walls and floors: a_{wall}, $a_{floor,1}$ and $a_{floor,2}$

The link loss is influenced to a great extent by the building's structure. The extracted parameters for the measurements of house A (Fig. 4.27) in the 2.4 and 5 GHz bands are given in the following table. The row "fit [%]" gives the fraction of measurements inside 6 dB tolerance with respect to the model. "σ_{Rest}" is the average deviation of the measurements after the coring (namely the objective).

Table 4.5 Results from the attenuation measurements

Parameter	Freq. [GHz]	House A
n	2.4	2.7
	5	2.8
$a_{floor,1}$ [dB]	2.4	11.0
	5	21
$a_{floor,2}$ [dB]	2.4	20
	5	N.A.
a_{wall} [dB]	2.4	0.0
	5	4.5
Fit [%]	2.4	98
	5	71
σ_{Rest} (objective)	2.4	0.4
	5	1

The path loss exponent *n* tends to smaller values in comparison to numbers taken from the literature, which were mainly measured in office environments.

Fig. 4.28 shows the attenuation for house A calculated with the presented path loss model corresponding to the measurement points of Fig. 4.27 in the 2.4 GHz band.

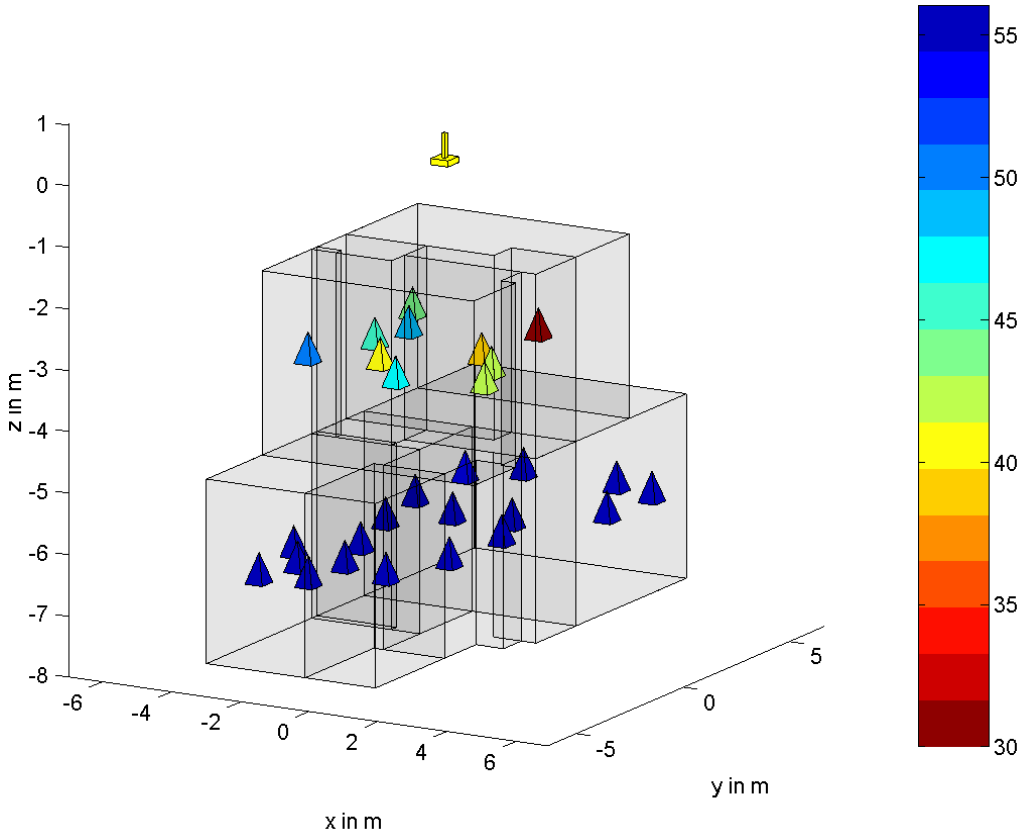

Fig. 4.28: Measurements in House A: attenuation in the 2.4 GHz band [dB].

5 Dynamic WLAN In-House Channel Measurements and Evaluations

Detailed and reliable understanding of the time-varying characteristics of the transmission channel is necessary to introduce link adaptation techniques such as dynamic frequency selection. For this purpose, new sets of dynamic WLAN channel measurements have been carried out.

Measurements of the time-varying wireless in-house channel imply exigent requisites by the measuring system. In the previous chapter, the static measurements in 2.4 GHz and 5 GHz bands were presented. This chapter shows dynamic measurements in time domain carried out in the 2.4 GHz ISM-Band in several home environments.

The acquisition of time varying scenes such as people moving or objects whose locations are changed, requires a high time resolution. It presupposes that the data need to be saved quickly. Statistical analyses of the results demand a long measuring time. For such measurements, a large memory storage is required for all the generated data. In the following sections, the measurement set up and the performed experiments are presented in detail. The next sections focus on the obtained results and on the evaluation of the proposed optimization technique DFS [AhFeVa05].

5.1 Measurement set-up

The measurements of channel dynamics are aimed at collecting information such as channel power traces and temporal characteristics of fading effects. For this purpose, the same set-up as for the static measurement has been reused (see Annex A). However, several modifications have been carried out according to the new requirements.

At the transmitter there are no significant changes. Identical devices compose the transmitter set, the signal generator AMIQ Rohde&Schwarz and the vector modulator SMIQ using quadrature modulation. Both form the transmitter side emitting a continuous 100 MHz bandwidth signal which modulates a carrier in the 2.4GHz band.

On the other side, the receiver has been simplified. Now the antenna positioner is not present anymore. The data acquisition continues being automatically carried out by a PC but the antenna remains fixed. The control algorithm for the data storage in C was modified to measure and save the values faster. The time resolution of the spectrum analyzer allows to measure seven spectra per second on average.

Fig. 5.1 illustrates the simplified set-up in comparison to the used for the static measurements. In principle, the basic structure remains equal except for the positioner: AMIQ, SMIQ and FSIQ of Rohde & Schwarz.

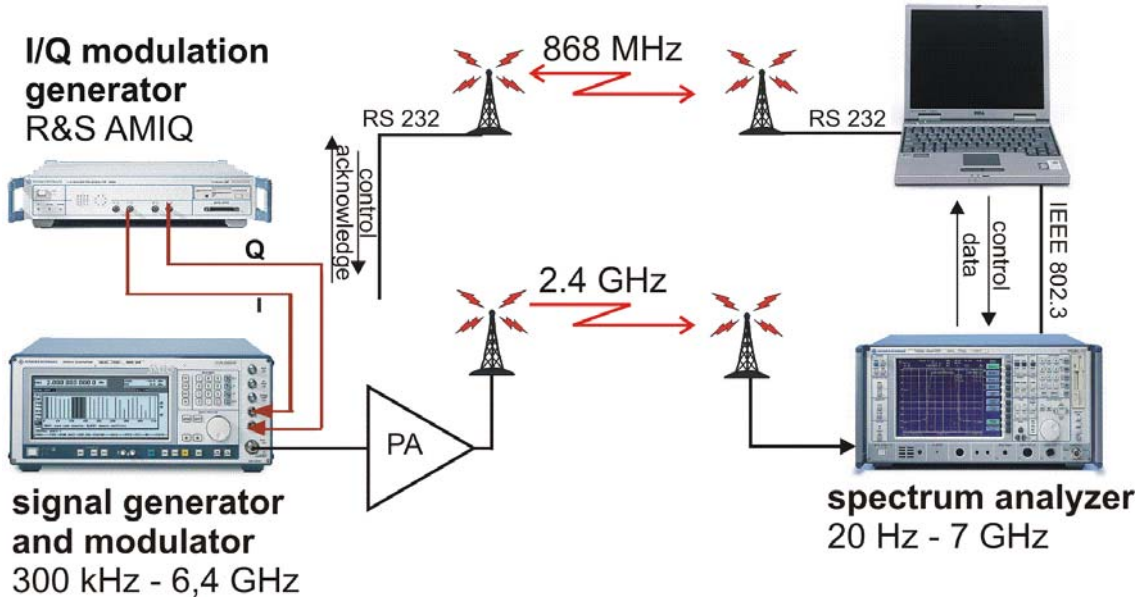

Fig. 5.1: Measurement set-up for registering the dynamic channel characteristics.

5.2 Measurement campaigns

The locations selected as scenario to carry out the dynamic measurements are three representative multistory residential buildings. In each household three, six, and two measurements have been performed, totalling more than 200 hours. The duration of each recording is limited by the operation system on the PC. The file system of Windows does not allow saving files larger than 4GB corresponding to a maximum duration of about 24 hours for each dynamic measurement.

The measurements have been carried out during the day as well as at night, in order to observe the influence of people moving around at different hours. A large database was created to achieve statistical significance. All the measured scenarios correspond to a NLOS transmission. The scenarios are diverse and the transmitter stays not only at the attic but also on the same floor in other rooms. In the following sections, when referring to the locations of these measurements by analyzing their results, the different scenarios will be labeled DA, DB and DC, to differ from the static ones, A and B.

In Fig. 5.2 a typical situation is represented that could take place in a home environment. Two people staying in a room, move their positions at the same time when some pieces of furniture are being displaced. These variations provoke a modification of the wireless medium along the time. The transmission path can vary from line-of-sight, Fig. 5.2 a), to one severely obstructed as shown in Fig. 5.2 b).

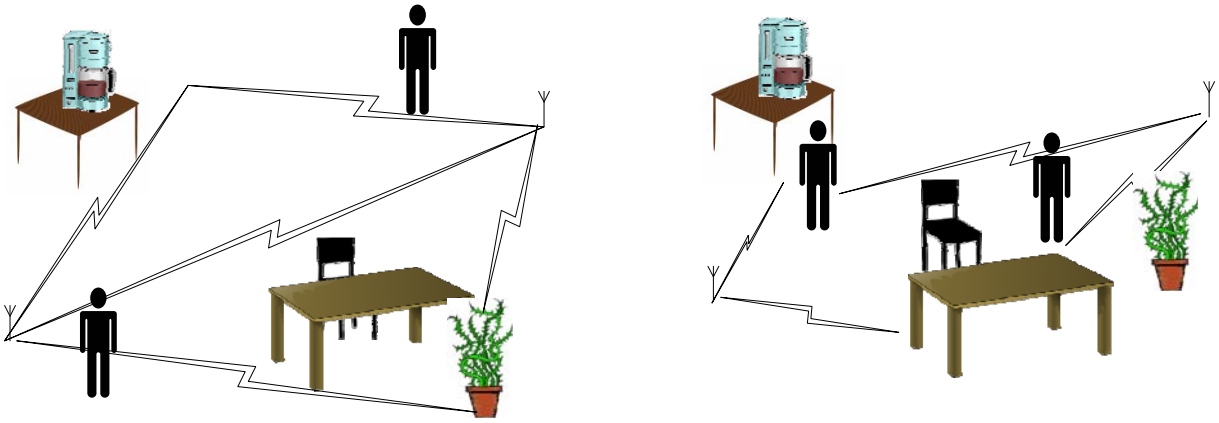

a) Situation of LOS transmission path b) Situation of NLOS transmission paths

Fig. 5.2: Sequence of two scenes in a home environment

The modifications on the channel lead to different effects, which will be shown and analyzed in the following sections.

5.3 Time sequences of spectra

The spectrum analyzer FSIQ captures sequences of spectra during hours. Fig. 5.3 shows a very short one truncated to three consecutive measured instants. The spectra are separated by approximately 150 ms, the time resolution of the used equipment that leads to 6-7 spectra per second. They were acquired on house DA at 22:24:54h during an activity phase on this scenario. It can be seen how fast the channel can change due to the varying environment. The main cause for that is the multipath effect explained in chapter 2.

As illustrated in Fig. 5.2, the variations in the room provoke an alteration of the transmission paths. This way, the propagation delays become lower or higher depending on each path length and therefore, the frequencies affected by selective frequency fading change from one channel to another in a random manner. That is clearly observed in the extract of the Fig. 5.3 and explained in the following paragraphs.

In this analysis, the four non-overlapping channels in the 2.4 GHz. ISM band are considered, whose frequencies according to the IEEE 802.11 *g* standard are:

- Channel number 1: [2402-2422 MHz]
- Channel number 5: [2422-2442 MHz]
- Channel number 9: [2442-2462 MHz]
- Channel number 13: [2462-2482 MHz]

It is observed in Fig. 5.3 that channel 9 at the beginning of the sequence at 22:24:54.79 h, suffers from an abrupt degradation.The fading depth defined in chapter 4 as the difference between the maximum and minimum value of the channel, constitutes approximately 20 dB. This deterioration reduces its transmission performance for a long time. The unfavourable multipath constellation possibly created by fixed objects in the room, leads to a destructive interference for this frequency, like in Fig. 2.4. The other channels present good conditions at this time regarding the fading depth at this time.

In the next milliseconds, at 22:24:54.92 h, a deep and straight fade occurs in channel 1 with a level of almost 20 dB as well. This degradation is very short and after a few milliseconds again, this channel recovers its former level.

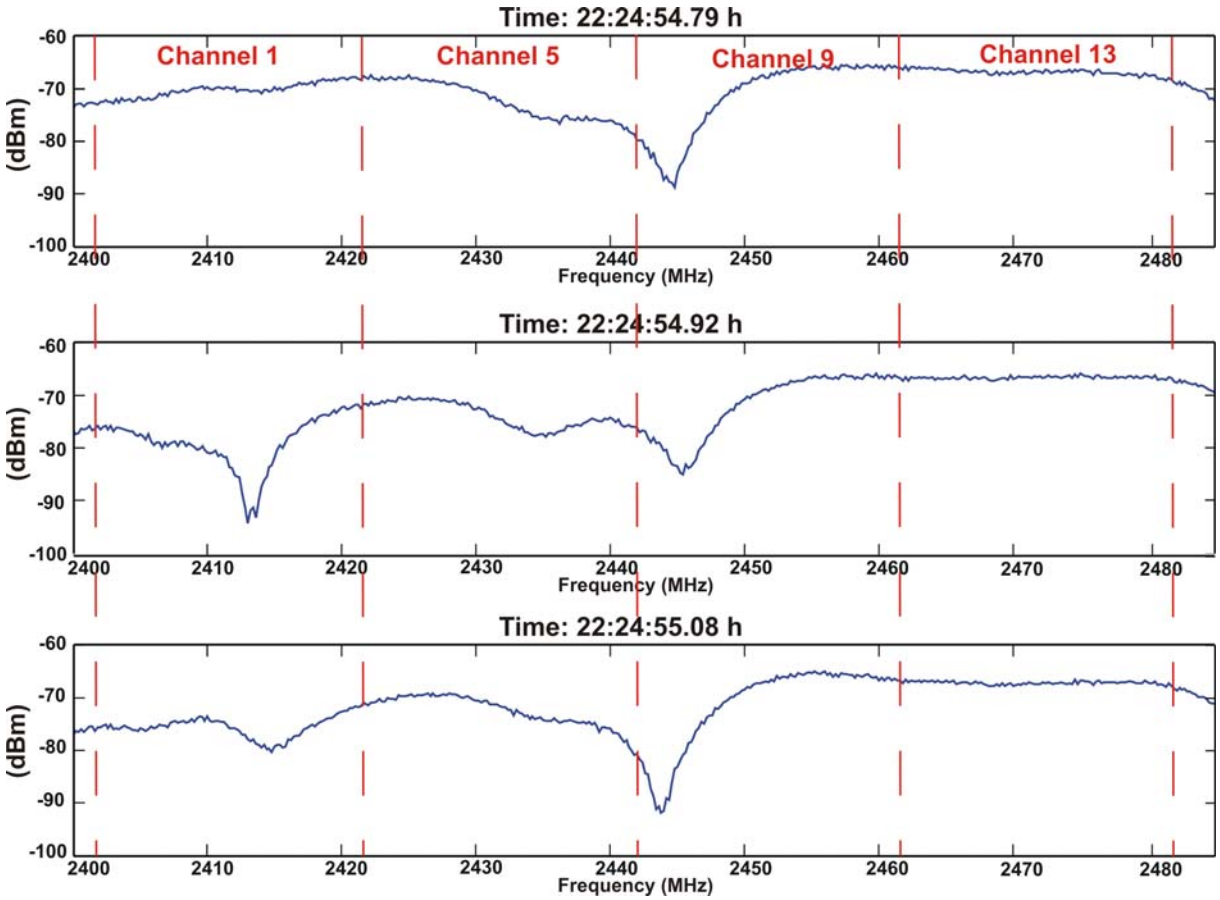

Fig. 5.3: Sequence of measured spectra.

This analysis pinpoints the improvement potential when applying an intelligent selection of the transmission frequency. With off-the-shelf WLAN products the user can select the transmission frequency during setup. Often the default setting of the product is kept. In this example, if the channel 9 would be the default one, a very low performace would occur on this channel. The case of sporadic degradations during some milliseconds seems to be harmless. However in transmission systems such as WLAN, this fading can be result in a OFDM frame error burst. Both degradations, constant and sporadic, can be avoided changing to a “sane” channel in time.

This link adaptation technique was evaluated in section 4.8.1 on the basis of the static measurements. A very efficient and promising performance of the method with a gain up to 7 dB in average for NLOS was shown. Now, it will be newly evaluated with a realistic time-varying scenario, i.e., on the basis of the dynamic measurements.

5.4 Time-varying received channel power

An important contribution to the knowledge of the dynamic WLAN channel behaviour is provided by the observation of the temporal variations of the received power. The signal-to-

noise ratio determines several important attributes such as packet loss, which directly affect the QoS. Thus, the channel power is a reasonable and meaningful attribute to characterize a link, although not the only one.

The channel power is calculated as the integral of the spectra in the corresponding frequency band, as defined in Section 4.6. As an example, Fig. 5.4 shows the channel power traces for the 4 non-overlapping channels observed during 9 hours in house DA. The measurement in this illustration has been selected as reference for all the analyses since includes diverse effects, such as small scale fading, non-stationarity or active and inactive phases. These traces willl be evaluated in detail in other sections of this chapter to exemplify analyses and to be referenced by comparying with other measurements, which have been evaluated likewise. Occasionally, one of these is also included to consolidate the conclusions.

From Fig. 5.4, the different phases of the day can be easily inferred. The first two hours correspond to a phase with variations affecting mainly the channels 1 and 5. Both present very low channel powers resulting in a link loss. In the second phase, from 23h to 00:30h approximately, frequent changes occur. The four channels reach similar channel power levels for a few moments, but then deeper fading levels in channel 1 and specially 5 irrupt their performances. Finally, an idle phase is achieved during the night period.

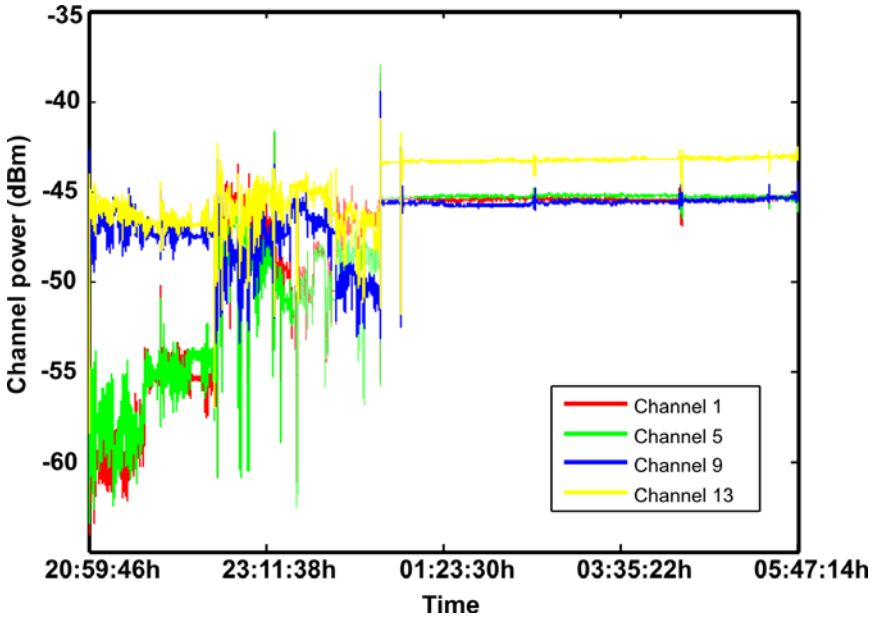

Fig. 5.4: Reference measurement: Received channel power

Hereupon and on the basis of the channel power, a ranking of the four candidate channels through the definition of a quality measure is performed. The channel with the highest channel power at a given time is the best one.

$$\text{Best channel}_t = i \mid_{\max\{ChPi\}} \qquad i = 1, 5, 9 \text{ and } 13 \tag{5.1}$$

This attribute is used in the following for several studies. Introducing intelligence to the system, an “optimal channel” could be determined for every time instant. For the example in Fig. 5.4, such a sequence of best channel number for every time is depicted in Fig. 5.5.

During the first two hours, channels 13 and 9 alternate as best channel. In the second phase from 23 h approximately, deeper fading levels than before are measured, and channels 1, 5, 9 and 13 take turns regarding the best channel attribute. During the night channel 13 acquires this first position and keeps it to the end. This analysis is focused on the DFS technique, which will be treated later in more detail.

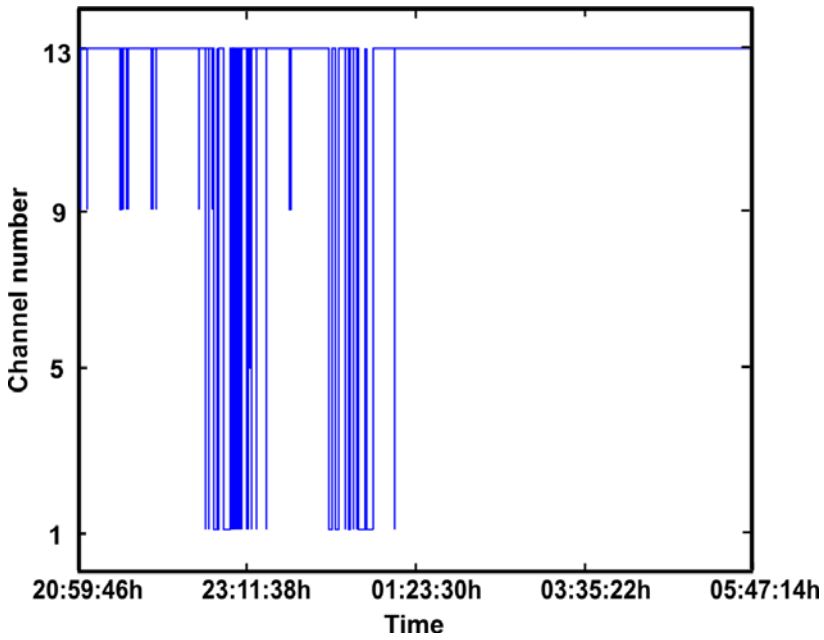

Fig. 5.5: “Optimal channel”: Best channel sequence

5.5 Time-varying fading

Selective frequency fades emerge within the WLAN frequency range of 20 MHz, as shown in Fig. 5.3, affecting the received channel power. Therefore, the fading depth is another important parameter to characterize a link. In Fig. 5.6, the fading depth traces associated to the channel powers of Fig. 5.4 are depicted for the 4 non-overlapping observed during 9 hours and calculated as defined before.

The fading traces show that the best channel regarding the received power, channel 13, is also the one that is least disturbed by fading. However, the channel with the deepest fading, channel 9, is not the channel with the lowest received power. The explanation for that can be found in Fig. 5.3, where only a steep and narrow fading in the frequency range between 2442 and 2462 MHz can be seen. The fact that this degradation is persistent in contrast to the variations in other channels can be due to an unfavourable path between the transmitter and the receiver, e.g. caused by a static object close to the receiving antenna. Therefore, the reduction of the channel power does not only depend on the fading depth but also on the bandwidth of the fade among other effects, as it will be explained in next sections.

It is also important to point out that different phases of the day affect the fading traces observed especially for channels 1 and 5. These channels are the most active in terms of channel power. In the first phase, both channels present a low channel power as a consequence of shadowing and it is aggravated by the high fading levels between 5 and 20 dB. In the second phase, the variation rate of their channel power traces increases in

contrast to the fades that are reduced. Finally, during the night time the fading levels remain constant. The constant degradation of almost 10 dB suffered by channel 9 is perceptible. It is also noticeable the rapidity of the fades, as it was seen in Fig. 5.3. From one instant to the next one there can be variations of up to 30 dB in the case of channel 9.

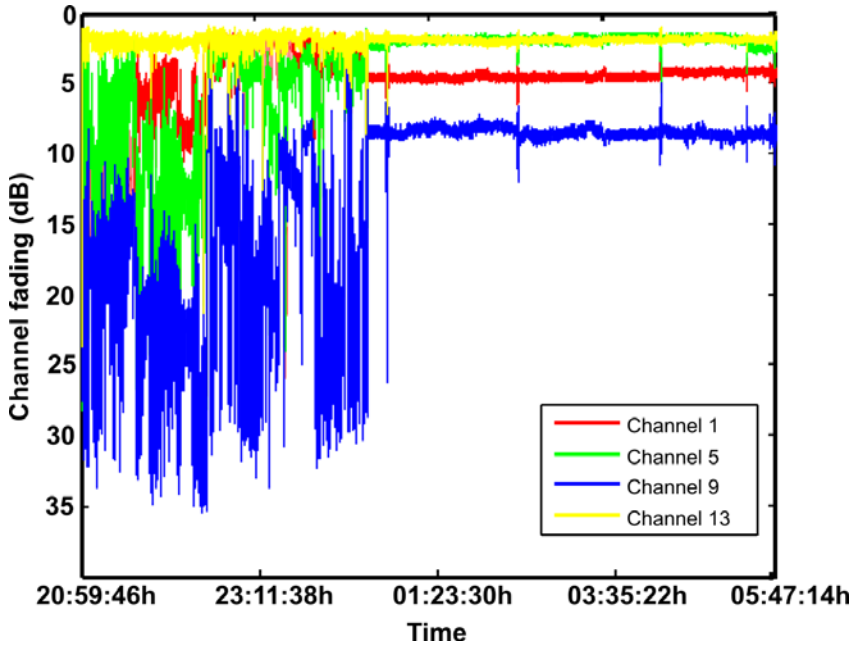

Fig. 5.6: Reference measurement: Channel fading levels

5.6 Correlation between fading depth and channel power

The main time-varying characteristics of the WLAN channel, received channel power and fading depth, have been separately described by means of an example of the carried out measurements.

Further analyses focus on finding the most convenient set of parameters to characterize both attributes for modeling. To facilitate the interpretation of the results, the long measurement time spans are divided into inactive and active phases.

For this analysis, the labeled reference measurement is used as an example. The inactive time corresponds to the night whereas the active time in the first four hours characterizes the channel in the evening.

5.6.1 Inactive Phase

Fig. 5.7 shows a spectrum of the 100 MHz measurement in the 2.4 GHz band during the night time and keeps this shape constant since approximately 1:00 h.

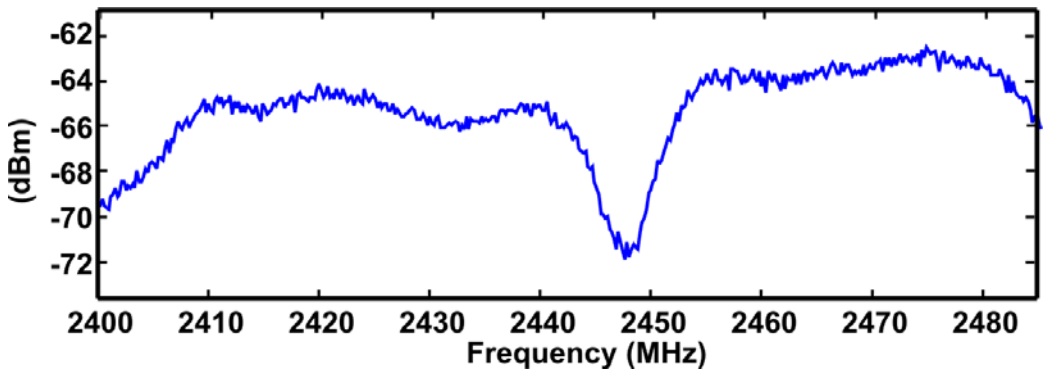

Fig. 5.7: Example of a 100 MHz measure trace in the 2.4GHz ISM band

The properties of the channel power and the fading depth are now analyzed in relation to each other in this phase. Thus, a two dimensional histogram is generated for the inactive phase of the reference measurement (from 1:00 h to 5:47 h) represented in Fig. 5.4 and Fig. 5.6. The chart in Fig. 5.8 reports the occurrences of the pair (ChP_i, F_i), where ChP_i is the received channel power at $t = i$ and F_i is the fading depth emerged in this channel at the same instant. This histogram has been calculated for all the 13 available channels in the 2.4 GHz ISM band. Due to the overlap between the channels (Fig. 3.6) there is a coherence between the calculated channel powers of consecutive channel frequencies.

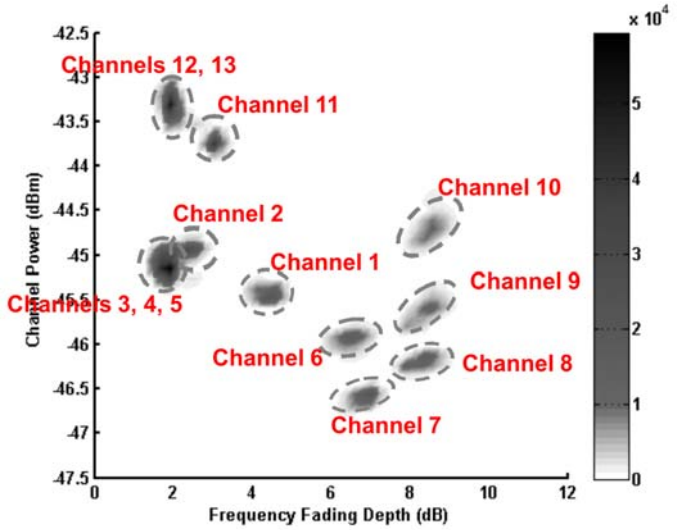

Fig. 5.8: 2D-Histogram: (*ChP-F*). Reference measurement: Inactive phase

Due to the absence of movements in the environment and thus, of changes in the transmission path, each frequency channel is recognizable in the histogram. Apparently, there is no dependency between the two measured factors, as deduced before.

Observing the outcomes more exhaustively, it can be assessed that, e.g. the channels 12 and 13 present higher channel powers than the channels 3, 4 and 5 under the same frequency fading depth. To eliminate additional effects that mask the impact of the frequency selective fading on the receiver performance, the maximum value in each channel spectrum is set to null. In the following, the integral of these spectra is labeled as normalized channel power. For the measured discrete data:

$$S\_dB_{j,norm}(f)\ [dB] = S_j(f)\ [dBm] - \max(S_j(f))\ [dBm] \tag{5.2}$$

$$S_{j,norm}(f) = 10^{\left(\frac{S\_dB_{j,norm}(f)}{10}\right)} \tag{5.3}$$

Finally, the normalized channel power is calculated analog to (4.17):

$$normalized\ ChP_j = 10 \cdot \log_{10}\left(\sum_{i=1}^{100} \frac{S_{j,norm}(f_i) * f_A}{\Delta f_{rbw}}\right) \tag{5.4}$$

where $S_{j,norm}(f)$ is the received linear signal in the corresponding frequency band deferred to null or normalized, Δf_{rbw} is the resolution bandwidth = 200 kHz, and f_A the sampling frequency = 200 kHz.

Fig. 5.9 exemplifies an arbitrary 20MHz WLAN channel deferred to null.

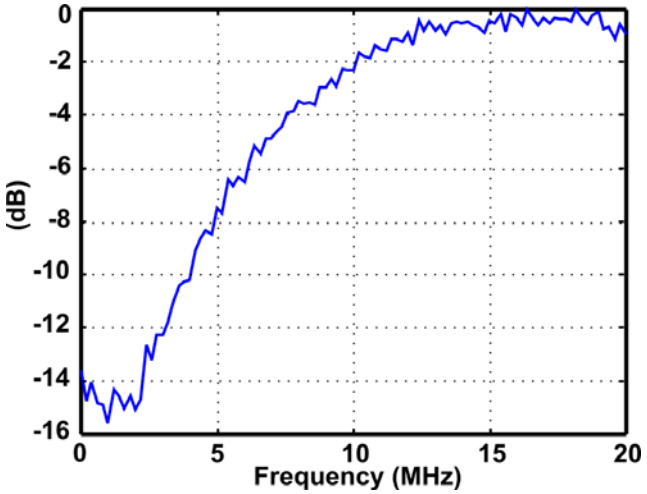

Fig. 5.9: Normalized 20 MHz channel spectrum

The normalized spectrum of the example shows a strong degradation *F*=15.6 dB and a normalized channel power *ChP*=17.32 dB. The new histogram for the same inactive phase of the measurement with the shifted spectra and the recalculated channel spectra is given in Fig. 5.10.

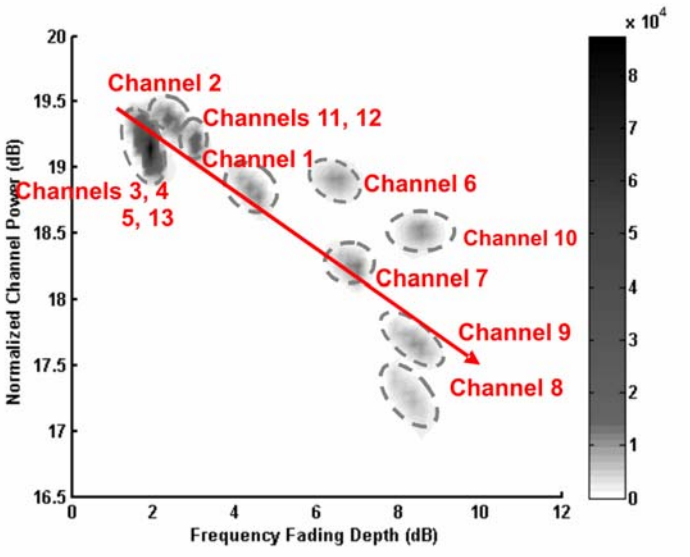

Fig. 5.10: 2D-Histogram: (normalized *ChP-F*). Reference measurement: Inactive phase

This distribution demonstrated an almost linear dependency between the two parameters. Deeper frequency fading corresponds to lower normalized channel power. However, the bandwidth of the fade also plays an important role. Channels 9 and 10, as well as 6 and 7, present different channel powers, although they have the same fading depth. The case of channels 1 and 6 is the contrary. They exhibit the same level of channel power with different fades. The explanation for both effects is the number of affected subcarriers in each channel. In Fig. 5.11, the overall 100 MHz spectrum is plotted with separating lines marking the frequency boundaries for channels 1, 6, 9 and 10.

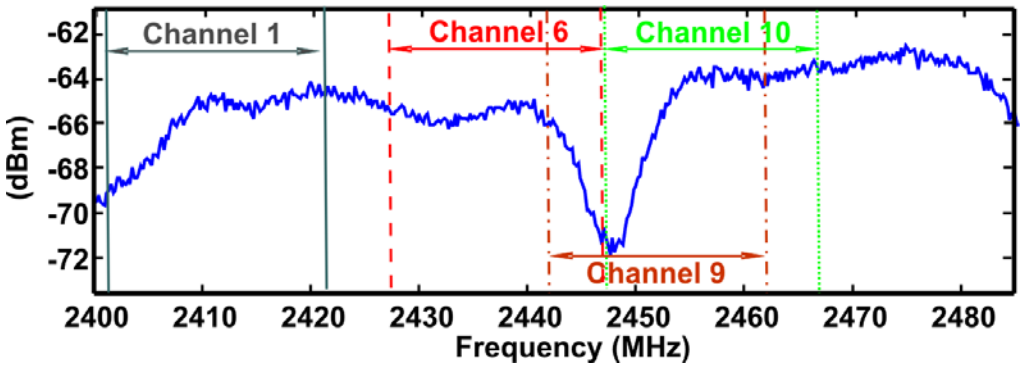

Fig. 5.11: 100 MHz measured Spectrum during the night

5.6.1.1 Aditional example

The relation between the relative channel power and fading depth has been verified by all other measurements. The next example in Fig. 5.12 is a measurement carried out in house DB during almost 21 hours. It depicts the progress for the 4 non-overlapping channels. In the course of this time the phases of a routine day are recognizable. By 23 h begins the time to go to bed. Until approximately 7:30h an idle period, similar to the given in the reference measurement, is recorded during more than 8 hours. Then, for a certain time, a bit longer than half an hour, there is an activity phase during the breakfast before the occupants leave the house to go to the work, reaching a calm state in the next four hours. At 12h somebody returns home and triggers a new activity period, which remains to the end of the measurement.

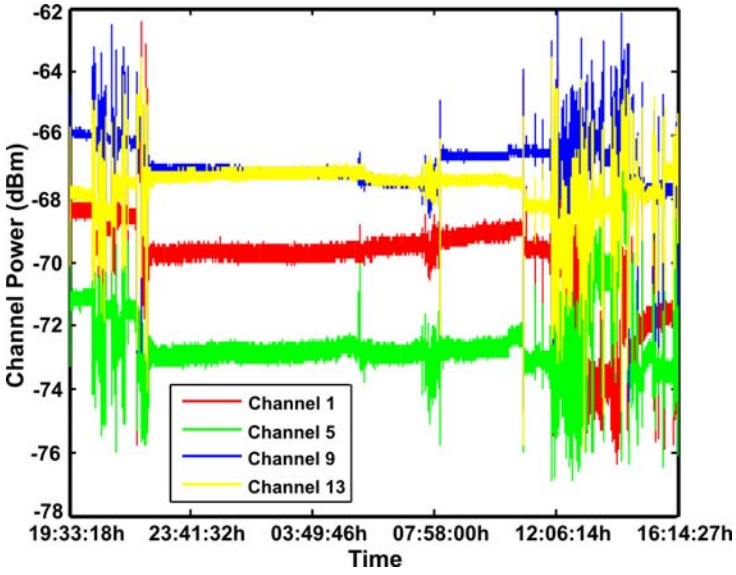

Fig. 5.12: Additional example: Received channel power

The next histograms in Fig. 5.13 resume the results of the correlation analysis between channel power and fading depth during the inactive phase in the night period. The histogram on the left side, Fig. 5.13 a), evaluates the measured power traces, whereas the one on the right uses the spectra normalized to their particular maximum value, as exemplified in Fig. 5.9. In this case, the outcomes show a pronounced dependency, even more linear than in the reference measurement.

In this case the upper channels in the band, from 9 to 13, present less fading depth than the lower ones and therefore, better channel power performance.

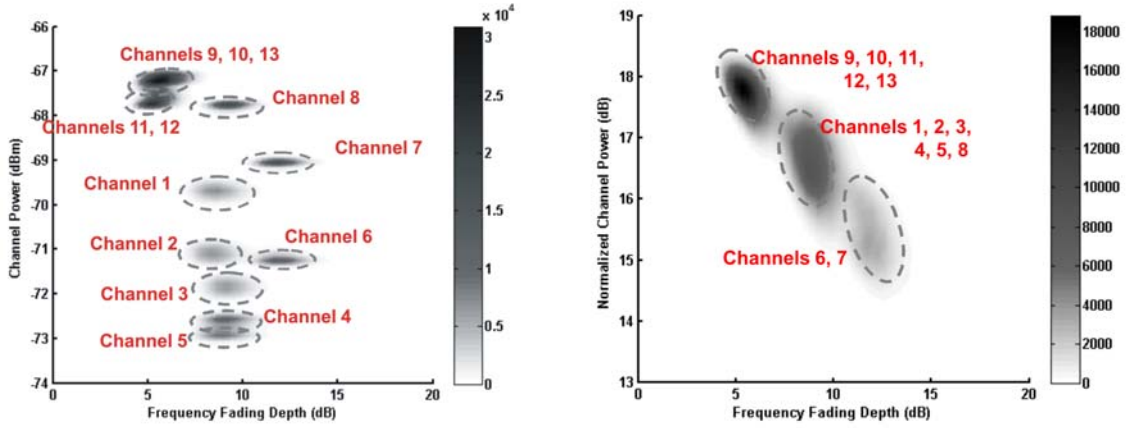

a) 2D-Histogram: (*ChP-F*) b) 2D-Histogram: (normalized *ChP-F*)

Fig. 5.13: Aditional example: Inactive phase

This aditional example consolidates the almost linear relationship between frequency selective channel and normalized power channel during the night period.

5.6.2 Active Phase

During the activity phases (from 20:59h to 00:45h in the measurement used as reference) intense variations are recorded for both parameters, channel power and fading depth. Therefore, the histogram in Fig. 5.14 looks more diffuse than in Fig. 5.8.

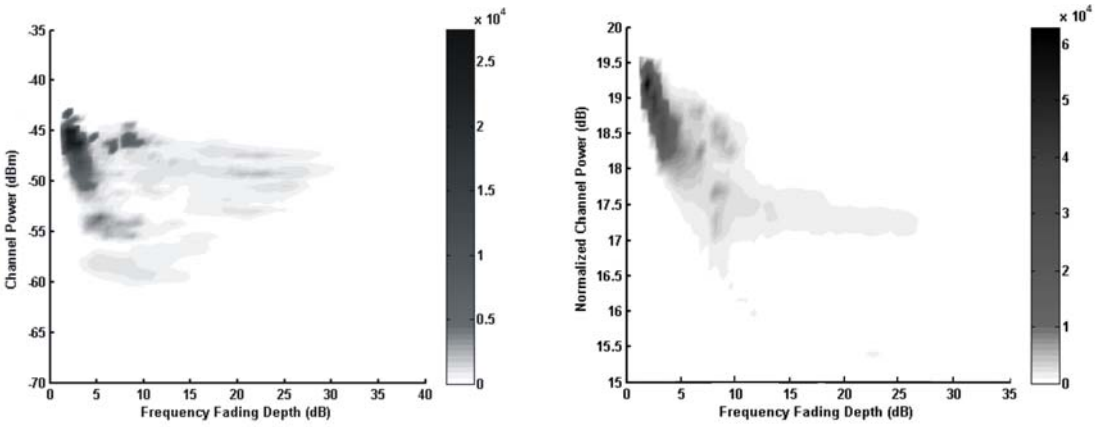

a) 2D-Histogram: (*ChP-F*) b) 2D-Histogram: (normalized *ChP-F*)

Fig. 5.14: Reference measurement: Active phase

In the active phases even though considering the normalized channel powers, Fig. 5.14b), the correlation between both parameters disappear when *F* > 12 dB. Now the single channels are no more distinguishable. Anyway, channel power and frequency fading are interdepending almost linearly up to *F*=12 dB. Higher F values do not largely influence *ChP*. These results were borne out by all other measurements.

Since it is not possible to separate the values belonging to each channel, the same histogram has been calculated apart for the four non-overlapping channels. Fig. 5.15 a), b), c) and d) correspond to channels 1, 5, 9 and 13 respectively, for the reference measurement of the house DA.

The most stable channel along the hours regarding both parameters is channel 13, despite the activities in the rooms. In the case of channels 5, 9 and 13, a linear proportion between the two random parameters can be once again indentified up to 12 dB fading depth. Channels 5 and 9 suffer from deeper fades, the channel power remaining in both cases almost constant, as mentioned before.

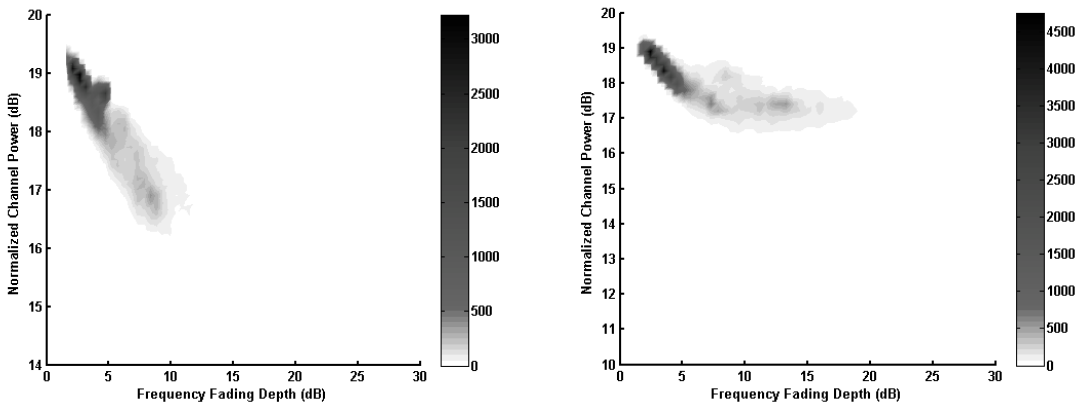

a) Channel 1 b) Channel 5

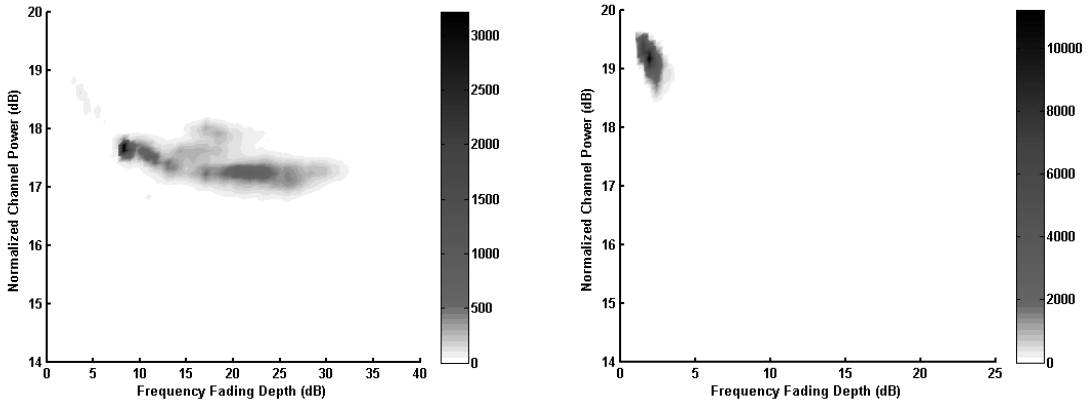

c) Channel 9 d) Channel 13

Fig. 5.15: 2D-Histogram: (normalized *ChP-F*). Reference measurement: Active phase

Furthermore, the measured traces showed that the received channel power as well as the fading depth are non-stationary processes due to people moving around the rooms. Therefore, a more accurate interpretation of this evaluation has been carried out for one channel during different sub-phases of the action period. The channel selected is the number 5, Fig. 5.16, one of the most instable of the reference measurement. The progress of its channel power trace can be divided into four intervals:

- Interval 1: from 20:59:46h to 21:40:20h (40 Min.)
- Interval 2: from 21:40:20h to 22:10:44h (33 Min.)
- Interval 3: from 22:10:44h to 22:30:47h (20 Min.)
- Interval 4: from 22:30:47h to 00:55:36h (144 Min.)

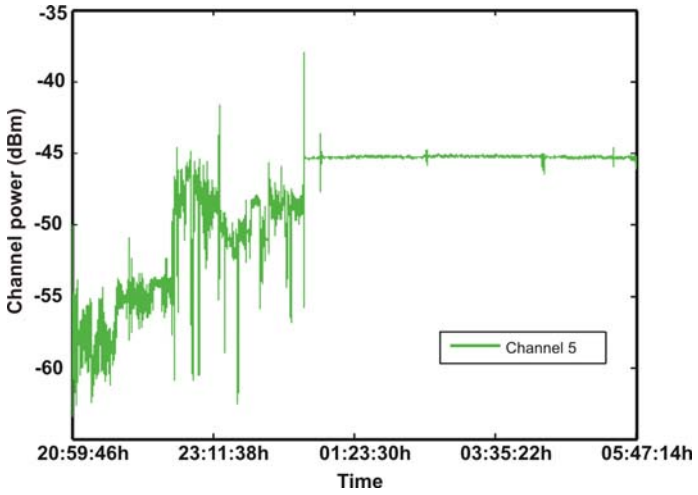

Fig. 5.16: Reference measurement: Channel 5

The goal of this thorough analysis is to evaluate whether this dependency varies in the time or if it is a generalized behaviour. In Fig. 5.17 the histogram on the left illustrates the interval from 20:59:46 to 21:40:20h and the right one from 22:30:47 to 00:55:36h. The first interval shows a wider deviation of the fading values than the second interval. The channel power variation range is around 2.5 dB, except for some cases in interval 1 where the bandwidth of the fade provokes a dramatic reduction of the channel power.

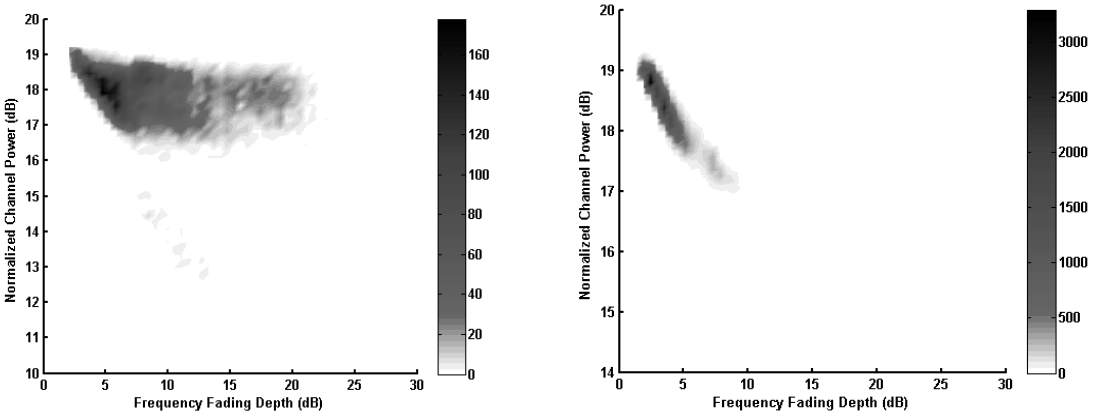

a) Interval 1: from 20:59:46h to 21:40:20h b) Interval 4: from 22:30:47h to 00:55:36h

Fig. 5.17: Channel 5: 2D-Histogram: (normalized *ChP-F*). Reference measurement: Active phase

However, by observing the measured channel power trace in Fig. 5.16, it can be assessed that much deeper incursions are produced in the fourth interval, Fig. 5.17 b), than in the first one, Fig. 5.17 a). It can be diagnosed that those degradations in channel power are caused by variations in the absolute power level during changing situations and not only by the frequency fading depth.

5.6.2.1 Aditional example

The second measurement, Fig. 5.12, is evaluated in an action period from 12:00 to 16:14h and similar properties are observed as in the reference measurement of house DA. The histogram in Fig. 5.18 shows the results for all 13 channels and Fig. 5.19 a), b), c) and d) split them for channel 1, 5, 9 and 13 respectively.

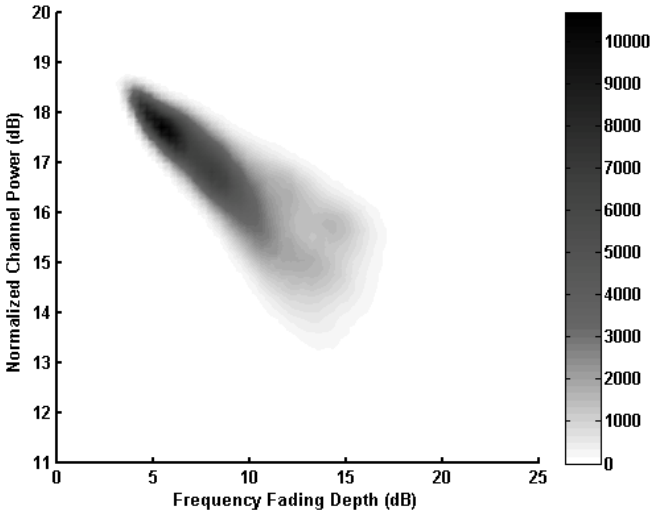

Fig. 5.18: 2D-Histogram: (normalized *ChP-F*). Additional example: Active phase

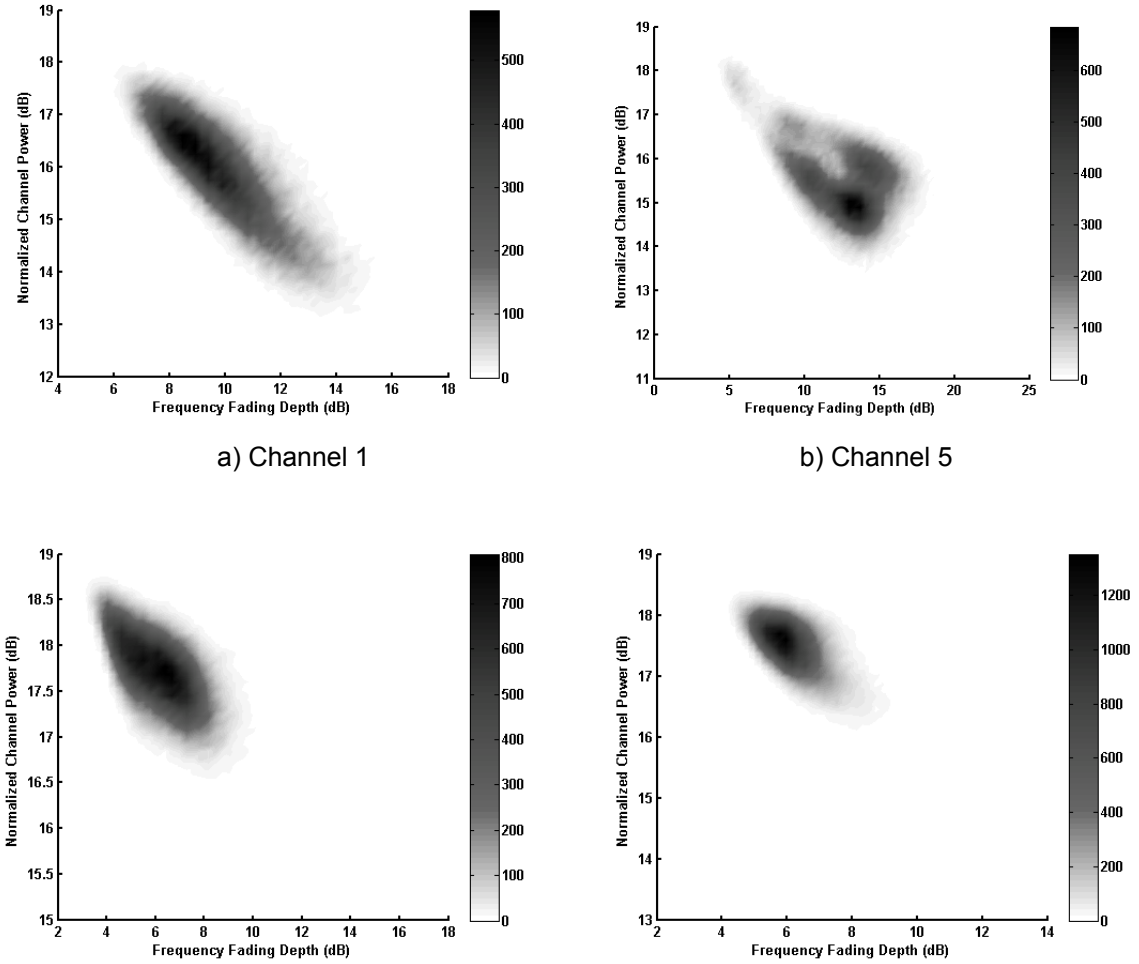

a) Channel 1 b) Channel 5

c) Channel 9 d) Channel 13

Fig. 5.19: 2D-Histogram: (normalized *ChP-F*). Additional example: Active phase

After this analysis of two characteristics of the transmission link, it can be pointed out that frequency fading depth and absolute channel power can not be independently treated for the dynamic modeling. In the following sections, the focus is on the channel power traces to characterize the dynamic channel behaviour for system performance simulations or for channel characteristics prediction for automatic link adaptation and network organization.

5.7 Dynamic Frequency Selection

Among the proposed optimization methods in Section 3.5, DFS and antenna diversity have been evaluated on the basis of the static measurements in Chapter 4. Both of them offer a high achievable gain according to these first assessments. In comparison to antenna diversity, DFS yields higher efficiency and less implementation effort. The advantage of compact, low-cost and low-complexity solutions makes DFS more suitable in the targeted application scenario than the use of multiple smart antennas, both at the transmitter and receiver like in MIMO (multiple-input multiple-output) techniques (e.g. IEEE 802.11n [IEEEn09], not approved).

To implement DFS in WLAN devices, it is sufficient to exchange control packets between the link partners. The control information flow between nodes in order to switch the transmission channel can be performed by means of in-band signaling (e. g. via the framework specified by IEEE 802.11h [IEEEh03] and the methods of IEEE 802.11k, not released) or by an external control network.

Due to these considerations the dynamic frequency selection technique is chosen to overcome the problems presented in Chapter 2. In the following section, the potential of this method in the 2.4 GHz ISM band will be analyzed. Nevertheless, the combination with some of the other techniques mentioned would be possible.

5.7.1 DFS Evaluation

For the analysis of this method a threshold value from 0.5 to 3 dB in steps of 0.5 dB is defined. As introduced in section 5.4 a channel becomes the best one when its channel power exceeds the previous best channel in this parameter. This threshold value is introduced in order to avoid continuous switching between channels. It has been analysed how much time between consecutive switches is needed, i.e. how long a channel tends to be the best one until degradation occurs in its frequency band or another channel becomes the best one. As seen in Fig. 5.3, the variations in spectrum are very fast and therefore, the time between consecutive switches is very short. It is obvious that this duration increases if the threshold is raised. It implies fewer channel switches and less protocol overhead but also less efficiency of the method due to a slow adaptation to the “optimal channel”, Fig. 5.5. The cumulative distribution function of this time duration is depicted in Fig. 5.20 a), corresponding to the reference measurement with a threshold Δ=0.5 dB.

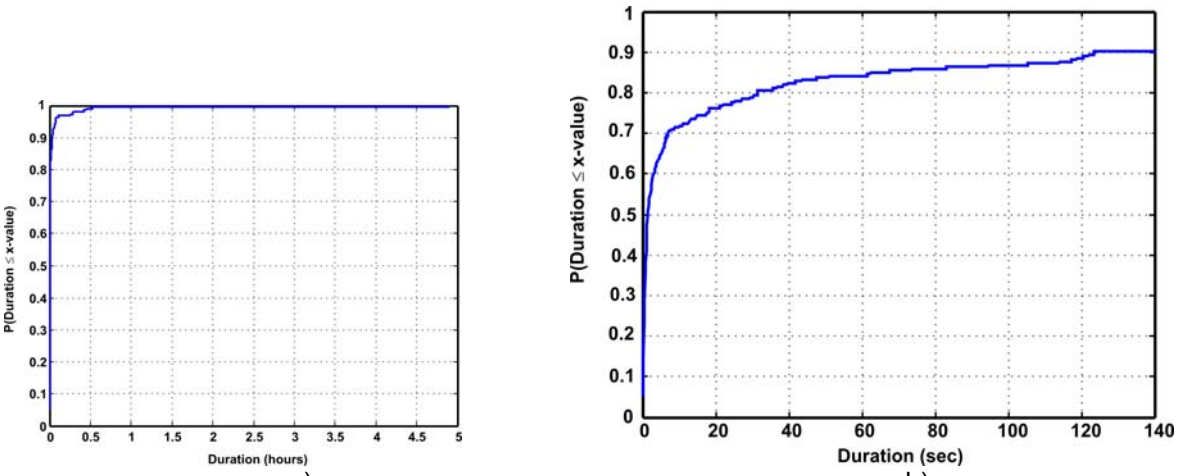

a) b)

Fig. 5.20: a) Duration between channel switches (b) Zoomed)

In this example, with Δ=0.5 dB the total number of switches is 227, and in 90% of the cases the period without changing the transmission frequency is less than two minutes, as shown in Fig. 5.20 b). For Δ=3 dB 30 switches occur with a duration of less than 30 minutes in 90% of the cases.

It can be seen Fig. 5.20 a) that the maximum of 1 of the CDF is reached for a much higher duration value. This effect is due to the idle phases in which no changes occur and the best channel keeps its state for a long time. In the reference measurement, this time represents nearly 5 hours.

The efficiency of the DFS method has been quantified. In Table 5.1, the achieved gains for each measurement are summarized. The maximal frequency selection gain describes the relation between the average received power when using the worst WLAN channel compared to the “optimal channel”. The maximal gain in the measurements is approximately 5 dB in average.

$$G_{max}\ (t) = (P_{optimal\ channel}\ (t) - P_{worst\ channel}\ (t)) \tag{5.5}$$

$$G_{max,lin} = \text{Mean}\left(10^{\left(\frac{G_{max}\ (t)}{10}\right)}\right) \tag{5.6}$$

$$G_{max,avg}\ [\text{dB}] = 10 \cdot \log_{10}\left(G_{max,lin}\right) \tag{5.7}$$

Table 5.1: Maximal gain of DFS

Measurement		$G_{max, avg}$ [dB]
House DA	1	2.73
	2	6.37
	3	6.92
House DB	1	2.96
	2	4.1
	3	1.66
	4	7.53
	5	6.09
	6	6.05
House DC	1	4.1
	2	5.17

However, during certain time phases the gain can be much higher. It can be seen in Fig. 5.4 that the gain of the dynamic frequency selection is more than 15 dB at 21:00h, whereas during the night time is less than average. Therefore, optimizing the transmission frequency according to the current link conditions is an efficient method in home environments, especially if the QoS requirements are more demanding. Also it is very helpful when interferences are acting. In the following section, the effects provoked by microwaves are analyzed as an example of interference for WLAN.

5.8 Microwave Effects

Microwaves are often present in households. They also operate in the 2.4GHz ISM-Band and its influence on the transmission has been analyzed. In Europe the maximum allowed leakage power is limited to 50 W/m^2 in 5 cm distance. The transmit power of the used WLAN measurement setup is 27 mW.

In order to observe the effect of this kind of interferences in the frequence spectrum and the consecuences over the channel power performance, a microwave was switched on several times for a short time interval during two measurements in house DA.

Fig. 5.21 shows the first measurement deteriorated with microwave interference and the moment of such interruption can be clearly recognized.

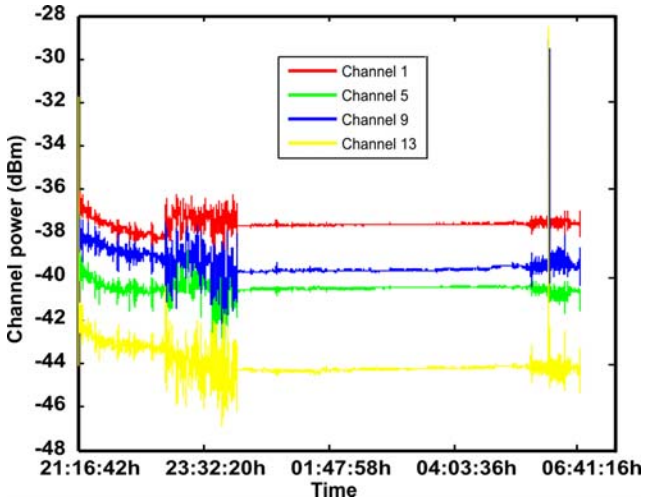

Fig. 5.21: First measurement with microwave interferences

In Fig. 5.22 the second measurement of these characteristics is represented. The first interfered point corresponds to the breakfast time, the second time was detected at 10h approximately and the third one is during the lunch time around noon. Otherwise, the traces are relatively undisturbed during the whole measurement except for these three intervals suffering under interference of the microwave.

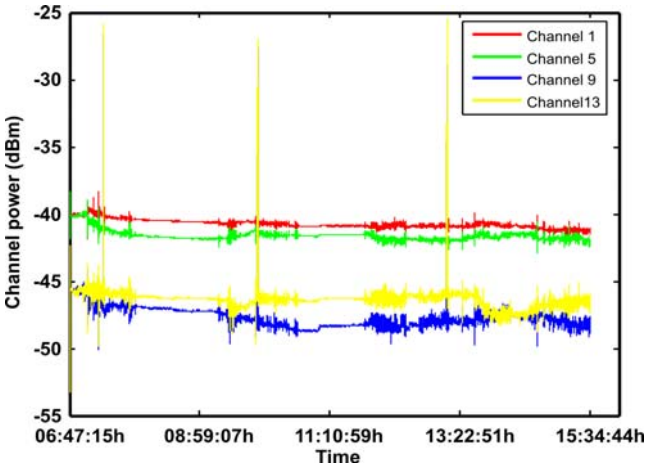

Fig. 5.22: Second measurement with microwave interferences

In Fig. 5.23 the disturbed minutes in the second interference are analysed in more detail by zooming in around 9:45h.

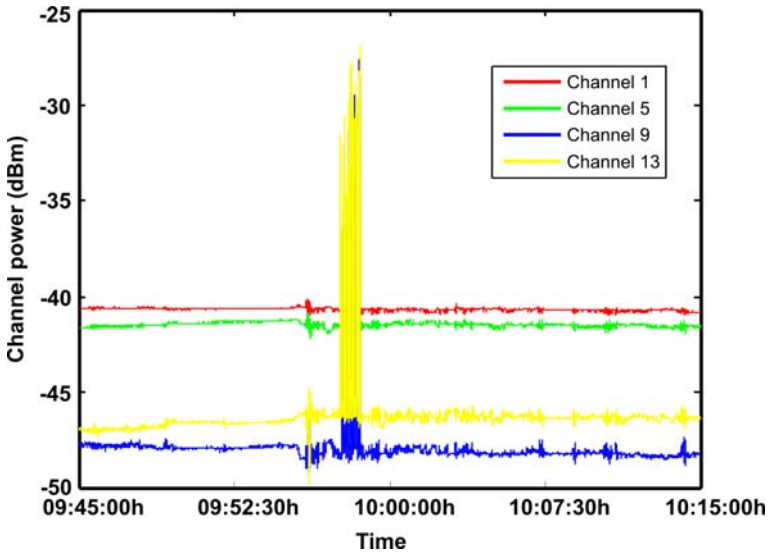

Fig. 5.23: Zoom of the second measurement from 9:45 h to 10:15 h

Fig. 5.24 illustrates a spectrum sequence of 3 measured seconds in two columns, from 9:57:44.109 h to 9:57:47.134 h. It is clear that the most affected channels are those with subcarriers on the frequency band between 2450 and 2470 MHz, i.e., channels from 9 to13. The reproduced sequence provides evidence that microwaves interfere intermittently like an impulse form. Due to the resolution of the utilized equipment, consecutive spectra are approximately separated by 150ms. The enormous impulse up to 20 dB provokes a large augmentation of the channel power seen in Fig. 5.23.

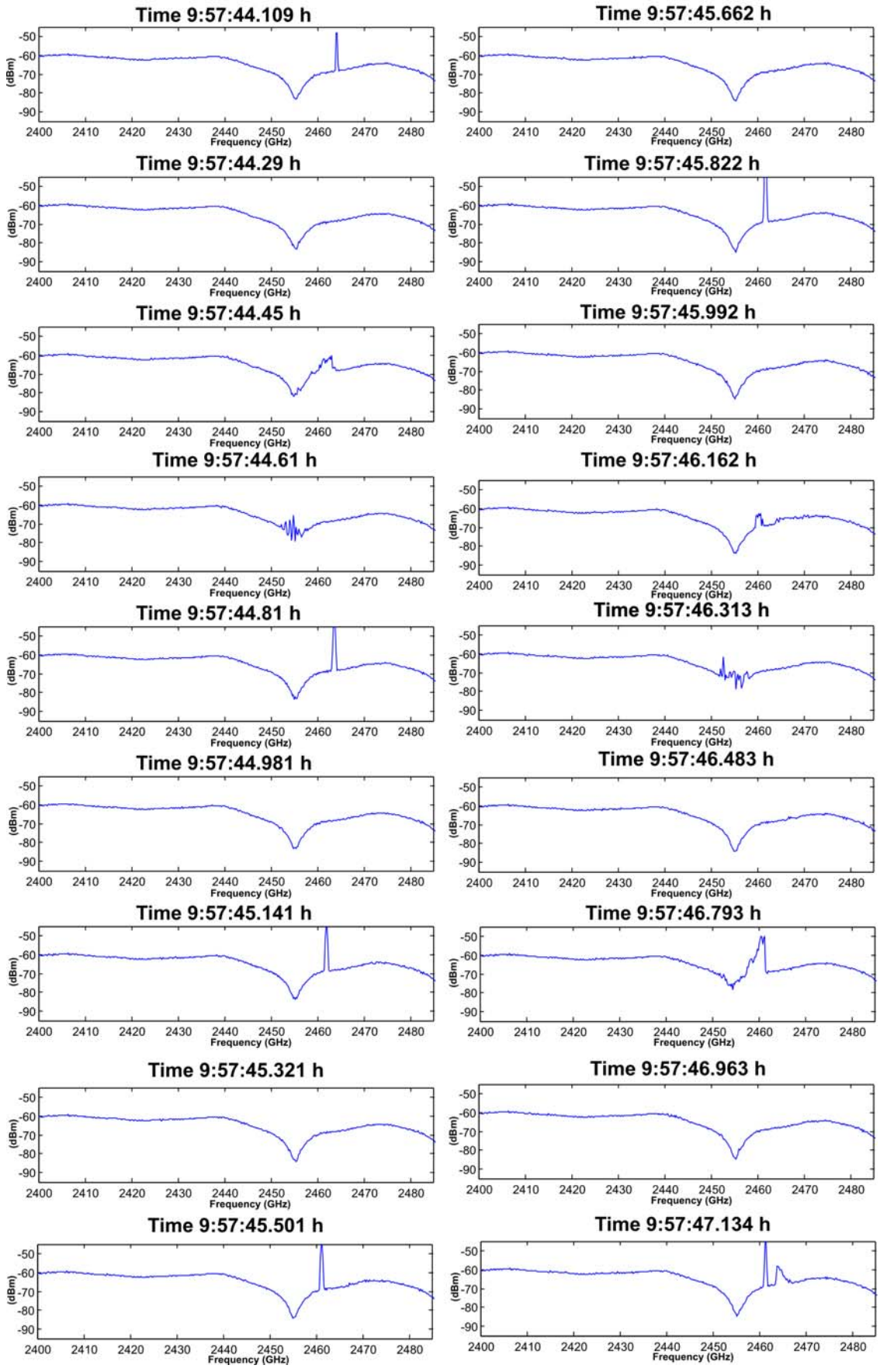

Fig. 5.24: Three seconds of the spectrum sequence from 9:44:109 h to 9:47:134 h.

The measurements show that the microwave irradiation is modulated with a half cycle of 50Hz and the interfering power is up to 20 dB higher than the transmitted signal power. The maximum power spectrum and the corresponding frequency of a microwave impulse are not constant but time-varying during the measurement. Therefore, in addition to the characteristics of the measured transfer functions, the effects of powerful interferences must be taken into account in the 2.45 GHz ISM-Band. The time dependent frequency position of the microwave impulse as well as its time-varying bandwidth and power must be considered.

5.9 Summary of the measurement results

In this chapter, a setup for carrying out in-house dynamic measurements in the 2.45 GHz ISM band has been described. With this configuration the time-varying transmission channel characteristics have been detected. The numerous measurements, approximately 200 hours, carried out in three different household scenarios, DA, DB and DC, have been thoroughly analyzed. The 4 non-overlapping channels were investigated with regard to the received channel power. In addition to this analysis, the channel fading was also evaluated.

Moreover, the dynamic frequency selection proposed as a method to improve wireless LAN capacity in home environments has been evaluated. It has been analyzed how often the channel has to be changed when always selecting the best channel. Short switching times were observed corresponding to the rapid fades emerged. Finally, it could be shown that this simple improvement method yields a significant gain and provides an effective and efficient technique to counteract the partly troublesome dynamic behaviour of WLAN channels.

Finally, a number of additional results regarding the changing environment and effects of interferences such as microwaves have been presented.

6 Modeling of the Dynamics of wireless In-House Channels

Channel modeling is an important research topic in wireless communications. The application areas for channel models are numerous. This chapter emphasizes the main goals and usefulness of modeling the dynamics of wireless channels in two fields of their application.

The analysis and design of wireless MAC protocols, coding schemes and transmission algorithms can significantly benefit from an understanding of the channel quality variation. All the optimization approaches to improve the overall system performance presented in Section 3.4.3 depend on the dynamic characteristics of the radio channel. Their parameters are adapted according to the state of the channel.

For systems that require periodic channel estimation such as MIMO systems, the knowledge of the time-varying characteristics is very important. A link with a short coherence time (Section 2.4.1.1) needs a higher rate of channel estimation.

From the point of view of error control mechanisms, the channel coherence time also determines the separation between packet retransmissions. In the digital broadcasting context, the packet length is often chosen to be longer than the average fade duration. The size of the interleaver should be larger than the fade duration to overcome burst errors so that corrupted bits can be recovered by error correction coding.

Characterization of depth and dynamics of fades is also important in the design of automatic gain control (AGC) loops needed for transceivers using high-order modulation schemes. AGC is used to compensate for variations in the channel gain, so that a nearly constant amplitude signal is used for symbol detection. Indoor localization represents another area where the dynamic channel model is essential, since in some methods the location is mainly accomplished by means of the received power.

In all these cases, the main goal of the channel model is to provide the system with a measure of fading speed. This work focuses on two applications: the prediction of channel characteristics for automatic link adaptation and network organization, and the simulation of system performance.

The diverse optimization techniques for the MAC parameters, transmit power, transmission mode, packet length and transmission frequency to improve the efficiency of wireless LAN for multimedia home networks are adapted depending on the state of the wireless channel. In order to design control algorithms, it is crucial to determine what the dynamic channel behavior is. This chapter analyzes the influence of moving obstacles, such as people over the propagation path inside a house, and the effect on received signal quality in a WLAN.

Also, characterizing the dynamic channel behavior is vital for a successful deployment of future wireless systems or to improve the current IEEE 802.11 based WLANs. Hence, it is

essential to provide simulations for realistic channel situations.

6.1 Background and literature research

There are two reasons why the channel can be referred to as dynamic. The first reason is due to the motion of the user terminal and the second one is the changing environment modifying the conditions of the transmission along the time, although transmitter and receiver remain static.

As explained in previous chapters, this work concentrates on fixed wireless links, i.e., the time variations are provoked by people moving around the room or by displacing pieces of furniture, as shown in the measurements presented in Chapter 5. These movements or changes are totally random and on that account cannot be predicted.

Since the received signal quality has a crucial impact on the network performance, accurate prediction of the received SIR (signal to interference ratio) is important for automatic optimal network deployment. The measurement of the temporal variation of the received power is an important contribution to the knowledge of the dynamic WLAN channel behavior. This ratio determines several important attributes like packet loss, which directly affect the QoS. Moving obstacles in the propagation path lead to selective frequency fades that emerge within the WLAN channel frequency range of 20 MHz. Several analyses have been carried out to determine the most convenient set of parameters to characterize fading depth and channel power, (*F*, *ChP*), for modeling. The correlation between both parameters is obvious and almost linear up to F = 12 dB. In the following sections, the focus is on the channel power traces for the dynamic modeling.

There is a number of publications describing modeling of the time-variance of in-house channels. In [WaMo95] a Finite-State Markov Channel (FSMC) is applied to shape the time-varying SNR at the receiver. [TuVanNo98] uses a Hidden Markov Model (HMM) to simulate the channel fading. In [ThVanDerEn02] a stochastic model is introduced specifically for indoor environments that reproduces the time variance of fixed links due to moving objects on the transmission path. They attempt to represent channel quality variation using a finite state birth-death Markov model [GuSa06]. They also outline a method to compute the parameters of the model based on measured traces taken from 802.11b access point networks using common hardware. Sajadieh studied and characterized the dynamics of a correlated Rayleigh fading channel with known phase. The model follows a continuous-time Markov double-chain for the random fading process with the Markov states corresponding to the quantized amplitude levels.

The assumption of all these approaches for dynamic channel modeling is that the indoor channel process remains stationary. However, this simplification of the in-house channel behavior cannot be made, as clearly shown in Fig. 5.4, where the statistic properties of the received channel power change and depend on the time of the day. This becomes problematic for the analysis and validity of the current time-varying channel models. Only two studies report non-WSSUS channel models (section 2.4.1.1). Nevertheless, they have not been developed for in-house environments. In the first investigation [JaMa05] a complex model is proposed based on a non-stationary vector autoregressive (AR) process to model the channel taps. They also present a Yule-Walker type approach to estimate the parameters of this vector time-frequency AR model. The second paper [AhFeVa05] presents the analysis

of the methodology and the interpretation of the results obtained in the measurement of the temporal Ricean *K*-factor and the time-autocovariance function of the received power for fixed narrowband wireless links in urban residential environments.

This chapter investigates the prediction of received signal statistics and investigates the influence of variable fading caused by the movement of people in the propagation path and its effect on the control algorithms for optimal network deployment and performance.

6.2 Dynamic channel model for network controllers

The quality of wireless links is decreased significantly by time variations of a channel. Current off-the-shelf devices are limited in their ability to adapt to these channel variations because they are designed with fixed values for most system parameters such as transmit power or transmission frequency, as dicussed in Section 5.7. The values for these parameters must be adjusted to maintain a desired link quality, by benign channel conditions as well as in a severely degraded channel.

Without adaptation at the link and physical layers, the channel variations would not achieve the QoS recommendations for applications in the multimedia network.

A key problem in wireless multimedia networks is to maintain acceptable throughput and delay over time-varying channels. The channel variations are noncontrollable, and their dynamic range is so large that it would not be efficient to design the link radio for the worst case with regard to, for example, the transmit power or data rate.

Results reported in [BaSu96] [ZoRa97] show that adapting the MAC layer packet schedule by deferring transmission when the radio channel is in fade, significantly improves link efficiency. Similarly, results in [LeSri98] and [Lettieri97] demonstrate that continuous adaptation of link-layer error control and packet length of the transmitter can also enhance the performance.

For an efficient implementation of such link adaptation techniques, it is necessary to adapt the speed of their algorithms to the dynamic channel behavior. In this section, a channel model is presented for adaptive control algorithms to efficiently meet the application requirements under widely varying channel conditions.

6.2.1 Action-Break-Idle Channel Model

The basic idea of this model is to classify the different characteristics of the channel into two stages: “active” and “inactive”. As shown in Fig. 6.1, the “active” stage is subdivided into *action* (A) and *break* (B) states.

The classification criterion is a margin Δ that indicates the variation of the channel power at the receiver along the time:

$$\Delta = ChP_t - ChP_{ref} \qquad (6.1)$$

where ChP_t is the current channel power and ChP_{ref} is the reference channel power, i.e., the last value in which a considerable variation ($> \Delta_{action}$) occurred. This reference value is updated along the time during the *action* state.

Therefore, while $|\Delta| < \Delta_{action}$ for at least T_{idle}, the model remains in (*I*) state. As soon as $|\Delta| \geq \Delta_{action}$, it switches to the *action* state (*A*) in order to be able to quickly adapt the parameters to the varying channel. This indicates that there are significant movements or changes in the environment and the timer t_{idle} is set to zero. During the stay in *(A),* t_{idle} can be either successively incremented or reset. At the same time, the parameter ChP_{ref} is refreshed as follows:

$$t_{idle}^{Action} = \begin{cases} t_{idle} ++ & \text{when} \quad \Delta < \Delta_{action} \\ 0 & \text{when} \quad \Delta \geq \Delta_{action} \Rightarrow ChP_{ref} = ChP_t \end{cases} \tag{6.2}$$

t_{idle} can be augmented until it is longer than T_{break}. At this moment, the channel will turn in a break state. Therefore, the activity phases alternate between (*A*) and (*B*) states. In break state, t_{idle} is incremented until the channel switches to the steady idle state (*I*) when t_{idle} μ T_{idle}, e.g. during the night time.

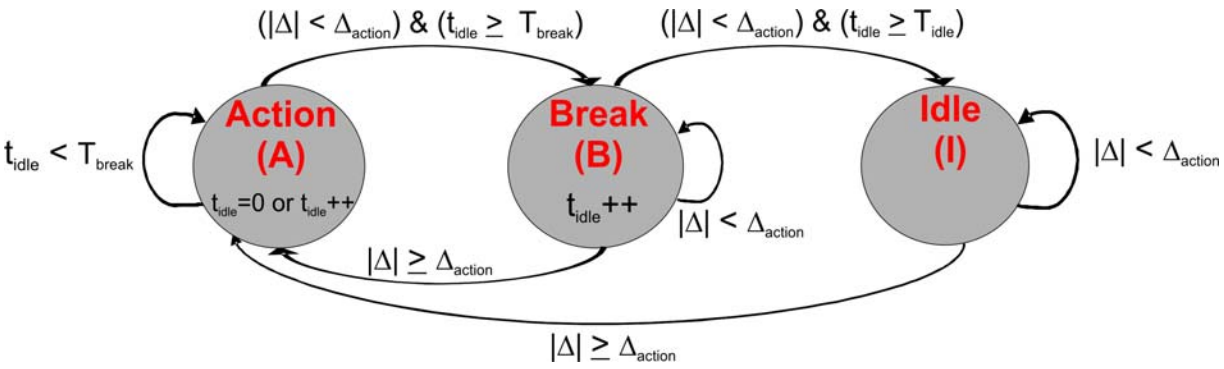

Fig. 6.1: Action-Break-Idle channel model diagram

Fig. 6.2 shows an arbitrary signal strength trace for one hour. In this example, the selected parameters are Δ_{action} = 2 dB, T_{break}= 30 sec. and T_{idle}= 5 min. It is indicated during each time interval what state the channel would be and for how long.

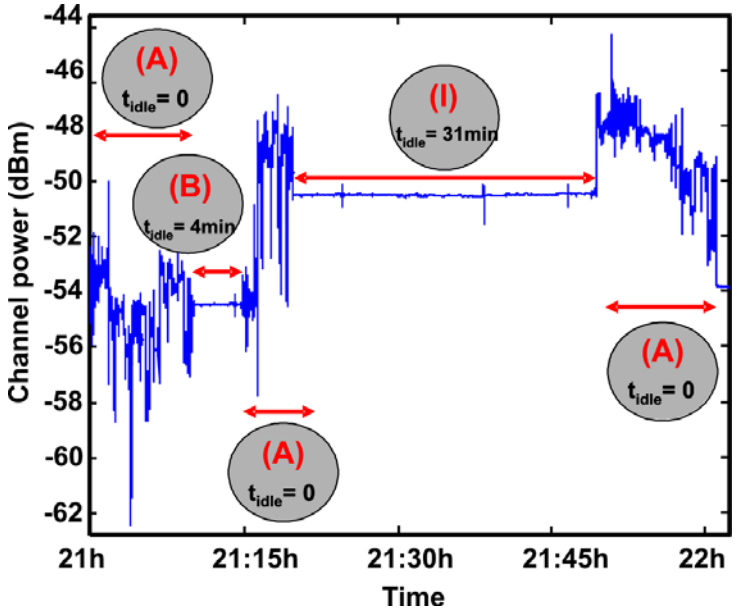

Fig. 6.2: Action-Break-Idle channel model example

The actual values for the thresholds Δ_{action}, T_{break} and T_{idle} depend on the control algorithm which uses the model. The overhead caused by the channel adaptation mechanisms has to be carefully considered when the parameters are selected.

6.2.1.1 Parameters

In order to determine a reasonable value for the parameter Δ_{action}, the channel power variation between two consecutively measured time points, $\gamma(n)$, separated by approximately 150 ms, has been analyzed for all the available measurements. The sequence $\gamma(n)$ is defined as follows:

$$\gamma(n) = ChP_{n+1} - ChP_n \tag{6.3}$$

where ChP_n represents the channel power samples from the measurements introduced in chapter 5.

In this context, the cdf of $\gamma(n)$ has been calculated and in Fig. 6.3 a) represented. The biggest measured difference between two samples is 12 dB. In the zoom in Fig. 6.3 b), it can be seen that in 99.34% of the cases, γ is smaller than 1 dB.

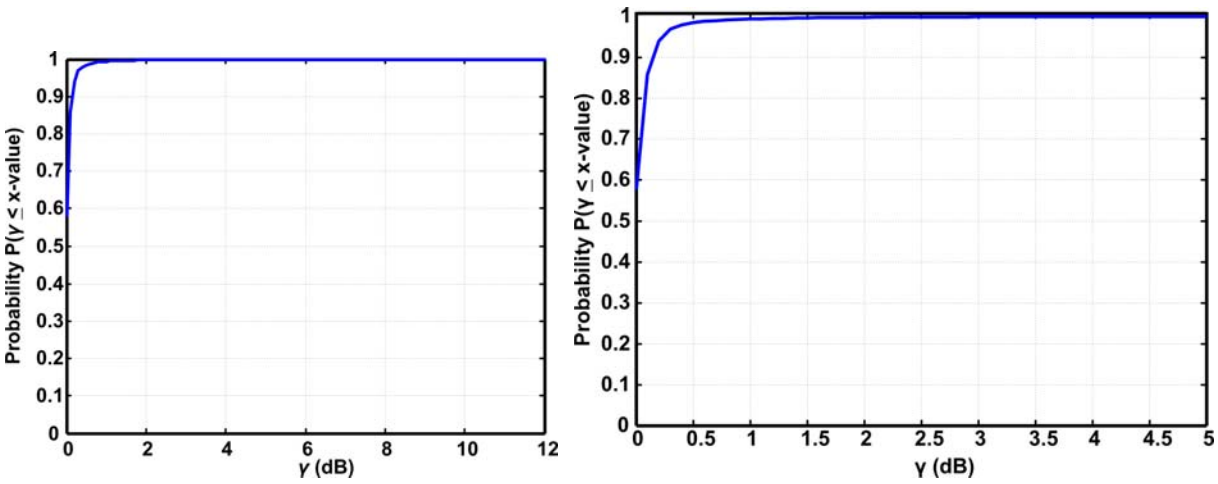

a) b)

Fig. 6.3: γ(n) cdf for all the measurements

Moreover, the active phases have been separately considered, since during the long night periods the variation γ(n) is clearly smaller than 1 dB in all cases. The results for two measurements during the active phases, (*A*) and (*I*) states, have been extracted. The selected measurements are the same ones, which were also analyzed individually in Chapter 5, the reference measurement and the additional example, and they are here newly illustrated in Fig. 6.4.

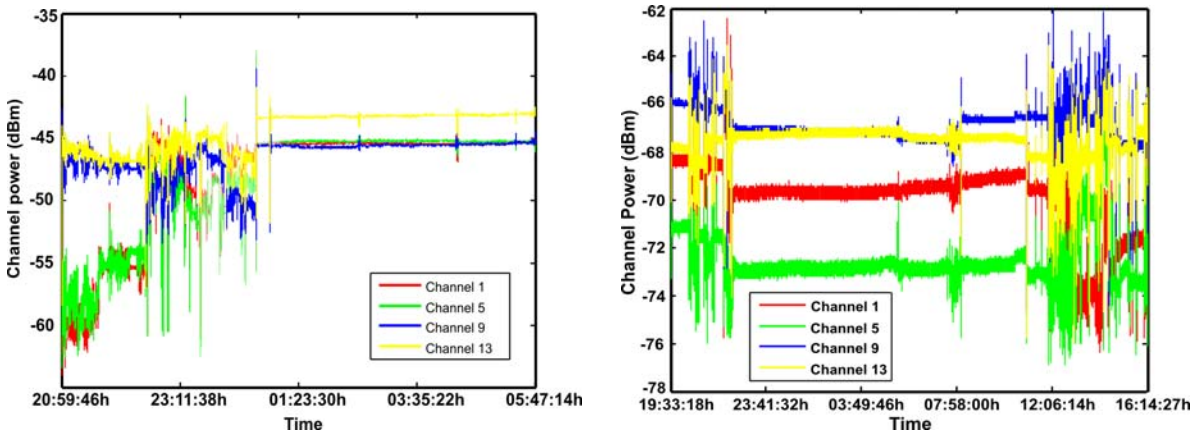

Fig. 6.4: a) Measurement 1 (reference) b) Measurement 2 (additional)

The corresponding sequences γ(n) for channel 1 are depicted in Fig. 6.5 a) and b) respectively for the total measured time span.

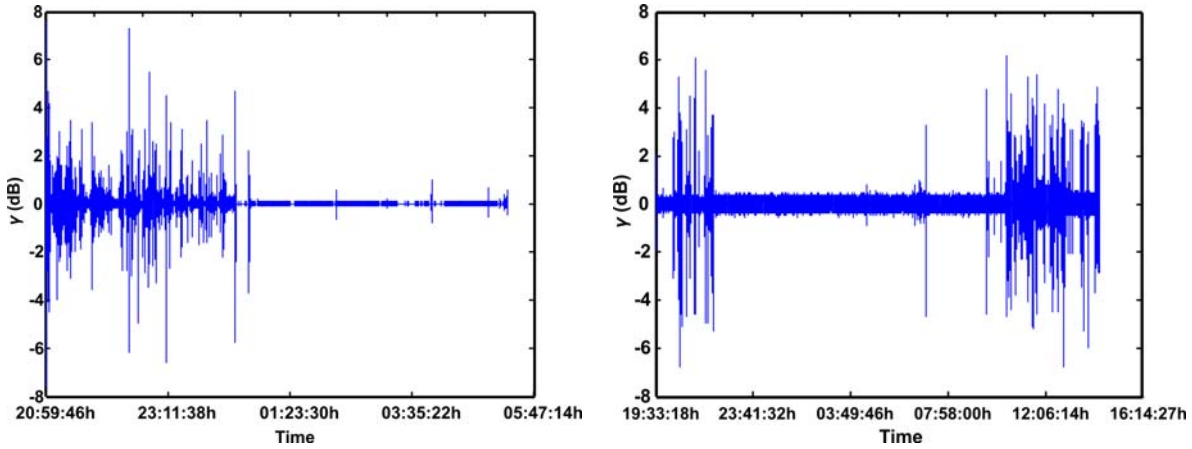

Fig. 6.5: γ(n) sequence for a) measurement 1 (reference) and b) measurement 2 (additional)

Considering only the active periods, the statistics listed in the Table 6.1 from the γ_{active}(n) cdf are obtained.

Table 6.1: Values of the γ_{active}(n) cdf for measurements 1 and 2

γ_{active}(dB)	**Measurement 1** (reference measurement)	**Measurement 2** (additional example)
≤ 1	98.46%	98.29%
≤ 2	99.64%	99.63%
≤ 3	99.88%	99.89%

Therefore, during the active phases, in 98.46% and 98.29% respectively, γ is smaller than 1 dB. As expected, this value is reduced in comparison to when the whole measurements (99.34%) are considered. According to the results, between 1 and 2 dB seems to be adequate for the threshold value Δ_{action}. In order to specify a precise value in this range by means of the correlation study between channel power and fading depth (section 5.6), the meaning of channel power variation in connection with fading depth has been investigated. The correlation is not obvious, since as already explained, more effects than frequency selective fading are provoking time-varying received power.

Based on Fig. 5.14 and Fig. 5.18 it can be interpreted that a power variation from 0.5 to 1 dB (depending on the fade bandwidth) could have been produced by a fading depth of 2 dB. A fluctuation from1 to 3 dB is related to a degradation of 8 dB and the power varies from 4 up to 5.5 dB with a fading depth of approximately 12 dB.

Based on these evaluations, Δ_{action} = 1.5 dB is selected.

To determine a value for the threshold T_{break}, diverse studies have been carried out regarding times. First, fifteen seconds of the sequence γ(n) of the Fig. 6.5 a) are zoomed in. Fig. 6.6 shows this time interval with the rapidity of the variations. In an active phase, large fluctuations of the channel power can continuously appear.

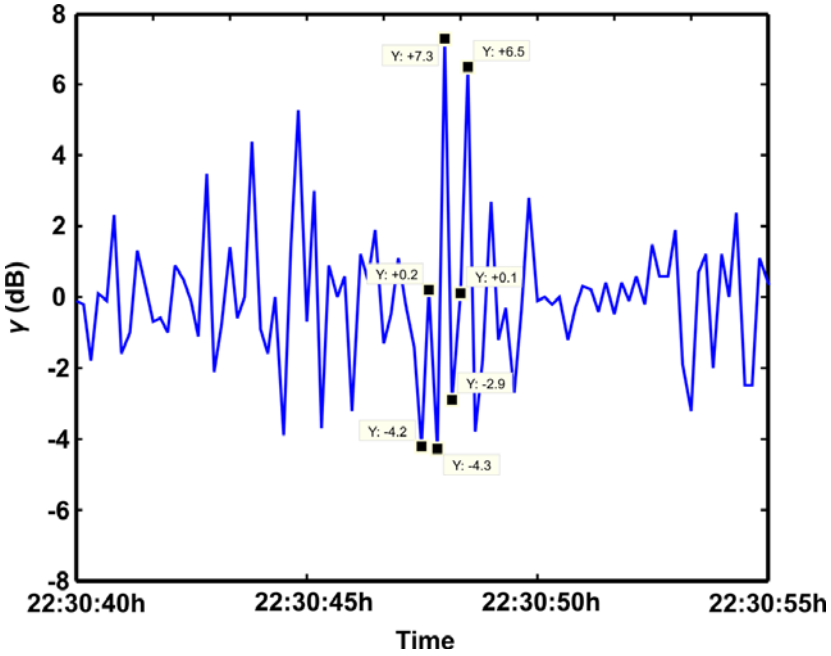

Fig. 6.6: Zoom of the $\gamma(n)$ sequence for measurement 1

The goal is to obtain the time period in which the channel variations are not greater than Δ_{action} to achieve a *break* state. During this state, the requisites to adapt the algorithm parameters are less restrictive than in the *action* state because of the absence of significant changes. Therefore, a compromise should be found between quick adjustment and overhead by channel adaptation. Long and unnecessary intervals in the *action* state should be neglected.

Taking into account a practical implementation of the channel model in a WLAN system, the channel power values are provided by receiving an OFDM frame. For a WLAN system (T_{symbol} = 4µs), during the interval of 150 ms between measured samples of channel power, a total of 37500 OFDM symbols can be sent. As illustrated in Fig. 3.8, an OFDM frame has a variable number of OFDM symbols in its data field. In Table 6.2 are listed the number of symbols per OFDM frame corresponding to the available data rates for IEEE 802.11 *g*. Thereby, it is considered a packet length of 1500 bytes, since it is the maximal user data quantity in an ethernet frame in IP-Networks according to the Path MTU Discovery [MoDe90]). To create a MAC frame, the LLC (logical link control) layer provides the IP packet with an 8 byte header. Furthermore, a MAC-layer extension of an additional 24 byte long header and a 4 byte CRC (cyclic redundancy check) sequence deliver a PSDU length of 1536 byte. The table also provides the number of OFDM frames that can be transmitted during this period of time taking into account the 13 OFDM symbols, which form the preamble and signal field of each frame.

Table 6.2: PSDU length =1536 Byte

Data rate (Mbit/s)	Modulation	Code rate	OFDM Symbols /OFDM Frame	OFDM Frames /150 ms
6	BPSK	1/2	513+13	72
9	BPSK	3/4	342+13	106
12	QPSK	1/2	257+13	139

18	QPSK	3/4	171+13	203
24	16-QAM	1/2	129+13	262
36	16-QAM	3/4	86+13	374
48	64-QAM	2/3	65+13	472
54	64-QAM	3/4	57+13	525

For the 6 Mbps mode, hardly 72 frames can be transmitted in 150 ms., whereas for the 54 Mbps mode this value increases to a total of 525 OFDM frames. That is a large number of frames and therefore, the measurement resolution of approximately 7 acquisitions per second seems not precise enough to determine the parameter T_{break}. Hence, an estimation of the channel coherence time is carried out.

As described in Section 2.3.2.2, the movement of the transmitter and the receiver as well as the continuously changing environment, produce so called Doppler Effect, whereby a frequency shift of the spectrum occurs. In a house, the fast fluctuations are produced predominantly by people moving around the room. Given that a person moves with a maximal velocity v_{max} =1 m/s and f_0 =2.4 GHz (frequency band of the modeled dynamic measurements), according to (2.10) a Doppler frequency can be calculated as $f_{D_{max}}$= 8 Hz. Based on (2.13) a coherence time, T_c, of 52.875 ms is obtained. Therefore, from one sample to the next available one, the channel cannot be considered as stationary. During T_c, the channel is considered, by definition, not to be changing. Thus, a time duration slightly longer than T_c is reasonable for T_{break}.

Based on all these evaluations, $T_{break}=1.5 \cdot T_c \approx 75$ ms is selected.

To calculate T_{idle}, further analyses of the more than 200 measured hours have been carried out. This should ensure that realistic duration of idle periods during the active phases will be determined. In that study, the inactivity periods of longer than one hour have been eliminated. In the remaining active phases, the duration in which the channel lasts with a variation shorter than Δ_{action}= 1.5 dB has been calculated. The resultant cdf for the 4 non-overlapped channels in all measurements is zoomed in and shown in Fig. 6.7.

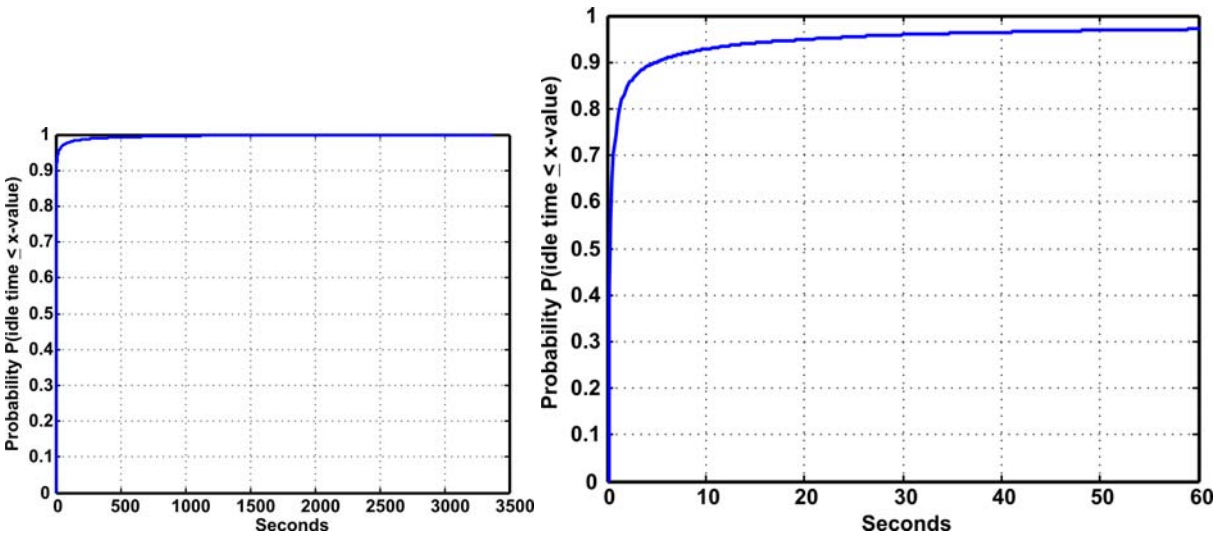

Fig. 6.7: Cdf of the channel power variation shorter than Δ_{action}= 1.5 dB during the active phases

Very seldom (1% of the cases), the “silence” intervals during the active phases are longer than 340 seconds. More frequently (10% of the cases), this period descends to 5 seconds.

Therefore, T_{idle} of 20 seconds (5% of the cases) is a good trade-off for the parameter as a threshold to switch to the steady idle state (*I*).

This general wireless channel model is applicable to different algorithms and could be modified according to their individual requirements. As an example, its use for dynamic data rate adaptation is presented in the following section.

6.2.1.2 Application: Data rate adaptation

The efficiency of a dynamic rate adaptation technique depends on a suitable reaction to the varying characteristics of the channel.

Current data rate adaptation algorithms implemented in off-the-shelf WLAN products such as ARF (Auto Rate Fallback) are based on packet loss statistics. They do not consider other reasons for packet losses such as, for example, collisions with competing transmissions. In this specific case, a reduction of the data rate is not beneficiary. On the contrary, the opposite effect is achieved because the channel will be occupied for longer time.

Within the framework of a research project funded by the German Federal Ministry of Economics and Technology, a new dynamic rate adaptation algorithm considering these aspects has been proposed. This algorithm computes parameters for the available data rates, which need to be adapted dynamically.

The requirements for the performance of the receiver specified by the IEEE 802.11 *a*/*g* are listed in Table 6.3.

Table 6.3: receiver performance requirements specified by the IEEE 802.11 a/g

Data rate (Mbit/s)	Minimum sensitivity Th_i (dBm)
6	-82
9	-81
12	-79
18	-77
24	-74
36	-70
48	-66
54	-65

The suggested algorithm takes into account the signal to interference plus noise ratio (SINR) and varies the threshold values for the performance requirements in a dynamic way as follows:

$$Th_i = a_1 \cdot Th_i + a_2 \cdot SINR \qquad a_1, a_2 \geq 0 \qquad SINR: \text{current } SINR$$
$$a_1 + a_2 = 1 \tag{6.4}$$

The adaptive minimum sensitivities Th_i are calculated based on error statistics of the last n transmitted OFDM frames. The parameters a_1 and a_2 weight the current values of Th_i and SINR and depend likewise on the dynamic characteristics of the channel.

The integration of the channel model presented in the previous section enables an efficient solution to adjust these parameters. At the receiver side, the channel state (*action*, *break* or *idle*) can be detected. In the *idle* state, the parameter adaptation rate should be much slower than in the active state. This can significantly increase the performance of the algorithm. Recalculation and measurement of link parameters can be restricted to relevant cases. When compared to other approaches, this data rate adaptation technique is able to send consecutive OFDM symbols without unnecessary computing and measurement overhead.

Therefore, the parameters should be adapted in each state as follows:

- *Action* (*A*): current SINR varies strongly in very short intervals $\Rightarrow a_1\downarrow$ ($a_2\uparrow$), $n\downarrow\downarrow$
- *Break* (*B*): current SINR does not vary in short intervals $\Rightarrow a_1\uparrow$ ($a_2\downarrow$), $n\downarrow$
- *Idle* (*I*): current SINR does not vary for long intervals $\Rightarrow a_1\uparrow$ ($a_2\downarrow$), $n\uparrow$

6.2.1.3 Model simplification

It is possible that, in some simple applications, the functionalities to be executed during *break* and *idle* states by the practical implementation are the same. Then, it would be feasible to simplify the channel model from three to two states: *action* and *idle*.

This would not be practicable for much more complex techniques such as, for example, dynamic frequency selection, whereby diverse parameters play an important role. This algorithm will profit the *break* state not only to measure the current channel conditions but also to scan all the other channels to confect a ranking list. Thus, during the active phase, when it will be necessary to select another transmission frequency, an updated channel list is available for the imminent switch. On the contrary, in the *idle* state, a stable channel is chosen and it remains for a long time, even for hours. Therefore, it should be sufficient to observe the current channel and to occasionally update the ranking list in order to reduce a useless overhead.

6.3 Dynamic channel model for simulation

In the previous section, a model as controller for the parameters of different link adaptation algorithms has been presented. It is more critical to select the adaptive techniques that provide performance improvements with regard to QoS for multimedia sessions. In order to evaluate link layer algorithms, physical layer algorithms or a combination of both, simulations with detailed channel models have to be conducted. Thus, the effectiveness of the proposed adaptive techniques can be validated.

For that purpose, two channel models are presented in the next sections. The objective of the first model is the reconstruction of typical traces to efficiently simulate a realistic dynamic channel using a minimum number of parameters.

When the low level processes are not of interest and it is more important what the physical link delivers to the MAC layer, an abstraction of the physical level can then be carried out. Hence, in Section 6.3.2 a simple stochastic model will be introduced. This model is described by few parameters to generate bit error patterns corresponding to the characteristics of wireless in-house transmissions.

Both models can substantially improve the design of efficient algorithms and can be useful for simulations that require low complexity models.

6.3.1 Physic layer simulation: Hierarchical Dynamic Channel Model Approach

The measurements in Chapter 5 have shown that the received channel power as well as the fading depth cannot be modeled by a stationary process. This is the goal for a novel approach of dynamic channel modeling. It is based on a hierarchical model. On the first level, the channel characteristics are coarsely described for a long period of time (hours). On the second level, the fast variations (seconds) are shaped. In Fig. 6.8 the basic structure of this model is outlined.

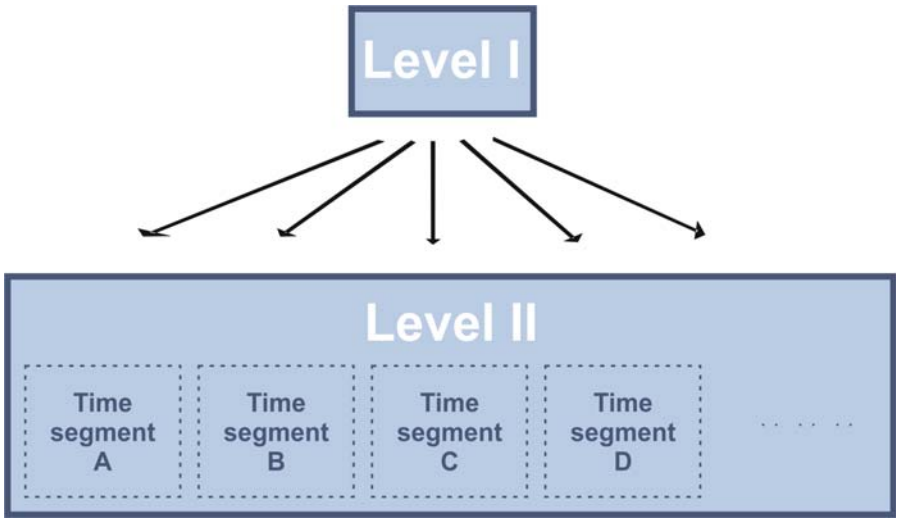

Fig. 6.8: Hierarchical dynamic channel model approach

6.3.1.1 Level I: Macroscopic Characteristics

The autocorrelation function of the measured traces φ_{xx} can be intuitively understood as an indicator of how the random received channel power changes with time. Since the process is nonstationary, this function is time-dependent $\varphi_{xx}(t, t+\tau)$. In this case, it is important to analyze the variations of the statistical properties throughout the day. Thus, the times of the day in which φ_{xx} changes more quickly are those with maximum activity rate in the environment.

In (6.5) an autocorrelation function of the received channel power has been defined:

$$\varphi_{xx}(n,n+k)=\frac{1}{M}\sum_{m=1}^{M}x(n)\cdot x_M(n+k) \qquad x_M(n)=\begin{cases}x(n) & 1\le n\le M\\ 0 & \text{otherwise}\end{cases} \qquad (6.5)$$

$$\varphi_{xx\ \max}=1$$

where x is the random power process, and M is the window length where the received power is considered as stationary. To determine the most convenient length of the window M, tests with different values from 1 minute to 30 minutes have been carried out. The functions of the four nonoverlapping channels in the 2.4 GHz band for the reference measurement in Fig. 6.4 have been calculated for the different windows length. A good trade-off is reached with M= 5 minutes.

The important information for this first level of the model is the statistical variation of $\varphi_{xx}(t,t+\tau)$ along the time which will determine the phase of the day.

6.3.1.2 Level II: Microscopic Characteristics

Once the current phase of the day has been extracted at level I, level II will try to reconstruct the corresponding signal characteristics.

For this part of the model, the received channel power trace is coded by using a differential approach. The difference between the current and the previous channel power values, γ(n), separated by approximately 150 ms due to the used measuring equipment, can be mapped with three possibilities:

- δ = 0 indicates that the channel power does not change (within a margin of ± 0.5 dBm due to the noise)
- δ = +1 indicates that the channel power ascends
- δ = -1 indicates that the channel power decends

The proposed approach works like the DPCM (differential pulse code modulation), whose principle is drafted in Fig. 6.9.

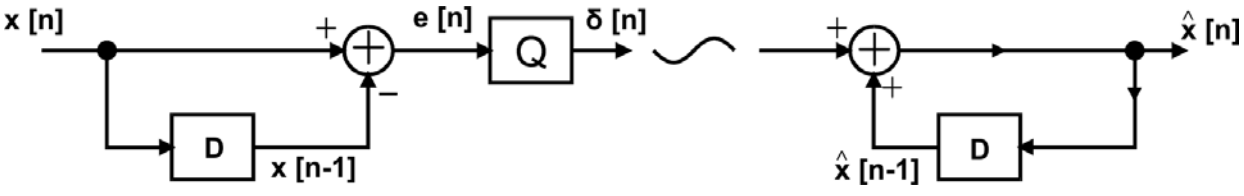

Fig. 6.9: DPCM scheme

In Fig. 6.10 a) shows the channel 1 of the reference measurement (Fig. 5.4), which has been coded and decoded differentially, as shown in Fig. 6.10 b). The accuracy of such a predictive encoder can be seen.

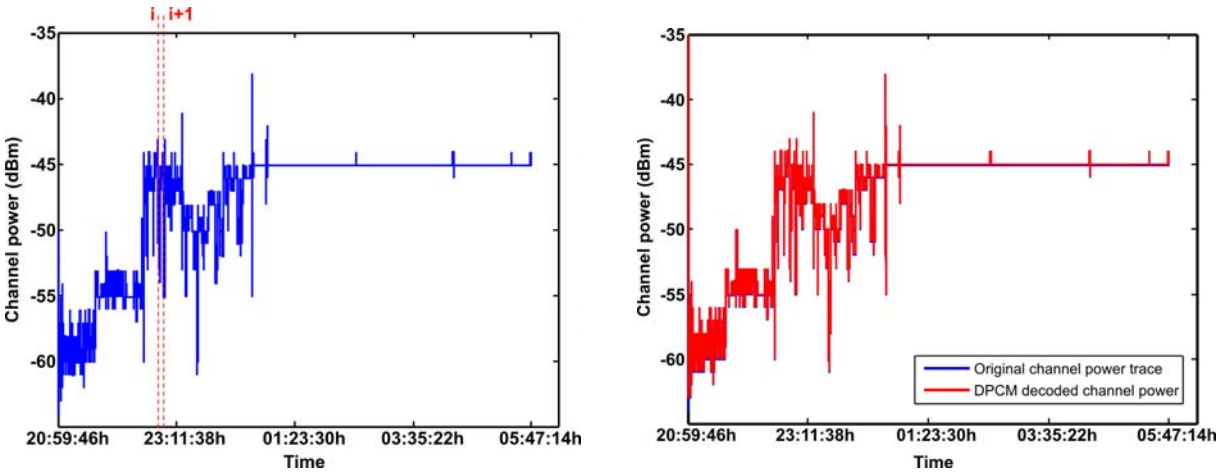

Fig. 6.10: a) Original signal b) Original and decoded signal

Afterwards, the total channel power range is quantized in 2 dB steps (a number which proved to be a good compromise between precision and complexity of the model) and the δ probabilities in each level P(δ | channel power) are calculated. As an example, Table 6.4 shows these probabilities for channel 1 for the entire measured period from 20:59:46h to 05:47:14h.

Table 6.4: P(δ | channel power) for channel 1

Channel power-level(ChP) (dBm)	P(δ=-1|ChP)	P(δ =0|ChP)	P(δ =+1|ChP)
-35.0000	1.0000	0	0
-37.0000	0.3333	0.6667	0
-39.0000	0.2041	0.6735	0.1224
-41.0000	0.2500	0.6111	0.1389
-43.0000	0.0478	0.9464	0.0058
-45.0000	0.0018	0.9971	0.0012
-47.0000	0.0115	0.9726	0.0159
-49.0000	0.0099	0.9782	0.0120
-51.0000	0.0221	0.9480	0.0299
-53.0000	0.0243	0.9624	0.0133
-55.0000	0.0080	0.9745	0.0175
-57.0000	0.0585	0.9162	0.0254
-59.0000	0.0266	0.9367	0.0367
-61.0000	0.0119	0.7954	0.1927
-63.0000	0	0.4000	0.6000
-65.0000	0	0	1.0000

The channel power range for channel 1 is very large, from -35 dBm to -65 dBm. Therefore, it is observed that the probability to descend, P(δ= -1), for the maximum power level (-35 dBm) is 1 and likewise for the probability to ascend, P(δ= +1), in the minimum level (-65 dBm).

With these probabilities, it was attempted to reconstruct the whole 9 hours for channel 1 and the results are shown in Fig. 6.11. The bad trace reproduction demonstrates once again the non-stationarity characteristic of the channel power process.

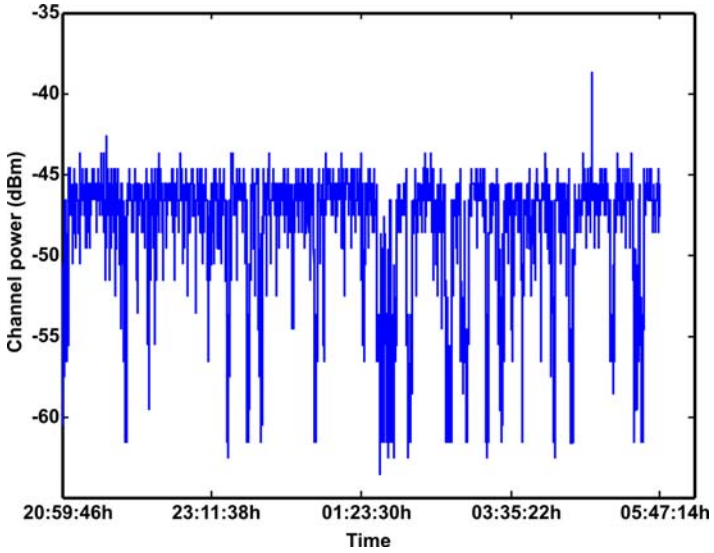

Fig. 6.11: Reconstruction for channel 1 for 9 hours

Due to the variations of the probabilities along the time, level I must limit the period of the day to be simulated. The probabilities P (δ | channel power) have to be recalculated for each time phase. Now an example for channel 13 is shown. Level I decides to simulate 1 minute of the evening phase whose probabilities are listed in Table 6.5.

Table 6.5: P(δ | channel power) for channel 13 from 22:35h - 22:36h

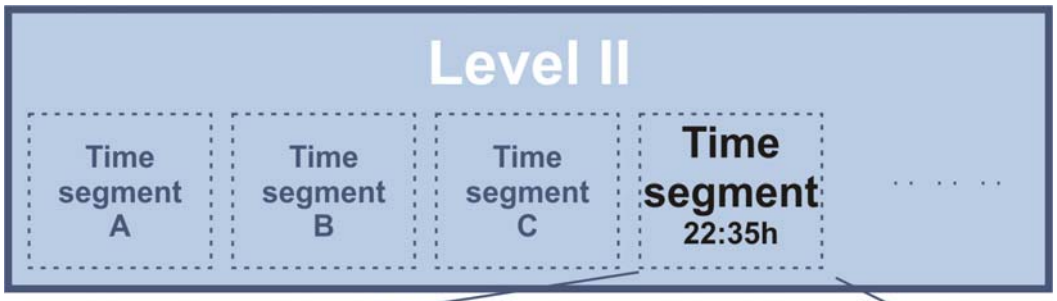

ChP (dBm)	P(δ =-1|ChP)	P(δ =0|ChP)	P(δ =+1|ChP)
-39.0000	1	0	0
-41.0000	0.3333	0.3333	0.3333
-43.0000	0.0145	0.9734	0.0119
-45.0000	0.1666	0.6929	0.1403
-47.0000	0.1459	0.6763	0.1776
-49.0000	0.1333	0.6888	0.1777
-51.0000	0	0	1

The channel power traces for the four non-overlapping channels observed from 22:35h to 22:36h are depicted on the left side of the Fig. 6.12. On the right, a random reproduction of these traces shows a good performance of the proposed dynamic channel model.

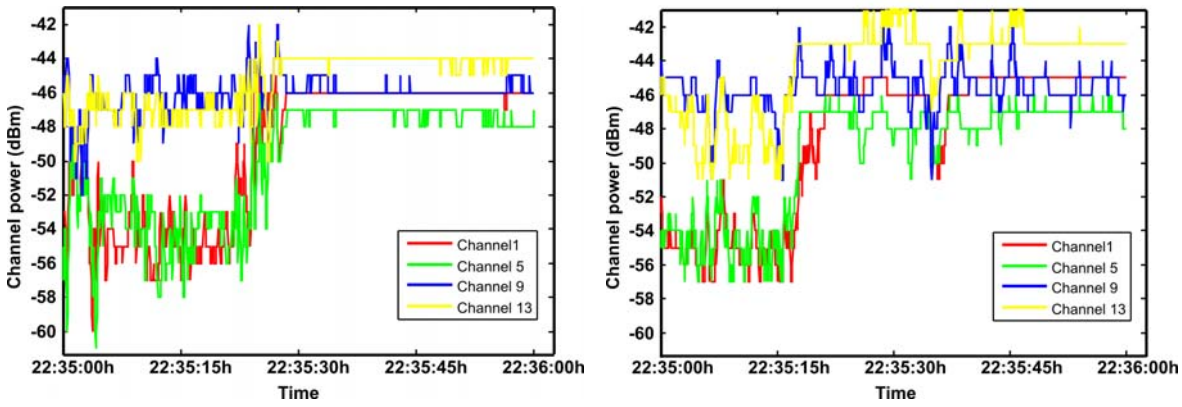

a)Original traces b) Reconstructed traces

Fig. 6.12: Level II: Example of reconstruction from 22:35h to 22:36h

Additional examples are shown in the following figures Fig. 6.13, Fig. 6.14 and Fig. 6.15. On the right, the traces for the intervals: from 23:16:30h to 23:17:30h, from 00:35:40 to 00:36:10h and from 00:51 to 00:52h, respectively are reconstructed. These examples further confirm the efficiency of the proposed model for physical layer simulations in the time domain.

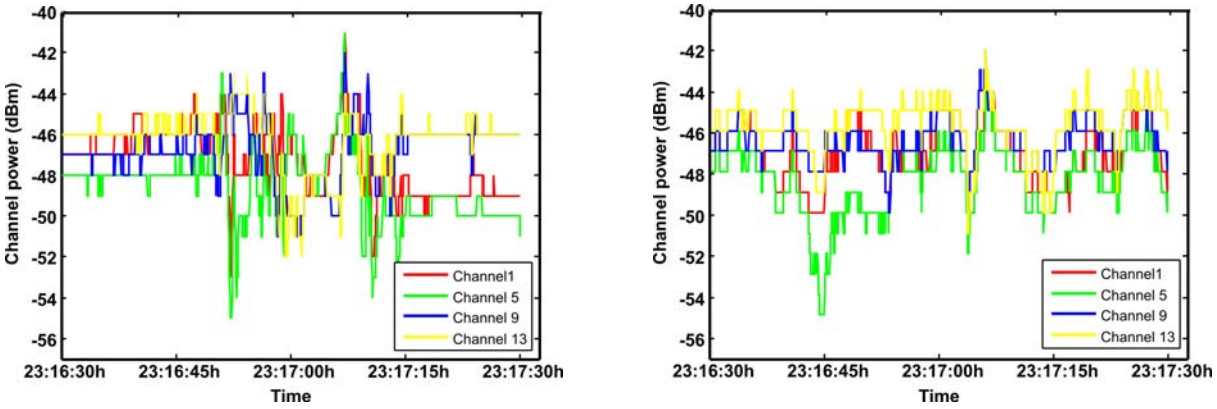

a)Original traces b) Reconstructed traces

Fig. 6.13: Level II: Example of reconstruction from 23:16:30h to 23:17:30h

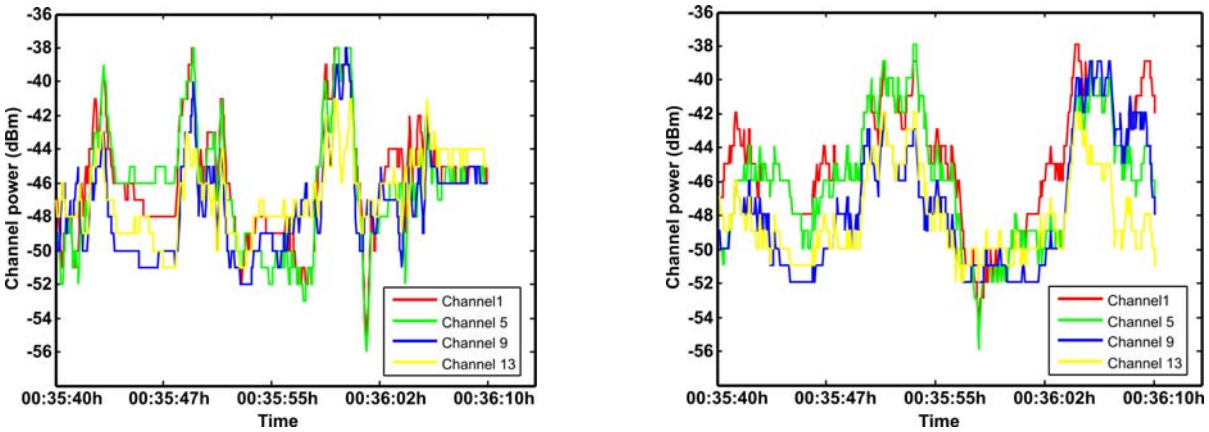

a)Original traces b) Reconstructed traces

Fig. 6.14: Level II: Example of reconstruction from 00:35:40h to 00:36:10h

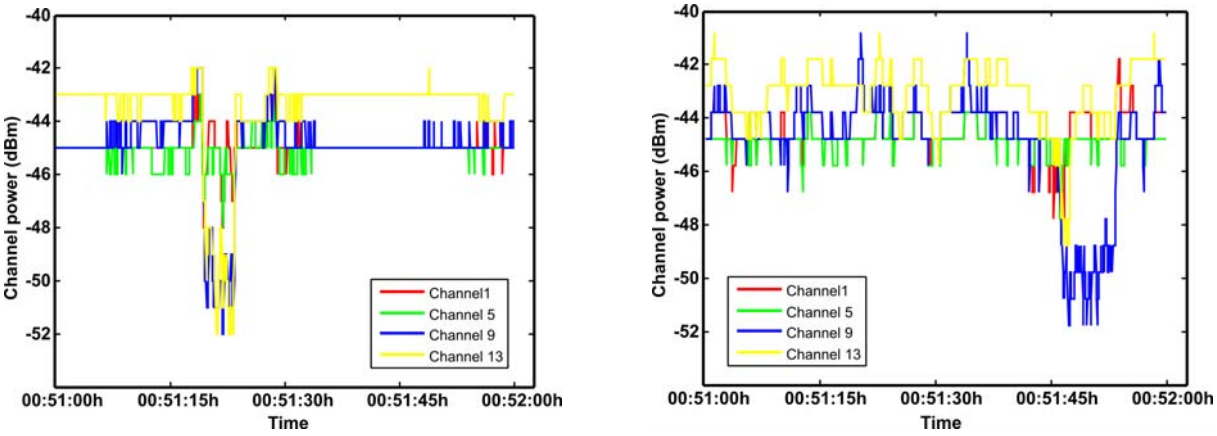

a)Original traces b) Reconstructed traces

Fig. 6.15: Level II: Example of reconstruction from 00:51h to 00:52h

Each channel power partition can be also viewed as a state of a Markov chain. Any partition of the received signal into a finite number of intervals forms a finite state channel model. In the case of the channel 13 from 22:35h to 22:36h in Fig. 6.12, there are 7 states or channel power levels, as shown in Fig. 6.16. For each state, three transition probabilities are possible corresponding to δ = +1, δ = 0 or δ = -1, and are defined as, e.g., $a_{-1,5}$= P(δ =-1|ChP_5),.

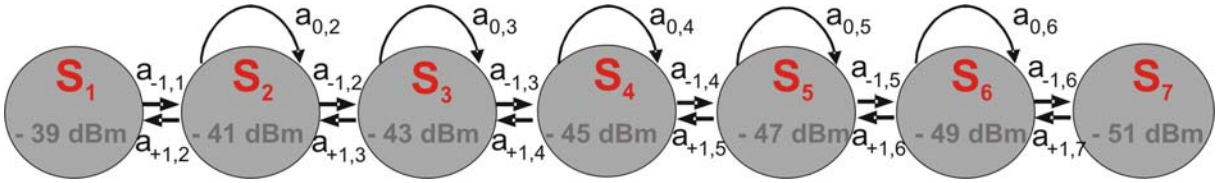

Fig. 6.16: Markov model for channel 13 from 22:35h - 22:36h

In contrast to the birth-death channel models presented in Section 2.6.2, this hierarchical approach can model frequency selective channels without simplifications. Moreover, due to the differential encoding, it is not necessary to simplify transitions to the neighbour states.

6.3.2 Link layer simulation: HMM Approach

For the design of MAC and link layer protocols, advanced knowledge of the error characteristics can help to select appropriate protocol mechanisms. For that purpose, a stochastic model is necessary to reproduce the statistics of given error patterns with some accuracy. Their computational complexity is low compared to the physical layer simulations, for which a multitude of other failure sources are also possible during the detailed implementation of the transmission blocks. This simplicity is beneficial for packet level simulations since simulation time is becoming an issue. Here, an approach based on a hidden Markov model (HMM) is presented.

An HMM is a probabilistic function of a Markov channel, as explained in Chapter 2. For frequency selective channels, it is more accurate than the two-state Gilbert Elliot model that is restricted by its simplicity [Fritchman67], [KaSa78], [Turin98]. An HMM is a doubly stochastic process. By simply observing the output sequence, the state that generated such an output cannot be determined.

HMMs allow finding closed-form expressions for various fading characteristics which are difficult to compute based on the continuous fading channel model. Some of these statistics are, for example, probability distributions of fade durations, error sequences or number of level crossings. Another advantage of using HMMs is the existence of powerful algorithms for fitting them to experimental data and approximating other processes.

The fading channel modeling with HMM was also discussed by Turin and van Nobelen [TuVanNo98], where HMM parameters were calculated from computer generated data. It has been demonstrated that Rayleigh fading can be modeled by an HMM, and therefore, bit errors and block errors in data communications over Rayleigh fading channels can be modeled by a HMM.

6.3.2.1 HMM as a special case of the first order Markov models

The main parameters of Markov models of the first order have been presented in Section 2.6.2. Another important statistic of such models is the error matrix. In a two state model, N=2, {g, b}, and assuming the binary case, this matrix is defined by B as follows:

$$B = \begin{pmatrix} P(\bar{E} \mid g) & P(\bar{E} \mid b) \\ P(E \mid g) & P(E \mid b) \end{pmatrix} \tag{6.6}$$

where $\bar{E}$ indicates that the bit was decided correctly (error sequence: “0”) at the receiver and E indicates that an error appeared, (error sequence: “1”). By multiplicating the steady state matrix by the transposed of the error matrix, the probabilities of a correct decision and an error are obtained by:

$$(P_{\bar{E}} \quad P_E) = \Pi_{SS} \cdot B^T \tag{6.7}$$

Assuming that all the elements in the matrix B are not null, an error can be produced independently of the state (i.e.good or bad). Thus, if an error is produced by the channel model, it cannot be directly estimated in which state the channel stays. The reasons for failures are occulted and therefore, these models are referred to as Hidden Markov Model.

In a Hidden Markov Modell with N states and binary transmission, the error matrix has dimensions 2xN:

$$B = \begin{pmatrix} b_{11} & b_{12} & \cdots & b_{1l} & \cdots & b_{1N} \\ b_{21} & b_{22} & \cdots & b_{2l} & \cdots & b_{2N} \end{pmatrix} \tag{6.8}$$

where:

$$b_{ki}(e_k) = P(e_k \mid S = s_i) \qquad \text{with} \qquad e_k = \{\bar{E}, E\} = \{0,1\} \tag{6.9}$$

The parameters A and B describe completely a discrete HMM. Fig. 6.17 presents a three state model and binary transmission as an example.

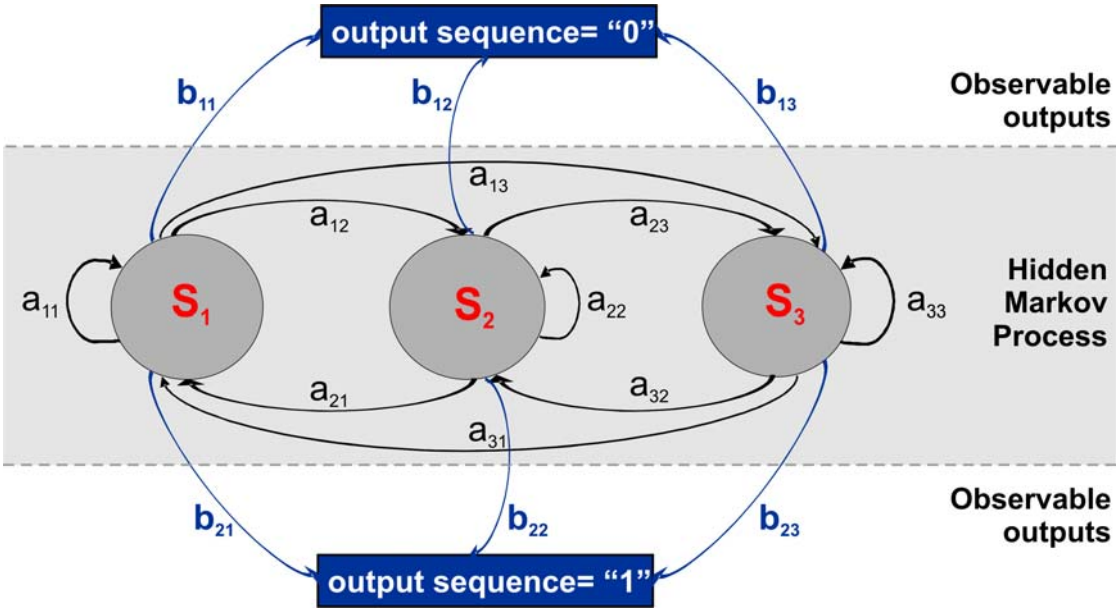

Fig. 6.17: Three state Hidden Markov Model and binary symbols

6.3.2.2 HMM Parameter estimation

To generate the error sequence that best matches statistically a given observed physical channel $O_i(t)$, the initial state distribution, π_0 , the transition probabilities, a_{ij}, and the output distribution must be determined by training the HMM.

To determine the model parameter set $\Gamma = \{A, B, \pi\}$, an aproach based on the Baum-Welch Algorithm (BWA) has been selected, since it is the most efficient algorithm for HMMs. The BWA [RaJu86] (see also annex B) has been used to train the HMM by means of the error sequence derived from detailed physical-layer simulations.

The BWA is an expectation-maximization (EM) algorithm that consists of fitting iteratively the probability distribution of the original process $\overline{O} = \{O_1, O_2, ..., O_t ... O_T\}$. The algorithm calculates the maximum likelihood estimation of Γ, whereby the probability $P(\overline{O} \mid \Gamma)$ is maximized.

The BWA must specify the initial transition, error and state matrix elements. They are defined as follows:

$$\hat{a}_{i,j} = \frac{\text{expected number of transitions from state } i \text{ to state } j}{\text{expected number of transitions from state } i} \tag{6.10}$$

$$\hat{b}_j(e_k) = \frac{\text{expected number of times } e_k \text{ is emitted from state } j}{\text{expected number of visits to state } j} \tag{6.11}$$

$$\hat{\pi}_j = \frac{\text{expected number of visits to state } j}{\text{total time observed}} \tag{6.12}$$

The estimated model parameters $\hat{\Gamma} = \{\hat{A}, \hat{B}, \hat{\Pi}\}$ are calculated from (6.10), (6.11) and (6.12) and they are employed by the iterative algorithm in its first step. In each of the next cycles $P(\overline{O} \mid \Gamma)$ is improved using the new Γ calculated in the previous loop.

6.3.2.3 Simulation and model performance

In order to train HMMs it is required to obtain binary sequences describing bit errors. One complex way to generate error sequences requires measurements to be performed. Once the model is parameterized, the outputs obtained from the model are compared with the measured statistics. An alternative way is to conduct a physical layer simulation.

In this work, the time-varying channel transfer functions obtained from the dynamic measurements presented in chapter 5, are used for simulations with different SNR values. A simulation environment programmed in Matlab has been created, which by means of the measured spectra implements a complete WLAN transmission based on the IEEE 802.11 *g* standard.

A total of three hours of the reference measurement, a very active period from 22:00h to 1:00h, has been simulated. A data packet simulation is carried out for each measured transfer function. Finally, each received packet is compared to the transmitted one and the result is appended to the saved error array. The final error sequence contains a "0" for the correctly received bits and "1" when an error occurred. An example:

Transmitted packet: 1 0 0 0 1 1 1 0 1 1 0 0 1 0 …. 1 1 0
Received packet: 1 0 1 0 1 1 0 0 1 1 0 0 1 0 …. 1 0 0

Error sequence: 0 0 1 0 0 0 1 0 0 0 0 0 0 0 …. 0 1 0

Since, the statistical channel characteristics must be reproduced by the HMM, it is important that by simulation sufficient errors appear. Therefore, it has been assured that at least 1000 errors for each SNR value have emerged. In this case the simulation has finished. If it is not the case, a further loop must be carried out. The simulation continues until the error number increases to 1000, or three loops with all transfer functions have been simulated. Through the simulations, very large error arrays are created paying attention to an efficient implementation in Matlab.

For all modulations and code rates used by 802.11*g,* a Hidden Markov Model for several SNR values was implemented.

The last decision is to choose the number of states in the HMM. In [HaFa04], the accuracy of these models was investigated leading to the observation that with three states it is possible to reproduce quite exactly the error distribution. In this section, the results obtained for Hidden Markov models with 2, 3 and 4 states are presented.

To calculate the HMM parameters, the BWA was used. As an example, the reconstruction of the error vector is presented for the 16 QAM and code rate 3/4. The pertinent HMM parameter sets obtained from the BWA for *N*=2, 3 and 4 are in (6.13), (6.14) and (6.15),

respectively:

N=2: (6.13)

$$A_{N=2} = \begin{pmatrix} 0.9981 & 0.0019 \\ 0.0217 & 0.9783 \end{pmatrix}$$

$$B_{N=2} = \begin{pmatrix} 1 & 0.5202 \\ 0 & 0.4798 \end{pmatrix}$$

$$\Pi_{SS,N=2} = \begin{pmatrix} 0.9210 & 0.079 \end{pmatrix}$$

N=3: (6.14)

$$A_{N=3} = \begin{pmatrix} 0.9927 & 0.0067 & 0.0006 \\ 0.2985 & 0.6294 & 0.0721 \\ 0.0059 & 0.0206 & 0.9735 \end{pmatrix}$$

$$B_{N=3} = \begin{pmatrix} 1 & 0.9972 & 0.5140 \\ 0 & 0.0028 & 0.4860 \end{pmatrix}$$

$$\Pi_{SS,N=3} = \begin{pmatrix} 0.9024 & 0.0205 & 0.0771 \end{pmatrix}$$

N=4: (6.15)

$$A_{N=4} = \begin{pmatrix} 0.9975 & 0.0016 & 0.0005 & 0.0004 \\ 0.1213 & 0.6704 & 0.1413 & 0.0670 \\ 0.0531 & 0.2872 & 0.5305 & 0.1292 \\ 0.0048 & 0.0134 & 0.0141 & 0.9673 \end{pmatrix}$$

$$B_{N=4} = \begin{pmatrix} 1 & 0.9982 & 0.6020 & 0.4959 \\ 0 & 0.0018 & 0.3980 & 0.5041 \end{pmatrix}$$

$$\Pi_{SS,N=4} = \begin{pmatrix} 0.9119 & 0.0134 & 0.0070 & 0.0677 \end{pmatrix}$$

In all three models when the error matrix *B* is taken into account, the first state is a “good state” where the probability that an error occurs is zero. The last state is respectively a “bad state”, where errors appear most frequently. This partitioning is also visible in the four state model. Thereby, the second state is a favourable state but not as good as the first one, and the third state is an adverse state, but not as bad as the last one. In the bad states, the probabilities to receive a correct or an erroneous bit are almost equal. Therefore, although the model is in such a state, a bit can be transmitted correctly.

As far as the transition matrix *A* is concerned, the probabilities to remain in a state is the highest in each state for all models. For example, with *N*=4 these probabilities are 0.9975 for s_1, 0.6704 for s_2, 0.5305 for s_3 and 0.9673 for s_4.

In order to reconstruct the observed error vector through the model parameters, a new first column with all zeros is joint to the transition matrix and each row of the new matrix is cumulatively added:

$$a_{i1}^{cum} = 0, \qquad a_{i(j+1)}^{cum} = \sum_{k=1}^{j} a_{ik} \qquad 1 \le i \le N, \quad j = 1,2,...,N \tag{6.16}$$

where *N* is the number of states.

The cumulative matrix, A^{cum}, with dimensions *N* x (*N*+1) is used to determine the next state. A random value α uniformly distributed between 0 and 1 is generated. Considering the row corresponding to the current state *i*, it is evaluated in which interval α resides, i.e. the next state *j* is calculated where: $a_{ij-1}^{cum} < \alpha \le a_{ij}^{cum}$.

Thereafter, it must be decided if the HMM delivers an error in the current state *i* and that is performed by means of the error matrix *B*. A new random number β is generated between 0 and 1. If β is higher than the value in the column *i* of the the first row of *B*, an error is produced. This results in an “1” being appended to the output sequence, otherwise, the ouput sequence= ”0”.

To evaluate the accuracy of the developed HMMs the error distribution statistic in the output sequence is analyzed. The adoption of such a model by packet orientated systems emphasizes the importance of a good fitting of the error free distribution, since long chains of correctly transmitted bit are necessary to properly receive a packet. $P(0^m|1)$ is the probability that after an error, “1“, follows a sequence with at least *m* zero values. This probability is calculated and analyzed for the three models and compared with the original error distribution.

The results shown in Fig. 6.18 correspond to *N*=2. The dashed curve represents the error-free distribution of the output sequence, whereas the solid plain line stands for the original error sequence from the simulations. Up to $m \approx 20$, the difference between the original and the reproduced distributions is very small. However, in the reconstruction, the model frequently remains such that no error appears, as can be derived from Π_{ss} in (6.13), and therefore, the long error-free intervals are more probable (dotted line). This effect increments from $m \geq 20$. The next bit sequence could be an example of the output sequence of the HMM with *N*=2 states, which parameters are defined in (6.13):

000000000000 01100111000110011001 0
“Good” “Bad”

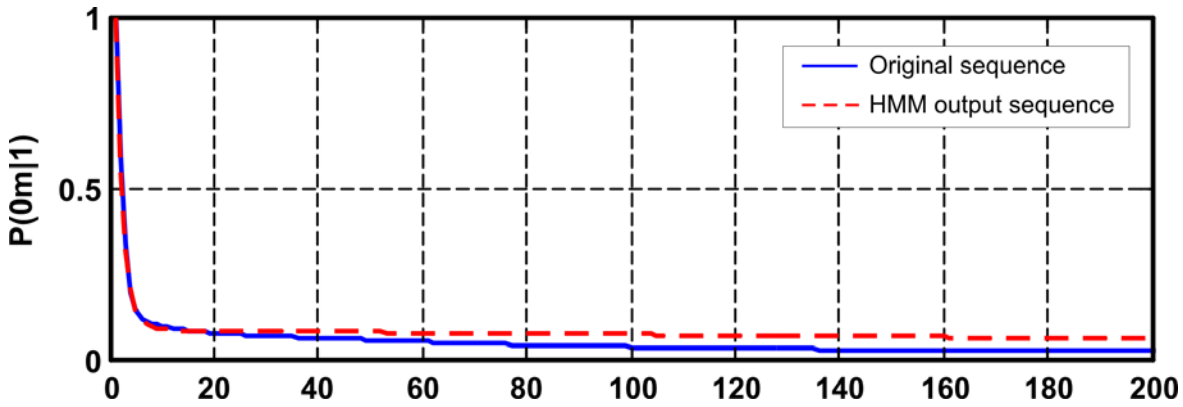

Fig. 6.18: Comparison original/reproduced error vector, N=2 states

For *N*=3, Fig. 6.19, the model shows a very good correspondence with the error statistic. The distribution of $P(0^m|1)$ is very accurate to the original error vector, much more than with *N*=2.

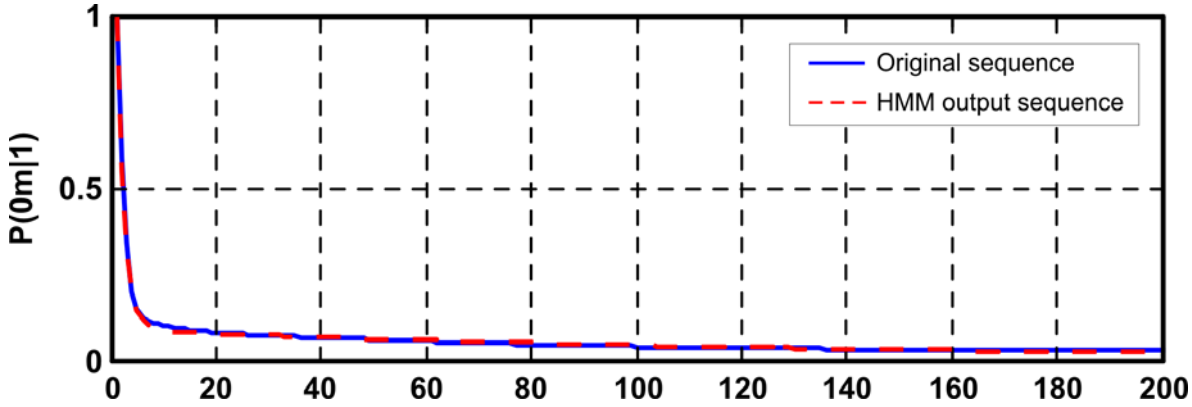

Fig. 6.19: Comparison original/reproduced error vector, N=3 states

Finally, the results for *N*=4 are illustrated in Fig. 6.20. Here, there are also deviations although not so large as by *N*=2. Now it is less probable to have long "0" intervals (up to a length of approximately 50) because in this model there are two additional states, s_2 and s_3, where errors can be produced as well, such as in s_4. The reproduction can be evaluated as good yet.

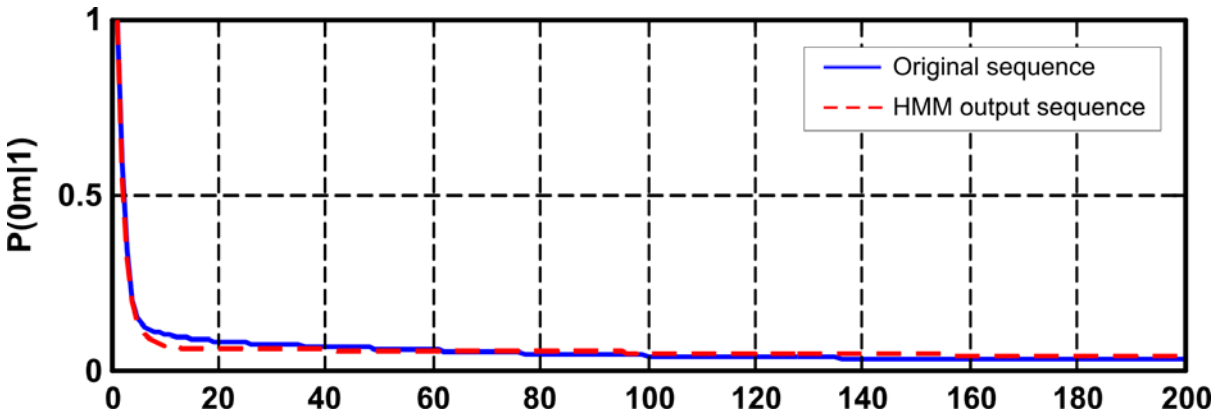

Fig. 6.20: Comparison original/reproduced error vector, N=4 states

The model that best fits the error statistics is the three state model. The results from [HaFa04] are therefore confirmed through the existing measured data.

This channel model can be used to develop the adaptive techniques presented in Section 3.5 under realistic dynamic situations. It has been already integrated into the mobility framework of OMNET++ (see Annex C). The operation mode is represented in Fig. 6.21.

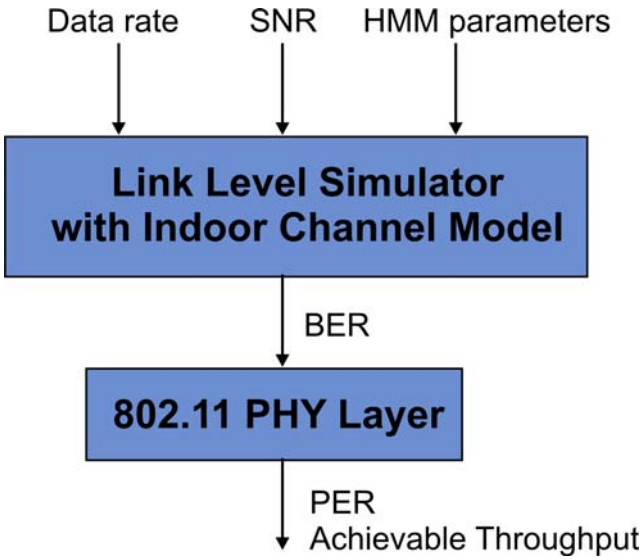

Fig. 6.21: A model of operation of a link layer simulator with HMM channel model

A transmitter entity passes the packets to the channel, where bit errors are injected to the channel that corrupts the data according to the current data rate and SNR. The packet error probability will depend on the error positions in the frame. Since only the parameters relative to the Hidden Markov model are additionally required for the simulation, this implementation of dynamic channel model is user-friendly.

6.4 Summary of the channel models

The presence of moving obstacles, such as people, seriously affects the performance of the system by introducing large variations in the received signal strength. These oscillations on the signal quality and signal to interference ratio (SIR) impact on the Bit Error Rate (BER) and therefore, also the achievable throughput.

In this chapter, two different channel model approaches have been proposed in order to characterize the dynamic behavior of WLAN channels in the 2.4 GHz band. The first approach contributes to improve link adaptation techniques such as data rate adaptation. The parameters of this algorithm are adapted to the dynamic channel conditions in order to maintain the QoS requirements.

The second approach has been used to simulate realistic scenarios of WLANs in home environments at the physical and link layer. Through simulations, the effectiveness of the proposed adaptive techniques can be evaluated. The error free burst lengths show great variability and they exhibit short term correlation. Therefore, discrete model channels based

on Markov chains such HMM are adequate due to the memory which they present. The best approximation to the original error statistics is given by the three-state model. It is also shown that an increase of the model complexity does not improve the performance.

7 Summary

IEEE 802.11 and its extensions are good candidates for media transmissions in home environments. In this application scenario, the devices are located in different rooms, forming a multi-dimensional arrangement. Common devices used for in-house multimedia distribution and presentation are PCs, set-top-boxes and multimedia home-servers. Multimedia services are distributed via individual wireless links between two or multiple interacting devices. A critical network situation occurs, if multiple high data-rate multimedia links operate simultaneously. The high density of communicating nodes and multimedia links requiring a high QoS, as well as the lack of suitable automatic configuration gives rise to numerous problems. Interfering wireless transmissions suffer from collisions that cause the QoS requirements of media streams to be missed. Further problems exist with regard to the reliability of data transmission due to the channel characteristics. A number of measurement results show the troublesome behavior of a standard wireless LAN link.

The channel's influence on the transmission can be reduced using methods of link adaptation. SNR improvements are possible by means of techniques such as dynamic frequency selection or antenna diversity, for example. The link adaptation approach will increase the individual link data rate as well as the overall throughput, so that a reliable distribution of A/V data can be possible in the home environment.

A user interaction should be avoided as much as possible. Therefore the efficient use of link adaptation as well as MAC parameter adaptation requires methods for self organization of the network nodes. The development and implementation of these methods will be a goal for future work.

In the framework of this dissertation, the properties of the wireless channel in the 2.4 GHz and 5 GHz ISM bands have been presented. The understanding of an in-house transmission channel has come from the results of the channel measurements. A network controller based on the time-varying measurements is proposed to dynamically adapt the parameters of the optimization methods. In addition, two channel models to simulate the in-house behavior have been developed and analyzed.

In Chapter 1 the penetration of the IEEE 802.11 WLANs in current home networking was introduced. In addition, the most common multimedia devices and applications such VoIP, gaming or video applications were presented together with their requirements. The concept of self-organised in-house wireless networks was also briefly outlined.

The wireless channel was mathematically described in Chapter 2. The stochastic functions of the wireless channel and the most representative parameters such as coherence time and bandwidth, and Doppler and multipath spread were defined and explained. Also, the principal effects of wireless propagation such as multipath propagation or Doppler effect and their consequences were described. A channel classification was presented based on the parameters previously defined. Moreover, a number of typical amplitude distributions described in the literature and appropriate for the in-house channels, such as Rayleigh, Rice or Nakagami were mentioned.

The most accepted model to perform simulations is the continuous-signal based tapped-delay-line. The benefits of digital channel models were pointed out through the well-known Markov chains and their different used structures: ARMA models, birth and death processes, Monte Carlo methods or Hidden Markov models.

In Chapter 3, the fundamental principle of the OFDM was explained. Advantages, disadvantages as well as the communication standards using this multicarrier technique were listed. The OFDM parameters for IEEE WLAN were briefly described and some optimization techniques to improve in-house WLAN performance were proposed.

To gain an insight into the wireless channel properties, several measurements in the 2.4 GHz and 5 GHz ISM bands were carried out and described in Chapter 4. First, the characteristics of the two scenarios selected for the experiments were presented. Then the used measuring equipment and signals were presented in detail, as well. Thorough evaluations regarding amplitude distributions for LOS and NLOS situations, coherence bandwidth, received channel power or frequency selective fading depth were the main focus of this chapter. Furthermore, the potential of two proposed optimization techniques were evaluated on the basis of these measurements obtaining very promising assessments. Finally, a path loss model with attenuators was parameterized for a concrete in-house measurement situation.

Encouraged by the initial results, new measurement experiments were carried out. This time, the goal was to gain a better insight into the time-varying characteristics of the in-house transmission channel in the 2.4 GHz band, as presented in Chapter 5. The test scenarios were three typical residential houses. Several sequences of the measured spectra were reproduced and investigated by defining an “optimal channel” at any time point. The analysis of the received channel power and frequency selective fading performance of the four non-overlapping channels helped to understand the dynamic behavior of the channel during different phases of the day. Interesting outcomes for a posterior modeling were found about the correlation between both parameters.

The dynamic frequency selection technique was more exhaustively examined in realistic time-varying situations. A significant gain can be achieved by selecting the best channel at any time, as was pinpointed in Chapter 4. During certain time phases, the gain can reach 15 dB. Therefore, when high QoS in home environments is demanded, adapting the transmission frequency to the link conditions is a simple and efficient method. Also it can be a useful technique when interferences such microwaves are present. They operate in the 2.4GHz ISM-Band as well. This appliance frequently used in home environment has influence on the transmission, irrupting with a 50 Hz impulse and affecting the highest channels of this band.

Finally, in Chapter 6 the modeling of the dynamics of wireless in-house channels is overviewed. Based on the literature research, it was pointed out that the current dynamic models for the in-house channels do not take into consideration the non-stationary characteristics of such transmission channels. In order to achieve the necessary QoS for multimedia sessions, the wireless links have to be adapted to the varying channel conditions. This task, which is essential for self-organization, is carried out by the network controller presented in this chapter. Its parameters have been carefully selected. The functionality of this model was exemplified using the optimization method of dynamic rate adaptation.

Two additional models were developed to simulate realistic dynamic situations in home

environments at physical or link layer. The first model is a hierarchical approach and reproduces very accurately the time-varying characteristics of the measured channel power traces for different phases of the day. The second model is an approach based on hidden Markov models. Three combinations with two, three and four states were tested and statistically compared to the results obtained from simulations with the measured dynamic channels. The best adjustment to the original error sequence was found with the three state model.

In conclusion, this work provides a comprehensive overview of the wireless channel in home environments. The dynamic behavior of WLAN channels in home environments is characterized to design link adaptation methods in adaptive ad-hoc wireless networks.

8 Bibliography

[AhFeVa05] AHUMADA, L.; FEICK, R.; VALENZUELA R.A.; MORALES, C.: *Measurement and Characterization of the Temporal Behavior of Fixed Wireless Links*. IEEE Transactions on Vehicular Technology, Vol. 54, No. 6, November 2005.

[Alexander82] ALEXANDER, S.E.: *Radio propagation within buildings at 900 MHz*. Electronics Letters, Vol. 18, No.21, pp. 913-914, October 14, 1982.

[AlexPugl83] ALEXANDER, S.E; PUGLIESE, G.: *Cordless communication within buildings: Results of measurements at 900 MHz and 60 GHz*. British Telecom Technology Journal, Vol. I, No. I, pp. 99-105, July 1983.

[BaKeLom99] BABICH, F.; KELLY, O. E.; LOMBARDI, G.: *A context-tree based model for quantized fading*. IEEE Transactions on Communications, Vol. 3, No. 2, pp. 46-48, 1999.

[BaKeLom00] BABICH, F.; KELLY, O. E.; LOMBARDI, G.: *Generalized Markov Modeling for Flat Fading*. IEEE Transactions on Communications, Vol.48, No.4, pp. 547-551, April 2000.

[BaLom00] BABICH, F.; LOMBARDI, G.: *A Markov model for the mobile propagation channel*. IEEE Transactions on Vehicular Technology, Vol. 49, No. 1, pp. 63-73, 2000.

[BaSu96] BADRINATH, B. R.; SUDAME, P.: *To send or not to send: Implementing deferred transmissions in a mobile host*. Proceedings 16th International Conference on Distributed Computing Systems, Hong Kong, pp. 327–333, May 27–30, 1996.

[Becker06] BECKER, R.: Entwicklung einer Simulationsumgebung zur Sendeleistungsregulierung in WLAN-Netzwerken. Technische Universität Dortmund, 2006.

[Bello63] BELLO, P. A.: *Characterization of randomly time-variant linear channels*. IEEE Transactions on Communication Systems, CS-11, No. 4, pp. 360–393, December 1963.

[BernSkl97] SKLAR, B.: *Rayleigh Fading Channels in Mobile Digital Communication Systems. Part I: Characterization*. IEEE Communications Magazine, Vol. 35, Issue 9, pp. 148-155, Sept. 1997.

[Bertoni00] BERTONI, L.B.: *Radio Propagation for Modern Wireless Systems*. Prentice Hall; 2000

[Billingsley61] BILLINGSLEY, P.: *Statistical methods in Markov chains*. The Annals of Mathematical Statistics, Vol. 32, pp. 12–40, 1961.

[Brak99] BRAKENSIEK, J.: *Ein Beitrag zu dezentralen,funkbasierten Inhouse-Netzen für breitbandige Kommunikation.* Doctor thesis1999.

[DAB95] ETSI: *Radio Broadcasting Systems: Digital Audio Broadcasting (DAB) to Mobile, Portable and Fixed Receivers*. Technischer Bericht ETS 300-401, European Telecommunication Standard, Februar 1995.

[DoSu97] DO, M.; Sun, S.: *Statistical Modeling of Broadband Wireless LAN Channels at 18 GHz Using Directive Antennas*. International Journal of Wireless Information Networks, Vol. 4, No. 1, pp. 21-30, 1997.

[Durgin02] DURGIN, G.D.: *Space-Time Wireless Channels*. Prentice Hall PTR, 2002.

[DVB97] ETSI: *Digital Video Broadcasting: Framing Structure, Channel Coding and Modulation for Digital Terrestrial Television*. Technischer Bericht ETS 300-744, European elecommunication Standard, August 1997.

[Elliot63] ELLIOT, E. O.: *Estimates of error rates for codes on burst-noise channels*. Bell Systems and Techonoly Journal, Vol. 42, pp. 1977-1997, September 1963.

[Forney72] FORNEY, G. D.: *Maximum-likelihood sequence estimation of digital sequences in the presence of intersymbol interference*. IEEE Transactions on Inform. Theory, Vol. IT-18, pp. 363–378, May 1972.

[Fritchman67] FRITCHMAN, B. D.: *A binary channel characterization using partitioned Markov chains*. IEEE Transactions on Information Theory, Vol. IT-13, pp. 221–227, April 1967.

[GaCr97] GARCIA-FRIAS, J.; CRESPO, P. M.: *Hidden Markov models for burst error characterization in indoor radio channels*. IEEE Transactions on Vehicular Technology, vol. 46, pp. 1006–1020, November 1997.

[Gillbert60] GILBERT, E. N.: *Capacity of a burst-noise channel*. Bell Systems and Technology Journal, Vol. 39,, pp. 1253-1265, September 1960

[GrHa94] GREENWOOD, D.; HANZO, L.: *Characterization of mobile radio channels in Mobile Radio Communications*. R. Steele, Ed. London, U.K.: Pentech, 1992, pp. 163-185.

[GrMiEr99] GREENSTEIN, L.J.; MICHELSON; D.G.; ERCEG, V.: *Moment-Method Estimation of the Rician K-Factor*. IEEE Communications letters, Vol. 3, No. 6, June 1999.

[GuSa06] GUHA, R.; SARKAR, S.: *Characterizing temporal snr variation in 802.11 networks.* Proceedings of IEEE Wireless Communications and Networking Conference (WCNC), April 3-6 2006.

[HaFa04] HARTWELL, J.; FAPOJUWO, A. O.: *Modeling and Characterization of frame loss process in IEEE 802.11 Wireless Networks*. IEEE Vehicular Technology Conference Fall 2004, September 2004.

[Hoeher92] HOEHER, P.: *A statistical discrete-time model for the WSSUS multipath channel*. IEEE Transactions on Vehicular Technology, Vol. 41, pp. 461–468, 1992.

[HOMEPLANE07] Home Media Platform and Networks [www.homeplane.org]

[HorTanMor86] HORIKOSHI, J.; TANAKA, K.; MORINAGA, T.: *1.2 GHz band wave propagation measurements in concrete buildings for indoor radio communications*. IEEE Transactions on Vehicular Technology, Vol. VT-35, No. 4, pp. 146-152, November 1986.

[IEEE97] IEEE 802.11, *IEEE Standard for Wireless LAN Medium Access Control (MAC) and Physical Layer (PHY) specifications*. November 1997.

[IEEEe05] IEEE 802.11e-2005, *Information technology - telecommunications and information exchange between systems - local and metropolitan area networks - Specific requirements, Part 11: wireless LAN medium access control (MAC) and physical layer (PHY) specifications, amendment 8: medium access control (MAC) quality of service enhancements*. November 2005.

[IEEEh03] IEEE 802.11h-2003*, Information technology - telecommunications and information exchange between systems - local and metropolitan area networks - Specific requirements, Part 11: wireless LAN medium access control (MAC) and physical layer (PHY) specifications, amendment 5: spectrum and transmit power management extensions in the 5 GHz band in Europe*. October 2003.

[IEEEn09] IEEE 802.11n-2009, *Higher throughput improvements using MIMO (multiple input, multiple output antennas)* (Draft 5.0, July 08). Status of Project IEEE 802.11n: http://grouper.ieee.org/groups/802/11/Reports/tgn_update.htm

[IEEE802.11WG] http://www.ieee802.org/11/Reports/802.11_Timelines.htm

[IntWStat] *http://www.internetworldstats.com/stats.htm*

[Jakes93] JAKES, W. C.: *Microwave Mobile Communicarions*. New York, IEEE Press, 1993.

[JaMa05] JACHAN, M.; MATZ, G.: *Nonstationary vector AR modeling of wireless channels*. Proceedings IEEE SPAWC-05, New York, pp. 648–652, June 2005.

[Jansen96] JANSSEN, G.J.M.: *Performance Enhancement of Indoor Channels Using Quasi-Coherent Combining of Multiple Antenna Signals*. Proceedings 7th International Therrenian Workshop on Digital Communications, Italy, pp. 15–26, September1995.

[JaStPr95] JANSSEN, G.J.M.; STIGTER, P.A.; PRASAD, R.: *Wideband Indoor Channel Measurements and BER Analysis of Frequency Selective Multipath Channels at 2.4, 4.75 and 11.5 GHz*. IEEE Transactions on on Communications, Vol. 44,No. 10, pp. 1272–1288, 1996.

[JeBaSha00] JERUCHIM, M. C.; BALABAN, P.; SHANMUGAN, K. S.: *Simulation of Communication Systems: Modeling, Methodology, and Techniques*. 2nd ed. Berlin, Germany: Kluwer, 2000.

[KaBo92] KARLSSON, P.; BORJESSON, H.: *Measurement system for indoor narrowband radio propagation at 1700 MHz and some results*. Proceedings IEEE Vehicular Technology Conference. VTC '92, Denver, Vol. 2, pp. 625-628, May 1992.

[KaElTaMa92] KALIVAS, G. A.; EL-TANANY, M.; MAHMOUD, S. A.: *Millimeter- wave channel measurements for indoor wireless communications*. Proceedings IEEE Vehicular Technology Conference. VTC '92, Denver, Vol. 2 pp. 609-612, May 1992.

[KaJoEn04] KAYS, R.; JOSTSCHULTE, K.; ENDEMANN, W.: *Wireless ad-hoc networks with high node density for home AV transmission*. IEEE Transactions on Consumer Electronics, Vol. 50, pp. 463-471, May 2004.

[KaSa78] KANAL, L. N.; SASTRY, A. R. K.: *Models for channels with memory and their applications to error control*. Proceedings IEEE, Vol. 66, No. 7, pp. 724–744, July 1978.

[KeBi80] KEASLER, W.E.; BITZER, D.L.: *High speed modem suitable for cooperating with a switched network*. U.S. Patent No. 4,206,320, June 1980.

[KeHan00] KELLER, T.; HANZO, L.: *Adaptive multicarrier modulation: a convenient framework for time-frequency processing in wireless communications*. Proceedings of the IEEE, Vol. 88, No. 5, pp. 611-640, May 2000.

[LeSri98] LETTIERI, P.; SRIVASTAVA, M. B.: *Adaptive frame length control for improving wireless link range and energy efficiency*. Proceedings IEEE INFOCOM '98 Conference on Computer Communications, San Francisco, CA, Vol. 2, pp. 564–571.

[Lettieri97] LETTIERI, P.: *Low power error control for wireless links*. Proceedings 3rd ACM/IEEE International Conference on Mobile Computing and Networking 1997 (MobiCom'97), Budapest, Hungary, pp. 139–150.

[LoBeBo92] LOTSE, J.; BERG, E.; BOWNDS, R.: *Indoor propagation measurement at 900 MHz*. in Proceedings IEEE Vehicular Technology Conference, VTC '92, Denver, Colo., May 1992, pp. 629-632.

[MaNiWa95] MARZETTA, T. L., NICHOLS Res. Corp.; WAKEFIELD, MA.: *EM algorithm for estimating the parameters of a multivariatecomplex Rician density for polarimetric SAR*. Proceedings ICASSP' 96 Detroit, MI, USA. Vol. 5, pp. 3651-3654, May 1995.

[Miniwatt06] ENDEMANN, W.; KAYS, R.: *Alternative Frequency Bands for Local Networks*. Miniwatt Report, June 2006.

[MoDe90] MOGUL, J.; DEERING, S.: *Path MTU Discovery*. RFC 1191, November 1990

[Molish05] MOLISH, A. F.: *IEEE 802.15.4a channel model - final report*. Document IEEE 802.15-04-0662-02-004a, 2005.

[OhmLueke04] OHM, J.R. and H.D. LÜKE: *Signalübertragung*. Springer, Berlin, 2004.

[Paetzold99] PÄTZOLD, M.: *Mobilfunkkanäle - Modellierung, Analyse und Simulation*. Vieweg-Verlag, Wiesbaden, 1999.

[Papadakis97] PAPADAKIS, N.: *Wideband Propagation Measurements and Modeling in Indoor Environment*. International Journal of Wireless Information Networks, Vol. 4, No. 2, PP 101-110, 1997.

[Parsons92] PARSONS, J.D.: *The mobile Radio Propagation Channel*. New York: Wiley, 1992, pp. 134-136.

[PoonHo03] POON, A.S.Y.; HO, M.: *Indoor Multiple-Antenna Channel Characterization from 2 to 8 GHz*. Communications and Interconnect Laboratory, Intel Corporation. IEEE International Conference on Communications, 2003. ICC '03.

[RaGo75] RABINER, L. R.; GOLD, B.: *Theory and Applications of Digital Signal Processing*. Englewood Cliffs, NJ: Prentice-Hall, 1975

[RaJu86] RABINER, L. R.; JUANG, B. H.: *An introduction to hidden Markov models (speech recognition and processing)*. IEEE ASSP Magazine, pp. 4–16, January 1986

[Rappaport02] RAPPAPORT, T.S.: *Wireless Communications - Principles and Practice*. Prentice Hall, 2. Auflage, 2002.

[SalehValenz87] SALEH, A.A.M.; VALENZUELA, R.A.: *A statistical model for indoor multipath propagation*. lEEE J. Selected Areas in Communications, vol. SAC-5, no.2, pp. 128-137, Feb. 1987.

[StratAnal] http://strategyanalytics.com/ default.aspx?mod=PressReleaseViewer&a0=3004

[Suzuki77] SUZUKI, H.: *A statistical model for urban multipath channels with random delay*. IEEE Transactions on Communications, Vol. COM-25, pp. 673–680, July 1977.

[TaLa91] TALUKDAR, K.K.; LAWING, W.D.: *Estimation of the parameters of the Rice distribution*. Journal of Acoustical Society of America, Vol.89, No.3, pp.1193– 1197, 1991.

[ThMcGee88] THAREK, A. R.; McGEEHAN, J. P.: *Indoor propagation and bit error rate measurements at 60 GHz using phase-locked oscillators*. Proceedings IEEE Vehicular Technology Conference, VTC ’88, Philadelphia, June 1988, pp. 127-133.

[ThVanDerEn02] THOEN, S.;; VAN DER PERRE, L.; ENGELS, M.: *Modeling the Channel Time-Variance for Fixed Wireless Communications*. IEEE Communications letters, Vol. 6, No. 8, August 2002.

[Turin98] TURIN, W.: *Performance Analysis of Digital Transmission Systems*. 2nd ed. New York: Computer Science, 1998

[TuVanNo98] TURIN, W.; VAN NOBELEN, R.: *Hidden Markov Modeling of Flat Fading Channels*. IEEE Journal on Selected Areas in Communications, Vol.16, No.9, December 1998.

[ToTur92] TOLEDO, A. F.; TURKMANI, A. M. D.: *Propagation into and within buildings at 900, 1800, and 2300 MHz*. Proceedings IEEE Vehicular Technology Conference.

[Turin72] TURIN, G. L.: Simulation of urban vehicle monitoring systems. IEEE Transactions on Veh. Technol., pp. 9–16, Feb. 1972.

[VanPr00] VAN NEE, R.; PRASAD, R.: *OFDM for Wireless Multimedia Communications*. Artech House Publishers universal personal communications library ISBN 0-89006-530-6.

[WaMo93] WANG, H. S.; MOAYERI, N.: *Modelling capacity and joint: source/channel coding for Rayleigh fading channel*. Proceedings 43rd. IEEE Vehicular Technology Conference, May 1993

[WaMo95] WANG, H. S.; MOAYERI, N.: *Finite-State Markov Channel- A useful Model for radio communication channels*. IEEE Transactions on Vehicular Technology, Vol. 44, No. 1, February 1995

[WeEb71] WEINSTEIN, S. B.; EBERT, P.M.: *Data Transmission by Frequency Division Multiplexing Using the Discrete*. IEEE Transactions on Communications, 19:628–634, 1971.

[WyZe00] WYSOCKI, T.A.; ZEPERNICK, H.J.: *Characterization of the indoor radio propagation channel at 2.4 GHz*. Journal of telecommunications and information technology 3-4/2000.

[YaSmHe05] YANG, H., SMULDERS, P.F.M.; HERBEN, M.H.A.J.: *Indoor Channel Measurements and Analysis in theFrequency Bands 2 GHz and 60 GHz.* Proceedings PIMRC'05, Berlin, September 2005.

[YipNg95] YIP, K. W.; NG, T. S.: *Efficient simulation of digital transmission over WSSUS channels*. IEEE Transactions on Communications, Vol. 43, pp. 2907–2913, December 1995.

[YipNg96] YIP, K. W.; NG, T. S.: *Discrete-time model for digital communications over a frequency- selective Rician fading WSSUS channel*. Proceedings IEEE Communications, vol. 143, pp. 37–42, February 1996

[ZhKa99] ZHANG, Q.; KASSAM, S. A.: *Finite-state Markov model for Rayleigh fading channels*. IEEE Transactions on Communications, vol. 47, No. 11, pp. 16881692, 1999

[ZoRa97] ZORZI, M.; RAO, R. R.: *Error control and energy consumption in communications for nomadic computing*. IEEE Transactions on Computers, Vol. 46, pp. 279–289, March 1997.

A. Measurement Set-up

Transmitter

The first element in each communication system is the signal source. The easiest solution to generate an OFDM signal, as described in Chapter 3, would be the utilization of one off-the-shelf IEEE 802.11*a* or *b*/*g* access point. However, to determine the wireless channel effects it is necessary to send a continuous signal. The standard protocols such as the ones avoiding collision in MAC layer that is implemented in the hardware exclude the employment of an access point for the realization of the transmitter for measurements of the multipath propagation over the total available bandwidths.

Based on those requirements, the selected signal generator AMIQ, which is able to emit constantly in the frequency band corresponding to the IEEE 802.11 *a* and *b*/*g* PHY, is depicted in Fig. A.1.

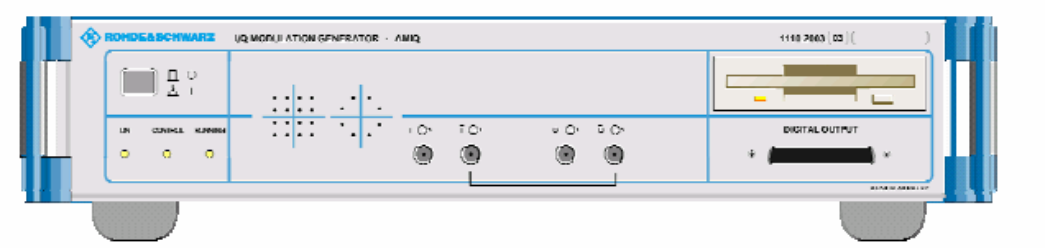

Fig. A.1: I/Q Signal generator Rohde & Schwarz AMIQ

The device is essentially a two channel synchronized D/A (digital to analog) converter. It consists of a fast RAM (random access memory), which is provided with data. The synchronization of both D/A converter enables the output of independent signals to be shifted by 90° in phase. This allows analog I/Q baseband signals to be modulated.

The AMIQ has a floppy disk drive and a built-in harddisk to store the waveforms. It itself has no signal controls. The device can be controlled through the vector modulator Rohde & Schwarz SMIQ or from a PC via GPIB (general purpose interface bus) or RS-232 (recommended standard 232) interface.

In order to generate a signal and to change the configurations of the AMIQ, Rohde & Schwarz provides the software WinIQSim. It is regularly updated and can be downloaded from the Internet website of the company Rohde & Schwarz. This software is used for the communication with the device through a serial port RS-232. The test signals have been created with the software WinIQSim, e.g. a spectral profile of the IEEE 802.11*g* based signal depicted in Fig. A.2. In menu "Multi-Carrier System Mode", “Carrier Settings" the 64 subcarriers with a subcarrier interspace of 312.5 kHz, can be enabled and disabled according to the channel profile, as shown in Fig. A.3. The carrier remains unmodulated to reach a time constant signal.

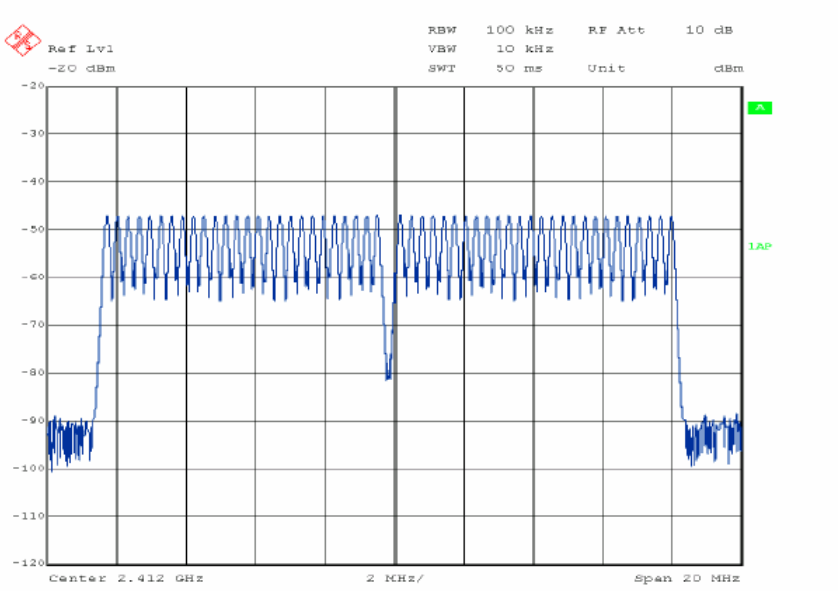

Fig. A.2: IEEE 802.11g PHY OFDM with 52 subcarriers by AWGN channel at the spectrum analyzer Rohde & Schwarz FSIQ

The "Minimize Crest Factor" option reduces the formation of strong impulses in the time domain. Such impulses are often a problem particularly for high-frequency amplifier and can lead to nonlinearity of components. The crest factor or peak-to-average power ratio (PAPR) is defined as the ratio between the peak amplitude divided by the rms value of the waveform P_{peak}/P_{rms} and may be reduced significantly with this option in the carrier settings panel. The in-phase superposition of all signal components results in the maximum voltage. The “Minimize Crest Factor” option randomizes the start phases of the subcarriers and in that way reduces the peak value of the signal.

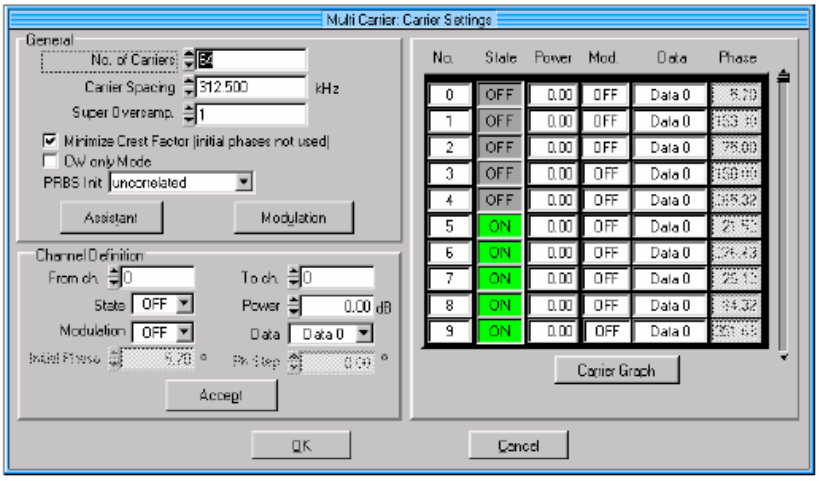

Fig. A.3: Configuration of the WLAN-OFDM profile in WinIQSim

To be able to measure the available spectrum for the IEEE 802.11*a* or *b*/*g* standards, a wideband signal was created. It is an OFDM signal with 500 subcarriers totalling a bandwidth of 100 MHz. It arises from an OFDM subcarrier interspace of 200 kHz. This arrangement is such that with a spectrum analyzer at the receiver measuring 500 values, each spectral sample accurately represents the power of one carrier. Fig. A.4 exemplifies a received spectrum over a 100 MHz bandwidth by AWGN channel with this configuration.

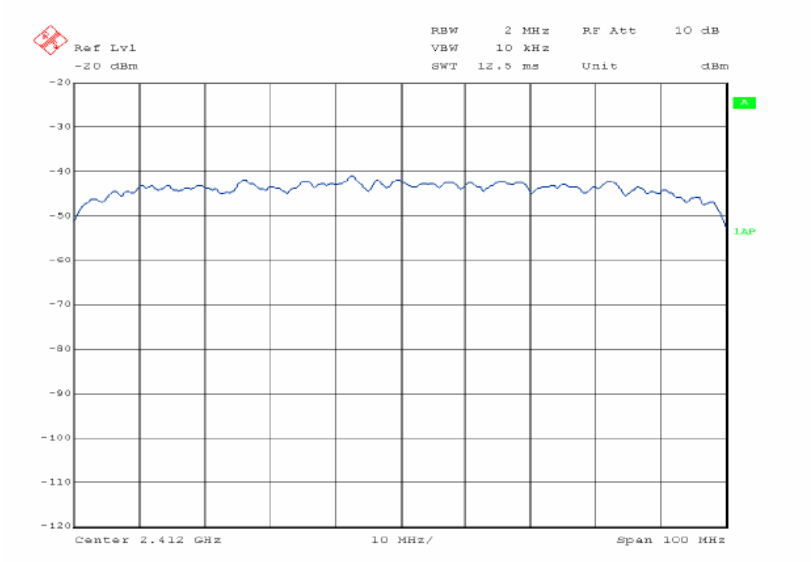

Fig. A.4: OFDM with 500 subcarriers for measuring the channel transfer function over a 100 MHz bandwidth at spectrum analyzer Rohde & Schwarz FSIQ by AWGN channel.

To send the complex baseband signal generated by the AMIQ through the investigated ISM bands, a vector modulator is needed, the Rohde & Schwarz SMIQ, shown in Fig. A.5. In this work, only basic functions from its diverse capabilities are used. To generate OFDM signals in the pass band, the vector modulation function of the SMIQ is utilized. The device receives the base band signal for the I/Q components separately from the signal generator via a 50 Ω BNC cable.

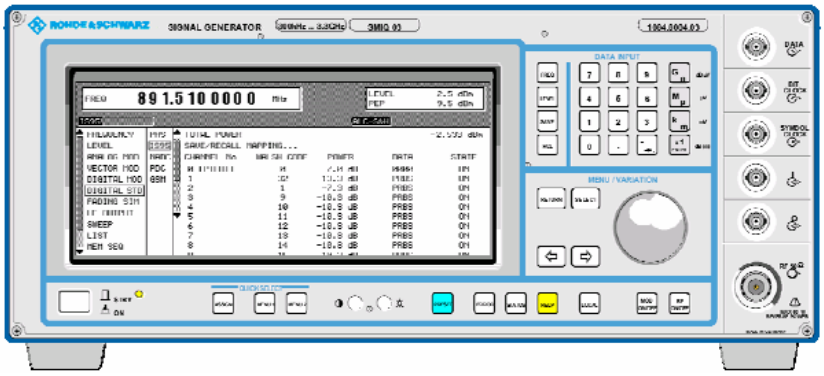

Fig. A.5: Rohde&Schwarz SMIQ Vector modulator used for the complex modulation

The vector modulator SMIQ provides an output signal with up to 16 dBm available by using a quadrature modulation. This is still lower than the IEEE 802.11*g* allowable 20 dBm EIRP (Table 3.3). To enhance the coverage range an additional amplifier is used.

According to the specifications of the amplifier, this shows a saturation power of 13 W when 50 mW input power. Because the amplifier has a fixed gain, the output power of the system is regulated via the power at the amplifier input and thus, via the power control of the vector modulator. The signal power at the transmitter output is 27 dBm.

Receiver

At the receiver side a spectrum analyzer is used for data acquisition. Many spectra with sufficient resolution have to be recorded for later analysis with MATLAB. For this reason, a

connected PC serves to store the saved spectra. The FSIQ has the RS-232, IEEE488.2/GPIB and IEEE 802.3 Ethernet 10-Base-5 interfaces available to transmit the measured data. To connect the PC to the spectrum analyzer the ethernet connection has been selected. The physical connection is via the MAU AUI DB15 connector on the rear panel.

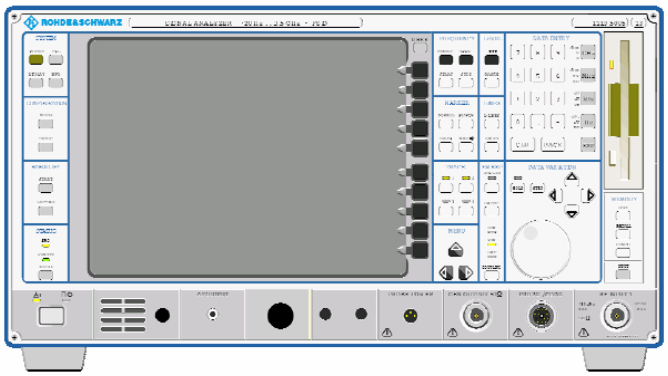

Fig. A.6: Rohde&Schwarz FSIQ7 employed spectrum analyzer at the receiver

The FSIQ7, shown in Fig. A.6, has a total measurement error <1.5 dB in the range from 2.2 - 7 GHz, a typical noise figure of 15 dB and a displayed average noise level (DANL) (with 0 dB RF attenuation, RBW =10 Hz, VBW =1 Hz, 20 averages, trace average, span 0 Hz, termination 50 Ω) of -145 dBm (maximum of -142 dBm) between 10 MHz - 6 GHz. For the measurements, the resolution bandwidth of the spectrum analyzer is chosen to be 200 KHz in order to adapt it to the intercarrier frequency space of the received OFDM signal. The FSIQ7 allows shorter measurement times than other tested equipments.

As mentioned before, the analysis of the recorded ASCII measurement data takes place offline, with the technical and mathematical software package MATLAB. Following it is shown how the data have been prepared for the later analysis.

The values generated by FSIQ are storaged in the ASCII format and written in lines in a file, as depicted in Fig. A.7.

```
%Measurement name: Livingroom1
%Position: X: 32 Y:0
%Frequency range 2400.00 - 2500.00 MHz
%Time: 12:57:04
%RBW: 0.20
%VBW: 0.20
%Center frequency: 2450.00 MHz
%Bandwidth: 100 MHz
%Spectrum values:
2400.00 -88.72
2400.20 -91.48
2400.40 -90.96
2400.60 -90.96
2400.80 -90.46
...
```

Fig. A.7: An example of generated data by the FSIQ by measurement “Livingroom1” in the 2.4GHz band.

Fig. A.8 depicts a number of devices during a measuring process. These include a laptop, a spectrum analyzer as well as antenna positioner form the receiver.

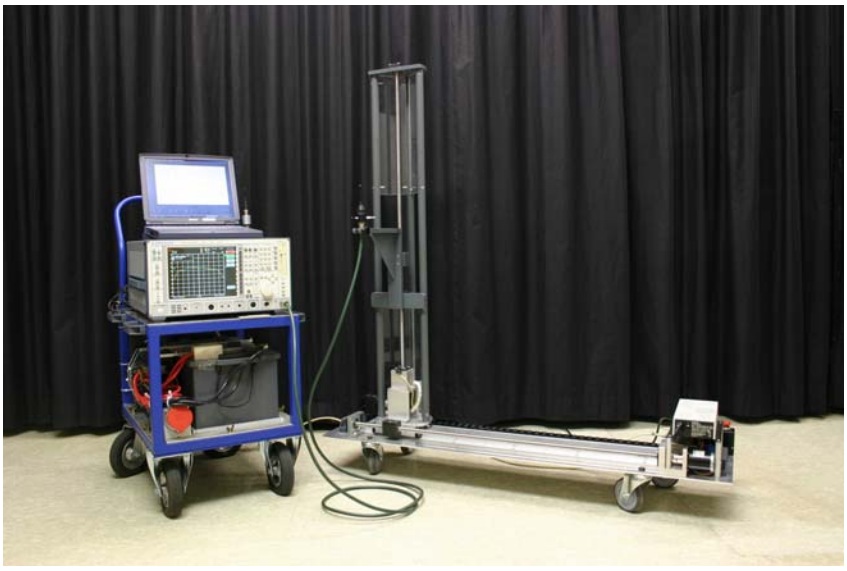

Fig. A.8: Receiving set-up for registering the channel characteristics.

B. Baum-Welch Algorithm

The Baum-Welch forward-backward algorithm is the most efficient and prevalent method for automatically estimating the parameters of a set of Hidden Markov Model based on error vectors. Long sequences are required to accurately estimate small transition probabilities a_{ij}. In communication systems, these small values are often critical for estimating system performance. The calculations required to implement the Baum-Welch Algorithm are described in the following steps.

Step 0: Start with an initial (assumed) model $\hat{\Gamma} = \{\hat{A}, \hat{B}, \hat{\Pi}\}$

$$\hat{a}_{i,j} = \frac{\text{expected number of transitions from state } i \text{ to state } j}{\text{expected number of transitions from state } i} \tag{B.1}$$

$$\hat{b}_j(e_k) = \frac{\text{expected number of times } e_k \text{ is emitted from state } j}{\text{expected number of visits to state } j} \tag{B.2}$$

$$\hat{\pi}_i = \text{expected number of times in state } S_i \text{ at time } t$$

Step 1: The "forward variables", $\alpha_t(i)$, and the "backward variables", $\beta_t(i)$, are computed as follows:

Forward variables

$$\alpha_t(i) = P[O_1, O_2, \ldots, O_t,\ s_t = i \mid \Gamma] \tag{B.3}$$

The calculation of the forward variables is carried out in three steps: initialization, induction and termination.

- Initialization:

$$\alpha_1(i) = \pi_i \cdot b_i(O_1), \qquad i = 1,2,\ldots N \tag{B.4}$$

- Induction:

$$\alpha_{t+1}(j) = \left[\sum_{i=1}^{N} \alpha_t(i) \cdot a_{ij}\right] b_j(O_{t+1}), \qquad 1 \le t \le T-1, \quad 1 \le j \le N \tag{B.5}$$

- Termination:

$$P\left[\overline{O} \mid \Gamma\right] = \sum_{i=1}^{N} \alpha_T(i) \cdot \beta_T(i) \tag{B.6}$$

Note that:

$$\sum_{i=1}^{N} \alpha_T(i) = \sum_{i=1}^{N} P\left[O_1,...,O_T,\ s_T = i \mid \Gamma\right] = P\left[\overline{O} \mid \Gamma\right] \tag{B.7}$$

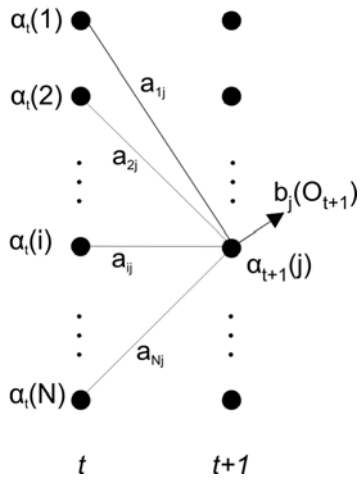

Fig. B.1: Forward Variables

Backward variables

$$\beta_t(i) = P[O_{t+1}, O_{t+2},..., O_T \mid s_t = i, \Gamma], \quad t = 1,2,...T,\ i = 1,2,...N \tag{B.8}$$

The calculation of the backward variables needs two steps: initialization and induction.

- Initialization:

$$\beta_T(i) = 1, \quad i = 1,2,...N \tag{B.9}$$

- Induction:

$$\beta_t(i) = \sum_{j=1}^{N} \beta_{t+1}(j) \cdot b_j(O_{t+1}) \cdot a_{ij}, \quad i \le t \le T,\ 1 \le j \le N \tag{B.10}$$

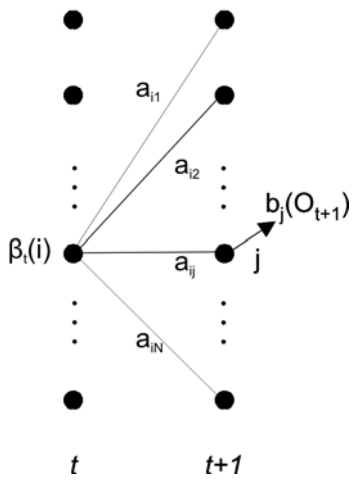

Fig. B.2: Backward Variables

Step 2: The next step is to compute $\gamma_t(i)$ and $\xi_t(i,j)$ according to:

$$\gamma_t(i) = P\left[s_t = i \mid \overline{O}, \Gamma \right] = \frac{\alpha_t(i) \cdot \beta_t(i)}{P\left[\overline{O} \mid \Gamma \right]}, \quad i = 1,2,...,N \tag{B.11}$$

$$\xi_t(i,j) = P\left[s_t = i, s_{t+1} = j \mid \overline{O}, \Gamma \right] = \frac{\alpha_t(i) \cdot a_{ij} \cdot b_j(O_t + 1) \cdot \beta_{t+1}(j)}{P\left[\overline{O} \mid \Gamma \right]} \tag{B.12}$$

Following, is computed:

$$a_{i,j} = \frac{\sum_{t=1}^{T-1} \xi_t(i,j)}{\sum_{t=1}^{T-1} \gamma_t(i)} \tag{B.13}$$

and:

$$b_j\left(e_k\right) = \frac{\sum_{t=1 \mid O_t = e_k}^{T} \gamma_t(j)}{\sum_{t=1}^{T} \gamma_t(j)} \tag{B.14}$$

Finally, it can be computed:

$$\pi_i(t=1) = \alpha_1(i) \cdot \beta_1(i) \tag{B.15}$$

Step 3: Go back to Spet 1 with the new values $\Gamma = \{A, B, \pi\}$ and repeat the three steps until the desired level of convergence is reached.

The computational effort associated with the Baum-Welch algorithm is quite high when the error vector is long, since the forward and backward variables are computed for all *N* states for each symbol in the given error sequence. In addition, convergence is sometimes slow, which adds to the computational cost. For low error probability applications, the error vector must contain a significant number of error events in order to accurately define the model for the error vector.

Scaling

The forward and backward vectors tend to zero exponentially for large data size and must be scaled properly in order to prevent numerical overflow. The scaling constant is defined as follows:

$$C_t = \sum_{i=1}^{N} \alpha_t(i) \tag{B.16}$$

The scaled values of the backward variables denoted by $\overline{\alpha}_t(j)$, are given by:

$$\overline{\alpha}_t(j) = \frac{\alpha_t(j)}{C_t} \tag{B.17}$$

This implies that:

$$\sum_{i=1}^{N} \overline{\alpha}_t(i) = 1 \tag{B.18}$$

Likewise, the scaled values of the backward variables, denoted $\overline{\beta}_t(\mathrm{i})$, are given by:

$$\overline{\beta}_t(i) = \frac{\beta_t(i)}{C_t} \tag{B.19}$$

with the initialization:

$$\overline{\beta}_T = \frac{1}{C_T} \tag{B.20}$$

where **1** denotes the column vector containing all ones.

Convergence and stopping criteria

Since the Baum-Welch algorithm is iterative, the number of iterations to be performed for a required level of model accuracy must be determined. Perhaps the best way to accomplish this is to display the estimation of *A* and *B* as the algorithm is executing. If one desires each element of *A* and *B* to be accurate to a given number of significant figures, execution of the algorithm is allowed to continue until the elements of *A* and *B* no longer change, within the given accuracy, from iteration to iteration. The algorithm is then terminated manually. This technique has considerable appeal, since the level of accuracy is known. Also, based on previous knowledge, one may simply perform a given number of iterations.

Another commonly used method for determinig convergence is to continue the iterations until successive values of $P[\overline{O} \mid \Gamma]$ differ very little. The Baum-Welch algorithm is guaranteed to converge to a maximum likelihood solution. The value of $P[\overline{O} \mid \Gamma]$ is determined in terms of the scaling constant C_t:

$$P\left[\overline{O} \mid \Gamma\right] = \prod_{t=1}^{T} C_t \tag{B.21}$$

For *T* large, this number will be very small and is usually expressed as:

$$\log_{10} P\left[\overline{O} \mid \Gamma\right] = \sum_{t=1}^{T} \log_{10} C_t \tag{B.22}$$

This is referred to as the log-likelihood ratio. It should be pointed out that the estimates of *A* and *B* for a given set of data are not unique, unless the initial estimates of *A*, *B* and π are specified. Since the error vector is a function of both *A* and *B*, various combinations may produce statistically equivalent results and a specific result will depend on the initial conditions.

C. OMNet++

OMNet++ is an object-oriented event simulator. It is an open source project under the General Public License (GPL). The source code is C++ and strongly object oriented. OMNet is very suitable to simulate communications systems and is extended through the mobility framework, which also allows configuring wireless systems. With the mobility framework, the propagation characteristics of a radio link are simulated. Thereby, the implementation of ad-hoc or centralized wireless networks is possible.

The Mobility Framework already includes several systems, for example an Aloha-network or the IEEE 802.11 *b* Standard. In scope of the work [Becker06] also the IEEE 802.11 *g* Standard was implemented. In this available communication network, the discrete in-house channel model based on a HMM approach has been integrated and described in Section 6.3.2.

In OMNet, the wireless links are managed by the “channelcontrol” module, as shown in Fig. C.1. It interconnects all the stations, which occasionally can interfere. This does not imply that these nodes can communicate all with each other. The physical layer has to decide if the message is decodable or must be treated as interference.

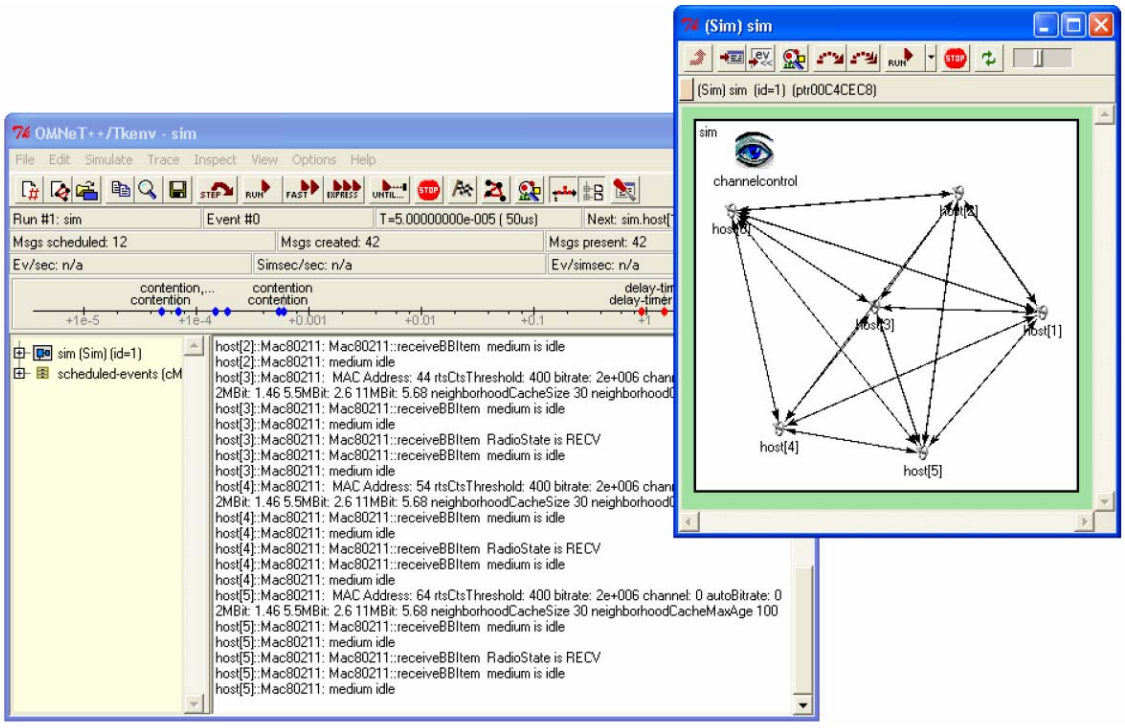

Fig. C.1: Simulation environment OMNet++ with Mobility Framework

A station in the simulator is referred to as *Host* and is built according to the ISO/OSI Model, see Fig. C.2. The NIC (network interface card) structure is formed by the receiver module (*snrEval*), the decider module (*decider*) and the MAC layer. These modules reproduce the

functionalities of the WLAN Standard.

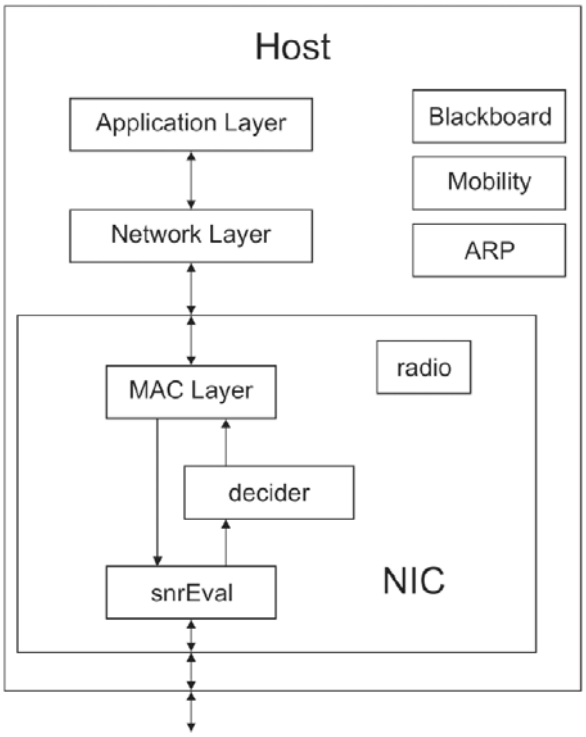

Fig. C.2: Configuration of a host

The *snrEval* module calculates an SNR value for each received packet. Afterwards, the packet with the SNR information is forwarded to the *decider* module.

On the basis of the datarate and the SNR value, the necessary model parameters are extracted from the data HMM_data.h. In this file, the HMM parameters {*A*, *B*, π} for the three-state model are classified depending on the code rate, modulation and E_b/N_0. Therefore, the assigned SNR value is converted into the corresponding E_b/N_0. In the file Decider80211g.cc, the function packetOK is implemented. Hier the output sequence (error sequence) of the channel model is generated. When the sum of this sequence is zero, it indicates the packet has been correctly received and the function returns “true”, otherwise returns “false”.